



Print ISSN: 2152-4157  
Online ISSN: 2152-4165

FALL/WINTER 2015  
VOLUME 7, NUMBER 2

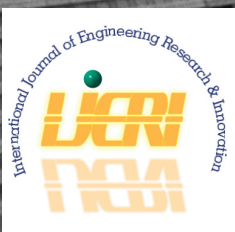
WWW.IJERI.ORG

# International Journal of Engineering Research & Innovation

**Editor-in-Chief: Mark Rajai, Ph.D.  
California State University Northridge**



Published by the  
**International Association of Journals & Conferences**



[www.ijeri.org](http://www.ijeri.org)

Print ISSN: 2152-4157  
Online ISSN: 2152-4165



[www.iajc.org](http://www.iajc.org)

## INTERNATIONAL JOURNAL OF ENGINEERING RESEARCH AND INNOVATION

### **ABOUT IJERI:**

- IJERI is the second official journal of the International Association of Journals and Conferences (IAJC).
- IJERI is a high-quality, independent journal steered by a distinguished board of directors and supported by an international review board representing many well-known universities, colleges, and corporations in the U.S. and abroad.
- IJERI has an impact factor of **1.58**, placing it among an elite group of most-cited engineering journals worldwide.

### **IJERI SUBMISSIONS:**

- Manuscripts should be sent electronically to the manuscript editor, Dr. Philip Weinsier, at [philipw@bgsu.edu](mailto:philipw@bgsu.edu).

For submission guidelines visit  
[www.ijeri.org/submissions](http://www.ijeri.org/submissions)

### **TO JOIN THE REVIEW BOARD:**

- Contact the chair of the International Review Board, Dr. Philip Weinsier, at [philipw@bgsu.edu](mailto:philipw@bgsu.edu).

For more information visit  
[www.ijeri.org/editorial](http://www.ijeri.org/editorial)

### **INDEXING ORGANIZATIONS:**

- IJERI is indexed by numerous agencies. For a complete listing, please visit us at [www.ijeri.org](http://www.ijeri.org).

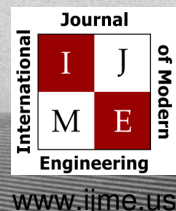
Contact us:

**Mark Rajai, Ph.D.**

Editor-in-Chief  
California State University-Northridge  
College of Engineering and Computer Science  
Room: JD 4510  
Northridge, CA 91330  
Office: (818) 677-5003  
Email: [mrajai@csun.edu](mailto:mrajai@csun.edu)



[www.tiji.org](http://www.tiji.org)



[www.ijme.us](http://www.ijme.us)

---

# **INTERNATIONAL JOURNAL OF ENGINEERING RESEARCH AND INNOVATION**

The INTERNATIONAL JOURNAL OF ENGINEERING RESEARCH AND INNOVATION (IJERI) is an independent and not-for-profit publication, which aims to provide the engineering community with a resource and forum for scholarly expression and reflection.

IJERI is published twice annually (fall and spring issues) and includes peer-reviewed research articles, editorials, and commentary that contribute to our understanding of the issues, problems, and research associated with engineering and related fields. The journal encourages the submission of manuscripts from private, public, and academic sectors. The views expressed are those of the authors and do not necessarily reflect the opinions of the IJERI editors.

## **EDITORIAL OFFICE:**

Mark Rajai, Ph.D.  
Editor-in-Chief  
Office: (818) 677-2167  
Email: [ijmeeditor@iajc.org](mailto:ijmeeditor@iajc.org)  
Dept. of Manufacturing Systems  
Engineering & Management  
California State University-  
Northridge  
18111 Nordhoff Street  
Northridge, CA 91330-8332

## **THE INTERNATIONAL JOURNAL OF ENGINEERING RESEARCH AND INNOVATION EDITORS**

*Editor-in-Chief:*

**Mark Rajai**

California State University-Northridge

*Manuscript Editor:*

**Philip Weinsier**

Bowling Green State University-Firelands

*Associate Editors:*

**Paul Wilder**

Vincennes University

*Copy Editors:*

**Li Tan**

Purdue University North Central

**Li Tan**

Purdue University North Central

**Ahmad Sarfaraz**

California State University-Northridge

*Production Editor:*

**Philip Weinsier**

Bowling Green State University-Firelands

*Technical Editors:*

**Marilyn Dyrud**

Oregon Institute of Technology

**Barry Hoy**

St. Leo University

*Subscription Editor:*

*Publisher:*

**Morteza Sadat-Hossieny**

Northern Kentucky University

**Bowling Green State University Firelands**

*Web Administrator:*

**Saeed Namyar**

Advanced Information Systems

---

# TABLE OF CONTENTS

<i>Editor's Note: 5th IAJC/ISAM Joint International Conference.....</i>	3
Philip Weinsier, IJERI Manuscript Editor	
<i>Evaluation of Intelligent Controllers for Improving Elevator Energy Efficiency.....</i>	5
Muhammad Z Hasan, Texas A&M International University; Rainer Fink, Texas A&M University; Muthuvel Raj Suyambu, Texas A&M University; Manoj Kumar Baskaran, Texas A&M University	
<i>Development of a Modified Experimental Setup to Evaluate the Effects of Shrinkage-Reducing Admixture.....</i>	13
Rajarajan Subramanian, Pennsylvania State University at Harrisburg; Mang Tia, University of Florida; Michael J. Bergin, Florida Department of Transportation; Charles A. Ishee, Applied Research Associates, Inc.	
<i>A Multi-Agent-Based Approach to Dynamic Scheduling of Machines and Automated Guided Vehicles (AGV) in Manufacturing Systems by Considering AGV Breakdowns .....</i>	32
Vahit Kaplanoğlu, University of Gaziantep; Cenk Şahin, Cukurova University; Adil Baykasoğlu, Dokuz Eylül University; Rızvan Erol, Cukurova University; Alper Ekinci, University of Gaziantep; Melek Demirtaş, Cukurova University	
<i>Introducing Kinematics into Robotic Operating Systems .....</i>	39
Asad Yousuf, Savannah State University; William Lehman, Bill's Robotic Solutions; Mir Hayder, Savannah State University; Mohamad Mustafa, Savannah State University	
<i>Fuzzy Logic Control of a Quadrotor .....</i>	48
Ming Li, University of Michigan-Flint	
<i>A Comparative Study on the Effectiveness of Coated and Uncoated Tungsten Carbide Tools for Dry Machining of Ti-6Al-4V.....</i>	53
Muhammad P. Jahan, Western Kentucky University; Gregory K. Arbuckle, Western Kentucky University; Abdulhameed Dawood, Western Kentucky University	
<i>Instructions for Authors: Manuscript Requirements .....</i>	61



# 5th IAJC/ISAM Joint International Conference

**November 6 – 8, 2016 – Orlando, Florida**



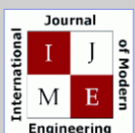
**The leading indexed high impact factor conference  
on engineering and related technologies.**



The editors and staff at IAJC would like to thank you, our readers, for your continued support, and we look forward to seeing you at the upcoming IAJC conference. For this fifth IAJC conference, we will be partnering again with the International Society of Agile Manufacturing (ISAM). This event will be held at the new Embassy Suites hotel in Orlando, FL, November 6-8, 2016, and is sponsored by IAJC, IEEE, ASEE, and the LEAN Institute.

The IAJC/ISAM Executive Board is pleased to invite faculty, students, researchers, engineers, and practitioners to present their latest accomplishments and innovations in all areas of engineering, engineering technology, math, science, and related technologies.

Main Sponsors



Selected papers from the conference will be published in the three IAJC-owned journals. Oftentimes, these papers, along with manuscripts submitted at-large, are reviewed and published in less than half the time of other journals. Publishing guidelines are available at [www.iajc.org](http://www.iajc.org), where you can read any of our previously published journal issues, as well as obtain information on chapters, membership, and benefits.

I am pleased to report that, based on the latest impact factor (IF) calculations (Google Scholar method), the *International Journal of Engineering Research and Innovation (IJERI)*, had a strong showing with an IF = 1.58, which is noteworthy, as it is a relatively young journal (in publication since 2009). *IJERI*'s sister journal, the *International Journal of Modern Engineering (IJME)*, also now has a remarkable IF = 3.0 and continues its march toward the top 20 engineering journals. Any IF above 1.0 is considered high, based on the requirements of many top universities, and places the journals among an elite group.

## EDITOR'S NOTE

Philip Weinsier, IJERI Manuscript Editor



Currently, there is no official ranking system for journals that publish engineering-related topics the way that *IJERI* and *IJME* do, but the following still apply:

- Both *IJME* and *IJERI* now are indexed in most well-known indexing databases including DOAJ, which is the most prestigious and comprehensive database for open-access journals worldwide.
- Both journals now are indexed by hundreds of libraries worldwide, and in several states where there is near complete indexing across their university and college libraries.
- Both journals now are indexed in the libraries of all 10 campuses of the University of California system and the 23 campuses of the California State University system.

The biggest achievement, though, is that now both journals also are indexed by all of the top 10 universities in the world:

- |     |  |
|-----|--|
| #1  | <b>California Institute of Technology</b>    |
| #2  | <b>Harvard</b>                               |
| #3  | <b>Stanford</b>                              |
| #4  | <b>University of Oxford</b>                  |
| #5  | <b>Princeton University</b>                  |
| #6  | <b>University of Cambridge</b>               |
| #7  | <b>Massachusetts Institute of Technology</b> |
| #8  | <b>Imperial College London</b>               |
| #9  | <b>University of Chicago</b>                 |
| #10 | <b>University of California, Berkeley</b>    |



---

## Editorial Review Board Members

Mohammed Addallah	State University of New York (NY)	Shiyoung Lee	Penn State University Berks (PA)
Nasser Alaraje	Michigan Tech (MI)	Soo-Yen Lee	Central Michigan University (MI)
Aly Mousaad Aly	Louisiana State University (LA)	Chao Li	Florida A&M University (FL)
Jahangir Ansari	Virginia State University (VA)	Jimmy Linn	Eastern Carolina University (NC)
Kevin Berrisso	Ohio University (OH)	Dale Litwhiler	Penn State University (PA)
Salah Badjou	Wentworth Institute of Technology (MA)	Guoxiang Liu	University of North Dakota (ND)
Pankaj Bhambri	Guru Nanak Dev Engineering (INDIA)	Louis Liu	University of New Orleans (LA)
Water Buchanan	Texas A&M University (TX)	Mani Manivannan	ARUP Corporation
Jessica Buck Murphy	Jackson State University (MS)	G.H. Massiha	University of Louisiana (LA)
John Birmingham	Clayton State University (GA)	Thomas McDonald	University of Southern Indiana (IN)
Shaobiao Cai	Penn State University (PA)	David Melton	Eastern Illinois University (IL)
Vigyan Chandra	Eastern Kentucky University (KY)	Shokoufeh Mirzaei	Cal State Poly Pomona (CA)
Isaac Chang	Cal Poly State University SLO (CA)	Bashir Morshed	University of Memphis (TN)
Bin Chen	Purdue University Calumet (IN)	Sam Mryyan	Excelsior College (NY)
Wei-Yin Chen	University of Mississippi (MS)	Wilson Naik	University of Hyderabad (INDIA)
Hans Chapman	Morehead State University (KY)	Arun Nambiar	California State University Fresno (CA)
Rigoberto Chinchilla	Eastern Illinois University (IL)	Ramesh Narang	Indiana University-Purdue University (IN)
Phil Cochrane	Indiana State University (IN)	Anand Nayyar	Institute Management and Tech (INDIA)
Michael Coffman	Southern Illinois University-Carbondale (IL)	Stephanie Nelson	Cal State LA (CA)
Emily Crawford	Southern Wesleyen University (SC)	Hamed Niroumand	Universiti Teknologi (MALAYSIA)
Brad Deken	Southeast Missouri State University (MO)	Aurenice Oliveira	Michigan Tech (MI)
Z.T. Deng	Alabama A&M University (AL)	Troy Ollison	University of Central Missouri (MO)
Sagar Deshpande	Ferris State University (MI)	Reynaldo Pablo	Indiana University-Purdue University (IN)
David Domermuch	Appalachian State University (NC)	Basile Panoutsopoulos	Community College of Rhode Island (RI)
Ryan Dupont	Utah State University (UT)	Shahera Patel	Sardar Patel University (INDIA)
Marilyn Dyrud	Oregon Institute of Technology (OR)	Jose Pena	Purdue University Calumet (IN)
Mehran Elahi	Elizabeth City State University (NC)	Karl Perusich	Purdue University (IN)
Ahmed Elsawy	Tennessee Technological University (TN)	Thongchai Phairoh	Virginia State University (VA)
Rasoul Esfahani	DeVry University (OH)	Huyu Qu	Honeywell Corporation
Dominick Fazarro	Sam Houston State University (TX)	John Rajadas	Arizona State University (AZ)
Morteza Firouzi	University of Technology (MALAYSIA)	Desire Rasolomampionona	Warsaw University of Tech (POLAND)
Rod Flanigan	University of Nebraska-Kearney (NE)	Mulchand Rathod	Wayne State University (MI)
Ignatius Fomunung	University of Tennessee Chattanooga (TN)	Mohammad Razani	New York City College of Tech (NY)
Ahmed Gawad	Zagazig University EGYPT)	Sangram Redkar	Arizona State University-Poly (AZ)
Daba Gedafa	University of North Dakota (ND)	Michael Reynolds	University of Arkansas Fort Smith (AR)
Ralph Gibbs	Eastern Kentucky University (KY)	Marla Rogers	Wireless Systems Engineer
Mohsen Hamidi	Utah Valley University (UT)	Dale Rowe	Brigham Young University (UT)
Mamoon Hammad	Abu Dhabi University (UAE)	Anca Sala	Baker College (MI)
Youcef Himri	Safety Engineer in Sonelgaz (ALGERIA)	Mehdi Shabaninejad	Zagros Oil & Gas Company (IRAN)
Xiaobing Hou	Central Connecticut State University (CT)	Ehsan Sheybani	Virginia State University (VA)
Shelton Houston	University of Louisiana Lafayette (LA)	Musibau Shofoluwe	North Carolina State University (NC)
Barry Hoy	St. Leo University (VA)	Siles Singh	St. Joseph University Tanzania (AFRICA)
Ying Huang	North Dakota State University (ND)	Ahmad Sleiti	University of North Carolina Charlotte (NC)
Charles Hunt	Norfolk State University (VA)	Jiahui Song	Wentworth Institute of Technology (MA)
Dave Hunter	Western Illinois University (IL)	Yuyang Song	Toyota Corporation
Christian Hyeng	North Carolina A&T University (NC)	Carl Spezia	Southern Illinois University (IL)
Pete Hylton	Indiana University Purdue (IN)	Michelle Sururus	Ohio University (OH)
Ghassan Ibrahim	Bloomsburg University (PA)	Vassilios Tzouanas	University of Houston Downtown (TX)
John Irwin	Michigan Tech (MI)	Jeff Ulmer	University of Central Missouri (MO)
Sudershan Jetley	Bowling Green State University (OH)	Mihaela Vorvoreanu	Purdue University (IN)
Rex Kanu	Ball State University (IN)	Phillip Waldrop	Georgia Southern University (GA)
Reza Karim	North Dakota State University (ND)	Abraham Walton	Purdue University (IN)
Tolga Kaya	Central Michigan University (MI)	Liangmo Wang	Nanjing University of Science/Tech (CHINA)
Satish Ketkar	Wayne State University (MI)	Jonathan Williams	Lake Erie College (OH)
Manish Kewalramani	Abu Dhabi University (UAE)	Boonsap Witchayangkoon	Thammasat University (THAILAND)
Tae-Hoon Kim	Purdue University Calumet (IN)	Alex Wong	Diligent Inc.
Doug Koch	Southeast Missouri State University (MO)	Shuju Wu	Central Connecticut State University (CT)
Sally Krijestorac	Daytona State College (FL)	Baijian Yang	Ball State University (IN)
Ognjen Kuljaca	Brodarski Institute (CROATIA)	Mijia Yang	North Dakota State University (ND)
Chakresh Kumar	Uttar Pradesh Tech University (INDIA)	Faruk Yildiz	Sam Houston State University (TX)
Zaki Kuruppalil	Ohio University (OH)	Yuqiu You	Morehead State University (KY)
Edward Land	Johns Hopkins Medical Institute	Jinwen Zhu	Missouri Western State University (MO)
Ronald Land	Penn State University (PA)		
Jane LeClair	Excelsior College (NY)		

# EVALUATION OF INTELLIGENT CONTROLLERS FOR IMPROVING ELEVATOR ENERGY EFFICIENCY

Muhammad Z Hasan, Texas A&M International University; Rainer Fink, Texas A&M University;  
Muthuvel Raj Suyambu, Texas A&M University; Manoj Kumar Baskaran, Texas A&M University

## Abstract

In recent years, conservation of energy without degradation in performance has become a major trend in the transportation sector. Elevator operations have two modes: running and stand-by. In this study, the authors developed an algorithm to achieve notable energy savings in elevator systems and designed an energy-saving elevator system capable of manipulating its speed in the running mode. Speed was varied based on the load carried and acceleration was varied based on the number of floors traveled. The total travel time of the system was examined in the context of enhancing overall performance. The algorithm was tested with various traffic patterns during peak and non-peak hours. Simulated performance was compared with that of constant-speed elevators. This method produced a 12.35% energy savings and 5.49% reduction in travel time during non-peak hours and 5.06% energy savings and 1.32% reduction in travel time during peak hours of traffic.

## Introduction

In recent years, energy savings in electrical systems has grown into an important consideration for sustainable development. With the growing urban population, the use of elevator systems has increased rapidly over the last 20 years. Figure 1 illustrates the approximate number of elevators installed in some major countries [1]. Surprisingly, efforts towards reducing energy consumption tend to degrade system performance. Thus, optimization in terms of performance and energy (facing a trade-off) is necessary.

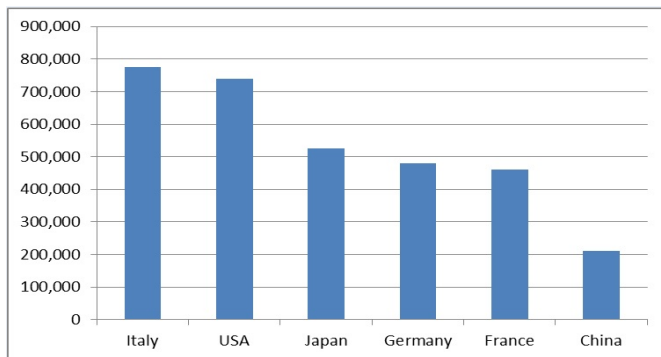


Figure 1. Installed Elevators across Different Countries

Various mechanisms are involved in the movement of elevators. Traction lifts have become prevalent in recent years. In traction lifts, the car is suspended by ropes wrapped around a sheave that is driven by an electric motor. The weight of the car is usually balanced by a counterweight that equals the mass of the car plus 45% to 50% of the rated load. The main purpose of the counterweight is to ensure that a constant potential energy is maintained in the system [2]. There are two types of traction: 1) geared lifts, typically used in midrise applications where high speed is not a prime factor, with a reduction gear to reduce the speed of the motor; and 2) gearless lifts, used in high-rise applications where the sheave is directly driven by the motor, thereby eliminating the losses in the gear. In such cases, both motor and sheave rotate at the same speed [2] and the counterweight balance ensures that sufficient tension is maintained in the suspension system. It enforces adequate traction between ropes/belts and the drive sheave. Also, the entire system maintains a near constant potential energy level, heavily reducing energy consumption [2].

There has been a significant development in optimization of elevator controllers in terms of energy efficiency and reducing average waiting and transit time. A recent study includes implementation of artificial intelligence and fuzzy logic in elevator controllers to optimize the passenger service. This paper examines speed manipulation of the elevator based on load to achieve energy savings. A trade-off between speed and the load torque is kept such that their product is constant.

## Related Work

In the recent past, several ideas have been proposed for energy savings in elevator systems. In this study, several methods for energy savings were considered: regenerative energy feedback, loss reduction to obtain optimum energy utilization, energy storage and discharge using capacitors [3], and speed manipulation. Similar other studies were carried out using super capacitors [4] and pulse width modulation (PWM) converters [5]. Another study [6] proved that, when observed for a prolonged duration, there exists a traffic pattern in multi-level buildings that repeats day to day. Furthermore, a simulation method was developed to analyze energy consumption based on elevator load and traffic pat-

terns. This method compared the energy savings of various drive systems and machinery as well as control systems. This provided insight for this current study on energy consumption of elevator systems.

Furthermore, several efforts have been established attempting to reduce waiting and transit time of the elevators as well. Current research has focused on implementation of artificial intelligence (AI) and neural networks in elevator group control systems, which assigns the elevator cage based on its demand at that instant in time. In these efforts, elevators undergo a training period in which the system establishes a definite traffic pattern corresponding to the building. This helps in the process of prioritizing the floors based on the requirement during up-peak and down-peak hours of the day. Energy consumption is reduced even in optimal assignment of an empty cage based on the historical need of each hour [7], [8].

Energy conservation is also made more effective in elevator group systems with intelligent algorithms to control all the lifts in the system, which requires optimal assignment of each cage to a particular floor [9]. This reduces energy use and improves passenger wait time. A recent study based on an ant colony algorithm documented improvement of energy conservation in elevators for peak traffic flow [10]. Another study examined a genetic algorithm designed for energy savings, which supports a 23.6% increase in conservation but also causes a significant increase in average service time [11]. Thus, energy savings beyond a particular limit may degrade the performance of the elevator; hence, the aim of this current study was to optimize energy savings without adversely impacting system performance.

## Development of the Idea

The authors considered energy conservation in traction elevators driven by electric motors. Normally, traction elevators move at a constant speed irrespective of the load they carry. This leads to inefficient use of energy. Adjustment of speed based on load is needed for more energy-efficient operation [12].

## Basic Algorithm of the Elevator System

With the aforementioned focus, elevator speed was varied based on the load carried by the cart. In determining the load, consideration was given to the counterweight of the elevator. Also, travel time was measured in order to estimate overall performance. A simple algorithm, by which a single elevator can decide how to move and where to stop, can be summarized as follows:

- 1) Continue traveling in the same direction while there are remaining requests in that same direction.
- 2) If there are no further requests in that direction, then stop and stay idle, or change direction if there are requests in the opposite direction.

According to the calls, the elevator determines the direction of movement and satisfies them based on a fixed priority (floors along the direction of movement are given priority). A constant-speed elevator moving at 1m/s was considered as the reference for this study. A MATLAB plot of elevator speed of such an elevator with respect to time is given in Figure 2 for a fixed traffic pattern. The elevator either travels at 1m/s (after acceleration) or remains idle at 0 m/s (after deceleration).

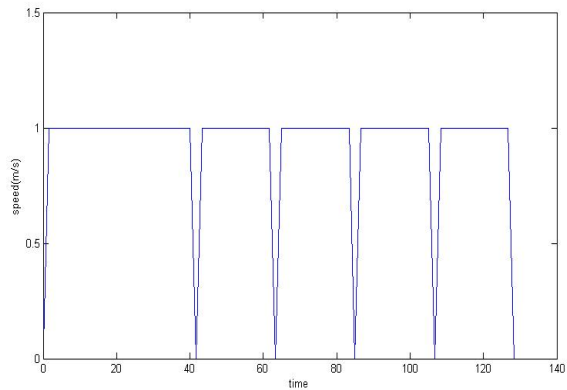


**Figure 2. Plot of Elevator Speed between Various Floors**

## Proposal of the Idea

The drive motor of a traction lift is required to move the load in the elevator cart. In order to reduce the size of the drive motor, the weight of the car plus a proportion of the maximum weight of the passengers (the rated load) is balanced by a counterweight. The commonly used value for counter balancing is 50%. For an elevator with 50% counter balancing, when it is partially full with passengers, the motor only needs to overcome a much smaller load in order to move the elevator. The rating,  $R$  (in N-m/s), of an elevator motor with efficiency  $\eta$  is related to the out-of-balance load,  $B$  (in kg), and rated speed,  $v$  (in m/s), as given in Equation (1) [13]:

$$R = 9.81 * (B * v) / (\eta) \quad (1)$$

Thus, for a fixed efficiency, any change in load gets compromised by a subsequent variation in the speed of the elevator. The initial idea is as follows:

- 1) Operate the motor at its rated full load power in order to achieve the maximum possible efficiency.
- 2) Vary the steady speed of the elevator, based on the weight carried, in a way that the motor operates closer to its rated full load power.
- 3) The upper limit on speed, taking passenger comfort into consideration, is decided by:  

$$TimeConstant \geq 4 * TimeAccDecel$$
, which is termed as the time constraint equation, where, TimeConstant is the time the elevator runs at constant speed, and TimeAccDecel is the time for acceleration or deceleration.

The lower limit for the elevator speed is the speed at which the elevator would run if the variable speed algorithm were not applied. This proposed algorithm will hereafter be referred to as “variable speed.”

## Implementation of the Algorithm

The time constraint equation previously explained prevented excess energy usage during acceleration/deceleration time. The algorithm was tested under varied traffic conditions and the result was compared with a constant-speed elevator. The algorithm was successful in producing energy savings and travel time reduction during non-peak hours of traffic, while during peak hours, it was found that more energy was consumed than the constant-speed method. Hence, appropriate manipulation of the algorithm was required in order to produce significant energy savings under varied traffic patterns during the day.

## Revised Algorithm to Increase Efficiency under Varied Traffic Intensity

The following changes were made to the algorithm:

- 1) Increase the speed range of operation by a small amount (the lower limit was decreased and the upper limit increased by a small amount).
- 2) Vary the acceleration based on number of floors the elevator has to move, relaxing the time constraint condition to ‘Time constant  $\geq 3 * TimeAccDecel$ ’, thereby significantly reducing the travel time. For example, in a 10-floor building, it would mean an acceleration value ( $u \text{ m/s}^2$ ) for moving eight levels would be different from an acceleration value ( $v \text{ m/s}^2$ ) for moving six levels. This modified version of the algorithm will hereafter be referred to as “speed variation II.”

## Analytical Model

The diagram representing the traction system considered in the simulation is shown in Figure 3 [14]. The maximum load on the elevator is 400 kg with a counter weight of 300 kg.  $T_M$  is the Motor Torque (in N-m),  $v$  is the speed of elevator (in m/s), and  $R$  is the radius of the pulley (in m). Equations (2)-(5) represent various relationships.

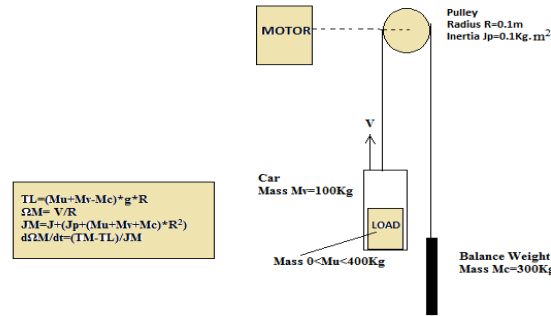


**Figure 3. Schematic Representation of the Elevator System under Study**

$$TL, \text{ Load Torque (in N-m)} = (Mu + Mv - Mc)*g*R \quad (2)$$

where,  $Mu$  is the mass of the load;  $Mv$  is the mass of the elevator cart;  $Mc$  is the mass of the counterweight; and,  $g$  is the gravity.

$$JM, \text{ Moment of inertia (in kg-m}^2\text{)} = J + J_p + (Mu + Mv + Mc) * R^2 \quad (3)$$

where,  $J_p$  is the inertia of the pulley.

$$\Omega M, \text{ Angular velocity (in radians/second)} = v / R \quad (4)$$

$$d(\Omega M) / dt, \text{ angular acceleration} = (TM - TL) / J \quad (5)$$

The basic operation of a constant speed elevator system is shown in Figure 4. According to the calls, the elevator controller determines the direction of movement and satisfies the calls based on a fixed priority (floors along the direction of movement are given priority).

The modified version of the algorithm is shown in Figure 5. This algorithm uses the “load on the elevator” to determine the speed of movement and the “number of floors to move” to determine acceleration. The elevator then satisfies the calls similar to the constant-speed case. Figure 6 shows how the calls are satisfied in a five-floor building using this algorithm.

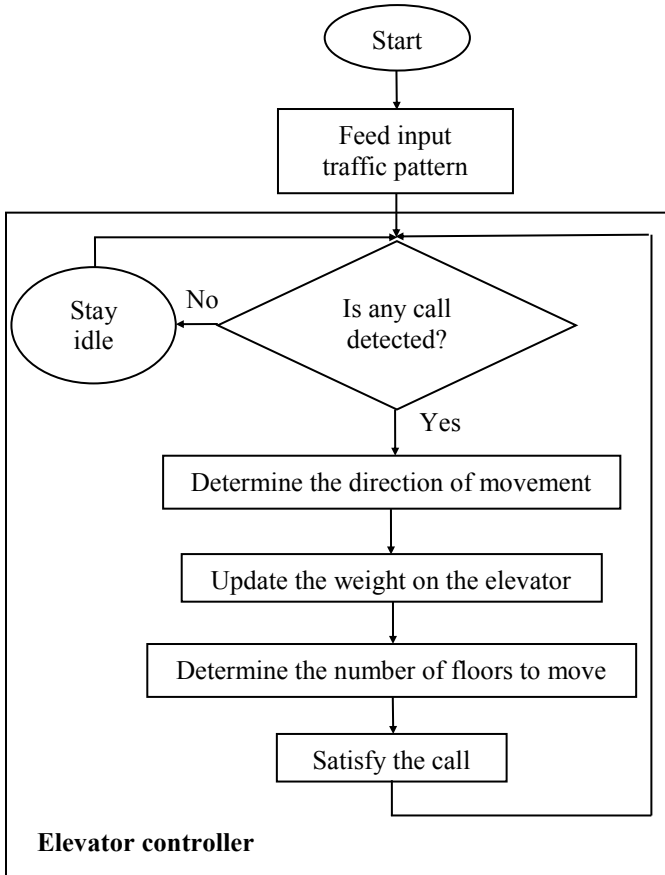


**Figure 4.** Flow Diagram Elaborating the Algorithm of the Constant-speed Case

## Result and Analysis

### Testing the Algorithms

The following three algorithms were simulated under multiple traffic patterns and the simulation results tabulated and compared.

- 1) Constant speed case: elevator running at a constant speed of 1m/s. This was used as the reference for comparison of energy consumption and travel time.
- 2) Speed variation I: elevator changing its speed based on load but fixed acceleration.
- 3) Speed variation II: elevator changing its speed based on the load as well as changing acceleration based on the number of levels moved. (This is a modified version of “speed variation I.”)

Case 1: Consider an elevator of maximum load 400 kg, running in a 10-level building during peak-hour traffic pat-

tern. The three algorithms were simulated and the results tabulated for analysis. In this simulation, peak hours of traffic intensity as mentioned by Cortés et al. [15] was used. Figures 7 and 8 depict the arrival rates at different halls during lunch-peak traffic. Most of the workers go out for lunch in the first hour (1-3600s), as shown in Figure 7, and return to the building during the second hour (3600-7200s), as shown in Figure 8.

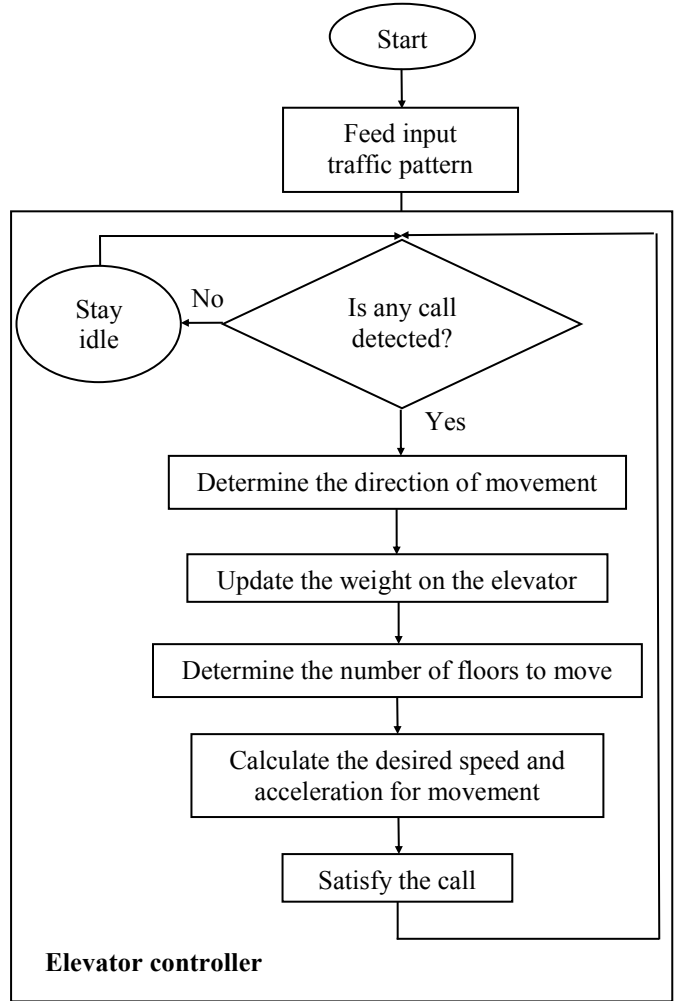


**Figure 5.** Flow Diagram Elaborating the Algorithm of the Modified Version

Speed versus time of the speed variation algorithm is shown in Figure 9. The simulation results of all of the algorithms over the same traffic intensity (peak hour) are tabulated in Table 1. In accordance with Table 1, using the speed variation II algorithm, both energy consumption and travel time were reduced significantly when compared to the constant-speed type. Hence, energy savings were achievable at a reduced travel time for peak-hour traffic patterns using “speed variation II” during peak travel hours.

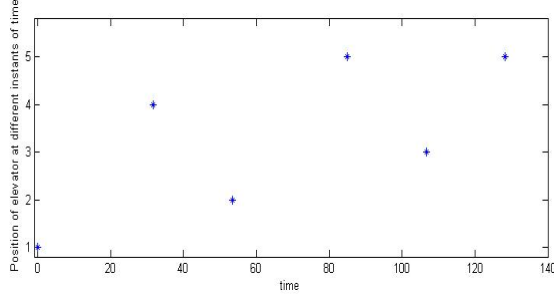


**Figure 6. Call Satisfying Pattern for 5 Floor Building**

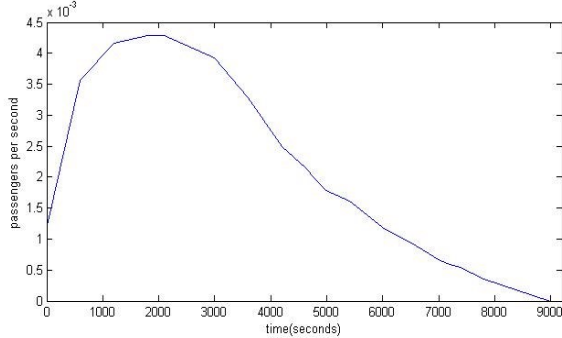


**Figure 7. Arrival Rate to the Hall of Other Floors**

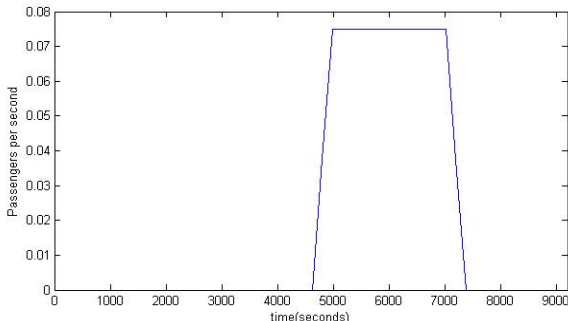


**Figure 8. Arrival Rate to the Hall of the Ground Floor**

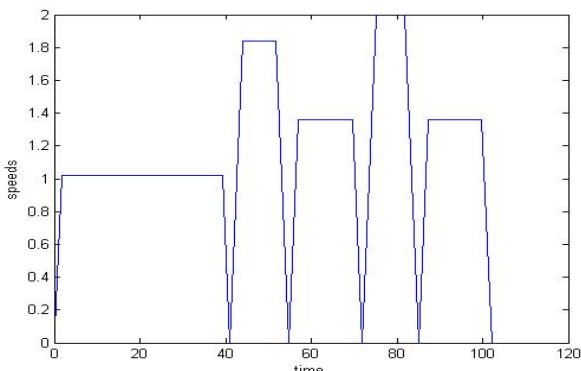


**Figure 9. Plot of Speed versus Time for the Speed Variation Algorithm**

**Table 1. Simulation Results for 10-floor Peak Hour Traffic**

	Constant speed	Speed variation I	Speed variation II
Consumption (KJ)	$3.45 \times 10^3$	$3.65 \times 10^3$	$3.27 \times 10^3$
Losses (KJ)	388.83	360.98	394.22
Regeneration (KJ)	$-2.88 \times 10^3$	$-2.92 \times 10^3$	$-2.81 \times 10^3$
Equivalent energy (kJ)	570.1	732.1	465
Total travel time (s)	$4.45 \times 10^3$	$4.21 \times 10^3$	$4.39 \times 10^3$
Efficiency (%)	88.72	90.10	87.96

**Case 2:** Consider an elevator with a maximum load of 400 kg, running in a 10-level building with a non-peak-hour traffic pattern. The three algorithms were simulated and the results tabulated for analysis. The pattern in which the calls were satisfied was very similar to that shown in Figure 7. All three algorithms were simulated using non-peak hours of traffic intensity. This traffic pattern was also used by Barney [16]. The resulting speed-versus-time plot of the speed variation II algorithm was also very similar to that shown in Figure 8. The simulation results of all of the algorithms over the same traffic intensity (non-peak hour) are tabulated in Table 2.

**Table 2. Simulation Results for 10-floor Non-peak-hour Traffic**

	Constant speed	Speed variation I	Speed variation II
Consumption (KJ)	$4.19 \times 10^3$	$3.96 \times 10^3$	$3.68 \times 10^3$
Losses (KJ)	400.62	337.83	365.00
Regeneration (KJ)	$-3.21 \times 10^3$	$-3.79 \times 10^3$	$-3.17 \times 10^3$
Equivalent energy (kJ)	$0.99 \times 10^3$	$0.18 \times 10^3$	$0.50 \times 10^3$
Total travel time (s)	$5.27 \times 10^3$	$4.88 \times 10^3$	$4.9761 \times 10^3$
Efficiency (%)	90.44	91.46	90.04

For the speed variation II algorithm, both energy consumption and travel time were significantly reduced when compared to the constant-speed type. Hence, energy savings were achievable at a reduced travel time for a non-peak-hour traffic pattern using “speed variation II.”

**Case 3:** Consider an additional case of an elevator with a maximum load of 400g, running in a 20-level building, using a non-peak-hour traffic pattern. The three algorithms were simulated and the results tabulated for analysis. The pattern in which the calls were satisfied was very similar to

that shown in Figure 6. All three algorithms were simulated using non-peak hours of traffic intensity, as used by Barney [16]. The simulation results of all of the algorithms over the same traffic intensity (non-peak hour) are tabulated in Table 3.

**Table 3. Simulation Results for 20-floor Non-peak-hour Traffic**

	Constant speed	Acceleration I	Acceleration II	Speed variation II
Consumption (kJ)	$3.44 \times 10^3$	$3.39 \times 10^3$	$3.31 \times 10^3$	$3.27 \times 10^3$
Losses (kJ)	388.82	388.58	401.60	394.22
Regeneration (kJ)	$-2.88 \times 10^3$	$-2.84 \times 10^3$	$-2.66 \times 10^3$	$-2.81 \times 10^3$
Equivalent energy (kJ)	570.1	545.5	654.5	465
Total travel time (s)	$4.45 \times 10^3$	$4.41 \times 10^3$	$4.35 \times 10^3$	$4.39 \times 10^3$
Efficiency (%)	88.716	88.52	87.88	87.96

From Table 3, it is clear that the speed variation II algorithm consumed less energy among the three for a fixed traffic pattern, irrespective of the number of floors in the building. Thus, from the tabulated analyses, it can be seen that the speed variation II algorithm produced significant energy savings in both peak and non-peak hours of traffic intensity. Additionally, the travel time of the elevator was reduced, thereby enhancing its overall performance. The authors further tested the algorithm by adding small variations in acceleration. From the simulation results for peak and non-peak hours of traffic intensity, the percentage of energy savings and travel time reduction of both the speed variation I and speed variation II algorithms with respect to the constant-speed case is shown in Table 4 [17].

**Table 4. Energy Savings and Travel Time of a 10-floor Building**

	Non-Peak hour traffic	Peak hour traffic		
	Energy saving	Travel time reduction	Energy saving	Travel time reduction
Speed variation I	5.63%	7.47%	-	5.438%
Speed variation II	12.35%	5.49%	5.06%	1.32%

## Search for a Near-optimal Algorithm

It is clear that, apart from varying the speed based on load carried by the elevator, acceleration should be varied to produce further energy savings. And, different cases of acceleration variation were tested in order to obtain the optimal value that would produce effective energy savings at a reduced travel time. The algorithm was subjected to minor variations as follows, where two types of acceleration were considered.

- 1) Acceleration variation—test cases involving different values of acceleration for upward and downward movement:
  - Acceleration variation I—downward movement given lesser values than upward movement
  - Acceleration variation II—upward movement given lesser values than downward movement
- 2) Speed variation II—the modified version of the algorithm consisting of the same values of acceleration for upward and downward movement.

As peak-hour traffic patterns tend to set the lower bound on energy savings, all of the algorithms were simulated under peak-hour traffic conditions with the same traffic pattern. Results are summarized in Table 5.

**Table 5. Optimal Search Results for 10-floor Peak-hour Traffic**

	Constant speed	Speed variation I	Speed variation II
Consumption (kJ)	$6.01 \times 10^3$	$5.99 \times 10^3$	$5.27 \times 10^3$
Losses (kJ)	552.17	418.91	405.86
Regeneration (kJ)	$-4.73 \times 10^3$	$-4.84 \times 10^3$	$-4.71 \times 10^3$
Equivalent energy (kJ)	$1.28 \times 10^3$	$1.14 \times 10^3$	$0.56 \times 10^3$
Total travel time (s)	$7.29 \times 10^3$	$5.86 \times 10^3$	$5.96 \times 10^3$
Efficiency (%)	90.78	93.00	91.90

The amount of energy savings and travel time reduction from the simulation are shown in Table 6. As per the tabulated results previously presented, though acceleration I and II produced energy savings at a reduced travel time, speed variation II still tended to be more efficient in terms of energy savings and travel time reduction. Hence, the speed variation II algorithm was determined to be optimal for obtaining the desired results.

**Table 6. Efficiency Calculation for 10-floor Peak-hour Traffic**

	Energy saving	Travel time reduction
Acceleration I	1.75%	0.9%
Acceleration II	3.8%	2.25%
Speed variation I	-	5.44%
Speed variation II	5.06%	1.32%

Thus by varying the speed of elevator based on load, and acceleration based on the number of levels moved, provided:

- 1) significant energy savings for varied traffic intensity;
- 2) reduction in the travel time for varied traffic intensity; and,
- 3) energy savings and travel time reduction varied according to peak and non-peak hours of traffic.

## Conclusion

Demand for energy efficient elevators is increasing worldwide [18]. In this paper, the authors presented an algorithm aimed towards energy conservation in elevators by manipulating the speed and acceleration of the system based on certain factors. Additionally, due to optimum variation in speed, the algorithm produced a significant reduction in travel time, thereby resulting in enhanced performance with minimal energy utilization. The algorithm was tested under various traffic conditions and the simulation results compared with constant-speed elevators. Results showed a significant reduction in energy consumption (between 5% and 12%) and a reduction in travel time (between 1% and 5%) under the variable-speed algorithm. Another way of optimizing the elevator operation was by implementing all three algorithms and by choosing the one based on the need of the hour. This may lead to additional energy savings and enhanced performance as well.

In future, the idea can be further appended with inclusion of artificial intelligence (AI), fuzzy logic, or neural network into the control algorithm of the system. This would allow the system to adapt to multiple factors in a more refined manner. For example, the prioritization of movement between floors based on load and number of calls obtained.

## References

- [1] National Building museum. (2011, Fall). [http://adultnumeracy.terc.edu/TIAN\\_statestandardsAZ.htm](http://adultnumeracy.terc.edu/TIAN_statestandardsAZ.htm)

- [2] Almeida, A. T., Patrão, C., Fong, J., Araújo, R., & Nunes, U. (2010). Energy Efficient Elevators and Escalators. *ISR -University of Coimbra (Portugal)*.
- [3] Tominaga, S., Suga, I., Araki, H., Ikejima, H., & Kusuma, M. K. (2002). Development of Energy-saving Elevator using Regenerated Power Storage System", *IEEE Power Conversion Conference*, 2.
- [4] Yao, Z., Wan, J., Li, B., Qian, J., & Wang, S. (2011). Research and Application of Elevator Energy Saving Devices with Super Capacitor to Store Energy. *Advances in Automation and Robotics*, 1, 429-436.
- [5] Liu, Y. Q., Wang, X. H., & Tian, L. F. (2011). Research of Elevator Energy Feedback System based on Converters using SVPWM. *Proceedings of IEEE International Conference on Transportation, Mechanical, and Electrical Engineering*, 998-1002.
- [6] Hakala, H., Siikonen, M. L., Tyni, T., & Ylinen J. (2012, spring). Energy Efficient Elevators for tall buildings. Retrieved from [http://www.kone.com/countries/SiteCollectionDocuments/MP/2001\\_energy\\_efficient\\_elevators\\_tall.pdf](http://www.kone.com/countries/SiteCollectionDocuments/MP/2001_energy_efficient_elevators_tall.pdf).
- [7] Zhang, T., Mabu, S., Yu, L., Zhou, J., Zhang, X., & Hirasawa, K. (2009). Energy saving Elevator Supervisory Control System with Idle Cage Assignment using Genetic Network Programming. *ICROS-SICE International Joint Conference*.
- [8] Brand, M., & Nikovski, D. (2004). Optimal Parking in Group Elevator Control. *Mitsubishi Electric Research Laboratories*. Retrieved from <http://merl.com>.
- [9] Dagdelen,U., Bagis, A., & Karaboga, D. (2005). An Efficient Control Method for Elevator Group Control System. *Springer-Verlag*.
- [10] Jing-long, Z., Jie, Z., & Jun-fang, Li. (2010). Energy saving Scheduling Strategy for Elevator Group Control System Based on Ant Colony Optimization. *IEEE*.
- [11] Hu, Z., Liu, Y. Su, & Huo, Q. J. (2010). A Multi-Objective Genetic Algorithm Designed for Energy saving of the Elevator System with Complete Information. *IEEE International Energy Conference*.
- [12] Reliance - Induction Motors B-7097-2. (2012, Spring). Retrieved from [http://www.reliance.com/prodserv/motgen/b7097\\_2.htm](http://www.reliance.com/prodserv/motgen/b7097_2.htm)
- [13] Barney, G. (2012, spring). Towards Low Carbon Lifts. Gina Barney Associates. Retrieved from [www.liftconsulting.org](http://www.liftconsulting.org)
- [14] Matlab/Simulink in Drives and Power Electronics. (2011, Fall). (Retrieved in June). Palestine Polytechnic University. Retrieved from [http://www.lgep.supelec.fr/uploads/images/lgep/Mocosem/Cocodi/Pages\\_perso/gremy/Hebron2009/Practice2\\_Intro\\_Simulink.pdf](http://www.lgep.supelec.fr/uploads/images/lgep/Mocosem/Cocodi/Pages_perso/gremy/Hebron2009/Practice2_Intro_Simulink.pdf)

- 
- [15] Cortés, P., Larrañeta, J., & Onieva, L. (2004). Genetic algorithm for controllers in elevator groups: analysis and simulation during lunch-peak traffic. *Applied Soft Computing*, 4(2), 159-174.
  - [16] Barney, G. C. (2003). *Elevator Traffic Handbook: Theory and Practice*. Spon Press.
  - [17] Hasan, M. Z., Fink, R., Raj, M., & Baskaran M. (2012). Assessment and Improvement of Intelligent Controllers for Elevator Energy Efficiency. *IEEE International Conference on Electro/Information Technology*.
  - [18] Kiker, P. (2015). *Study Finds Global Opportunities for Greater Elevator Efficiency*. American Council for Energy Efficient Economy (ACEEE).

## Biographies

**MUHAMMAD ZAFRUL HASAN** received his B.Sc. in Electrical and Electronic Engineering from Bangladesh University of Engineering and Technology. He received the Master of Electronic Engineering degree from Eindhoven University of Technology (the Netherlands) under Philips postgraduate scholarship program. He subsequently held several faculty positions in an engineering college and in a university in Malaysia. He obtained his Ph.D. in Computer Engineering from the New Jersey Institute of Technology. He was awarded the NJIT Hashimoto Fellowship. He taught at Texas A&M University in College Station. He is currently an assistant professor in the School of Engineering at Texas A&M International University. His research interests include the design, implementation, and testing of embedded systems for energy conservation, performance evaluation of computer architectures, and behavioral synthesis and testing of digital systems. Dr. Hasan may be reached at [muhammad.hasan@tamu.edu](mailto:muhammad.hasan@tamu.edu)

**RAINER J. FINK** received his Ph.D. degree in Bio-medical Engineering in 1995, M.S. in 1992, and B.S. in 1988, all from Texas A&M University. He is currently an associate professor in the Department of Engineering Technology and Industrial Distribution, Texas A&M University. He holds several patents in bio-medical devices. His semiconductor test educational efforts have been continuously supported by Texas Instruments (Dallas, TX), Teradyne Inc. (Boston, MA), National Instruments (Austin, TX), National Semiconductor (Santa Clara, CA), and IBM (Austin, TX). His research interests include analog electronics, semiconductor testing, medical device design and testing, product development, and entrepreneurship. Dr. Fink may be reached at [fink@tamu.edu](mailto:fink@tamu.edu)

**MUTHUVEL RAJ SUYAMBU** received his M.S. degree in Electrical and Computer Engineering in May, 2012,

from Texas A&M University. He is currently working with Asea Brown Boveri (ABB) in North Carolina. Mr. Suyambu, may be reached at [raj.muthuvel@gmail.com](mailto:raj.muthuvel@gmail.com)

**MANOJ KUMAR BASKARAN** received his M.S. degree in Electrical and Computer Engineering in December, 2012, from Texas A&M University. He is currently working with Intel Corporation in Oregon. Mr. Baskaran may be reached at [manojkumar.baskaran@intel.com](mailto:manojkumar.baskaran@intel.com)

# DEVELOPMENT OF A MODIFIED EXPERIMENTAL SETUP TO EVALUATE THE EFFECTS OF SHRINKAGE-REDUCING ADMIXTURE

---

Rajarajan Subramanian, Pennsylvania State University at Harrisburg; Mang Tia, University of Florida;  
Michael J. Bergin, Florida Department of Transportation; Charles A. Ishee, Applied Research Associates, Inc.

## Abstract

In this study, the authors developed a cutting-edge tool for evaluating the potential shrinkage-induced stresses in concrete and its potential for shrinkage cracking in service. The effects of a shrinkage-reducing admixture on the shrinkage-induced stresses of 30 different concrete mixes were evaluated by using a constrained long specimen (CLS) test. The existing apparatus was refined by the following modifications: 1) replacing the Whittemore gauge with a high-sensitivity linear variable differential transformer (LVDT); 2) replacing the proving ring with a load cell; 3) introducing an automation system to record strains and stresses through a data acquisition system; and, 4) replacing the existing single AC voltage function generator with eleven LVDT signal conditioners.

Using the CLS test method enabled the creep component to be properly considered, and a realistic determination of the expected induced shrinkage stresses in concrete in service. Also, the results of the CLS tests on 30 concrete mixes showed the possible benefits of using a shrinkage-reducing admixture and fly ash in reducing the potential shrinkage cracking of concrete in service. The results of the CLS tests on 30 concrete mixes showed the possible benefits of using a laboratory setup that measures the early shrinkage in concrete reasonably well.

## Introduction

Shrinkage cracking of concrete bridge decks is a critical problem in Florida and in many other states throughout the U.S. Many concrete bridge decks have been observed to develop plastic shrinkage cracks soon after construction. These cracks could shorten the service life of the bridge decks and increase the costs for maintenance and repairs. In recent years, the use of high-performance concretes in bridge decks might have aggravated this problem further. Results of several research studies [1-3] have indicated that high-performance concretes, which are usually produced by using high cement content and additives such as silica fume, have higher free shrinkage and a higher tendency for shrinkage cracking.

One possible solution to this problem is to modify concrete mix designs such that concretes would be less susceptible to shrinkage cracking, while maintaining their other high-performance properties. Another possible solution would be to modify the mix design by adding a shrinkage-reducing admixture and/or fly ash to reduce the possible drying shrinkage of the concrete and, thus, reduce the potential shrinkage-induced stresses in the concrete. The tendency of a given concrete to shrinkage cracking is not just a simple function of its free shrinkage but is also affected by factors such as the constraints on the concrete, rate of strength gain, temperature, and the elastic modulus of the concrete. The creep of the concrete during its plastic stage can also relieve some of the induced stresses due to shrinkage. All of these pertinent factors need to be fully considered in evaluating a concrete mix for its resistance to shrinkage cracking.

An effective test procedure and analysis method for evaluating the potential shrinkage-induced stresses in concrete and its potential for shrinkage cracking in service was developed by Tia et al. [4] at the University of Florida in 1998. The developed procedure was known as the modified constrained long specimen (CLS) test. Some additional improvements in the instrumentation for this test procedure were made subsequently. This developed test procedure and method of analysis was used to evaluate the effects of a shrinkage-reducing admixture on the potential shrinkage-induced stresses of different concrete mixes and their potential for shrinkage cracking in service.

## Literature Review

A literature review on methods for evaluating concrete for resistance to shrinkage cracking was conducted before the modified constrained long specimen (CLS) test apparatus was developed. Three existing test methods of particular interest are summarized here.

### Constrained Ring Specimen Method

The first test method of interest was a restrained shrinkage cracking test using a constrained ring specimen [1], [5].

---

The adopted ring test provided a high and nearly constant restraint, enabling tests on cement paste, mortar, and concrete.

The test specimen was made by casting a layer of concrete 1.4" thick and 5.5" high around a steel ring, which had an outer diameter of 8". A PVC tube was used as an outer mold for casting the concrete around the steel ring. To fabricate a specimen, the inner steel ring would be placed concentrically on a wooden base and the fresh concrete would be placed between the PVC mold and the steel ring. After the concrete had been cured for six hours at 20°C and 100% relative humidity (RH), the PVC mold would be removed. The top surface of the concrete would be sealed off using a silicon rubber so that drying would be allowed only from the outer circumferential surface. The specimen would then be exposed to a specified drying environment, and the cracks that might develop would be observed and used as indicators of shrinkage cracking potential of the concrete. Crack widths were measured by means of a special microscope.

### Constrained Plate Specimen Method

The second test method was another restrained shrinkage cracking test using rectangular plate specimens [6]. Specimens were made by casting concrete into forms to produce 24" x 36" rectangular panels with a thickness of 3/4". The forms were made of Plexiglas to prevent absorption of moisture from the concrete mix. An expended metal lathe was attached to the inside perimeter to provide edge restraint to the concrete. This test condition was intended to simulate the casting of a slab over a plastic vapor barrier. Temperature, relative humidity, and wind speed were controlled to simulate hot weather concreting conditions. Fans were placed next to the specimens to provide a controlled wind velocity of 7-8 mph. The length and average width of the cracks that might develop during the test were recorded and expressed as total crack area square inches.

### Constrained Long Specimen Method

The third test method studied was a restrained shrinkage test using a long specimen with flared ends [2]. The concrete specimen had a cross section of 1.6" x 1.6" and was 39" long. It increased gradually in width at the two ends, which fit into two end grips. One grip was fixed and the other was free to move and could be monitored by a dial gauge. To fabricate a test specimen, the fresh concrete would be cast directly into the apparatus. The two sides of the mold could be removed immediately after setting of the concrete. The concrete specimen could then be exposed to a specified drying condition and tested.

The apparatus could be used to measure the free shrinkage of the concrete as well as the load experienced by the specimen in a restrained condition. Free shrinkage could be measured by the dial gauge as the concrete was allowed to contract freely. To measure the load experienced by the specimen in a complete restrained condition, the movable grip could be returned to its original position by a screw assembly connected to the grip through a load cell, which could measure the load exerted on the concrete. Synthetic resin-coated rails were placed on both sides of the grip to reduce eccentricity and friction. To reduce friction, the mold was resin-coated and a gap of 0.08" was provided between the movable grip and the bar supporting the concrete specimen. Dial gauges could be mounted on both sides of the movable grip to monitor the extent of the eccentricity.

## Development of the Modified Constrained Long Specimen Method

The apparatuses for the three existing methods for evaluating shrinkage cracking resistance, as presented in the previous sections, were constructed and evaluated with regards to their effectiveness in determining shrinkage cracking potential of concrete in service. It was determined that the long constrained specimen method was one of the most promising approaches with regards to the ability to measure a concrete's potential shrinkage-induced stresses, which could be used to determine the concrete's potential for shrinkage cracking in service.

However, operational problems were encountered with the original design. Changes in design and test procedures were made in order to obtain better reliability and precision of the method. A detailed description of this investigation can be found in the report by Tia et al. [4]. Additional improvements in the instrumentation for this test method have also been made since the completion of that report. It is interesting to note that similar test setups have also been developed independently by other researchers for the same purpose. These researchers include Pigeon et al. [7], who used a specimen size of 2" x 2" x 20", and Altoubat and Lange [8], who used a specimen size of 3" x 3" x 36".

## The Modified Constrained Long Specimen Test Method

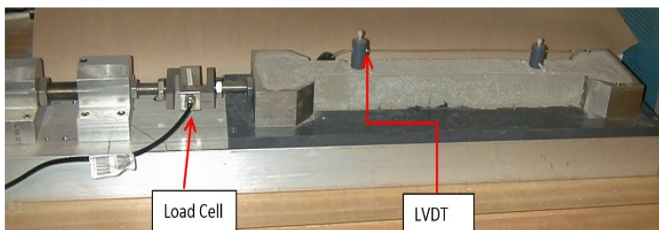
### Basic Test Setup

The existing apparatus was refined by the following modifications: 1) replacing the Whittemore gauge, which was used to measure the deformation of the specimen by a high-

sensitivity LVDT; 2) replacing the proving ring, which was used to measure the induced force in the constrained long specimen by a load cell; 3) introducing automation system recording strains and stresses through a data acquisition system, an Agilent 34970A unit (by Agilent Technologies) with a HP 34901A (20-channel armature multiplexer) plug-in module; and, 4) replacing the existing single AC voltage function generator with eleven LVDT signal conditioners (Model LPC-2100 by Micro Sensors) to overcome a lack of needed excitation voltage of 3.0 Vrms at 2.4 kHz. The LVDTs (CD375-025 by Macro Sensors) provided the needed excitation voltage of 3.0 Vrms at 2.4 kHz to demodulate the AC output signal from the LVDT into a DC signal, and to amplify the DC signal before outputting it to the data acquisition system.

Another observed problem with the constrained long specimen apparatus was that the long concrete specimen appeared to be sticking to the steel plate below it. Wax paper was placed over the steel base plate in an effort to reduce the friction between the concrete specimen and the base plate. However, the wax paper got soaked by the wet concrete, which exacerbated the problem; thus, the idea was abandoned. Finally, Teflon sheets were introduced to take care of this sticking problem [9]. Figure 1 shows a picture of the test apparatus with a test specimen. Basically, this test involved casting the concrete to be tested in a test apparatus, which was constrained from movement, placing the test specimen under a specified exposure condition and measuring the induced force in the specimen during the test. Since the specimen could not be perfectly constrained from movement, due to the possible movement of the load cell and other components of the apparatus, the movement of the specimen was also monitored during the test.

**Figure 1. Picture of a Constrained Long Specimen Apparatus**



**with a Test Specimen Showing the Load Cell and LVDT**

The specimen was 21.25" long and 1.5" thick. The specimen was 1.5" in the middle and 3.25" wide at the two enlarged ends, which were held by two end grips. One of the end grips was fixed, while the other end grip was connected to a load cell, which measured the induced force in the specimen during the test.

### LVDT for Measurement of Strain

Two gauge studs were installed in the mid-portion of the test specimen at a distance of 10" from each other. An AC LVDT was used to measure the relative movement between these two studs, which was used to determine the strain in the test specimen during the test. The LVDT was held by a holder that was attached to one of the two gauge studs. The end of the rod that was connected to the LVDT core was held by another holder, which was attached to the other gauge stud. The LVDT used was a CD375-025 by Macro Sensors. It had a stroke of  $\pm 0.125"$  and a weight of 2.8 grams (0.1 oz.). Each AC LVDT was connected to a separate LVDT signal conditioner (Model LPC-2100 by Micro Sensors). This LVDT signal conditioner provided the needed excitation voltage of 3.0 Vrms at 2.4 kHz. It also demodulated the AC output signal from the AC LVDT into a DC signal and amplified the DC signal before outputting it to the data acquisition system. Each LVDT signal conditioner was calibrated such that a full stroke of the LVDT of  $\pm 0.125"$  produced an output of  $\pm 10.0$  VDC from the signal conditioner. The displacement between the two gauge points could be computed from the voltage output as:

$$\text{displacement (in inches)} = \text{output (in volts)} \times 0.0125$$

The strain was then computed from the displacement as  $\text{strain} = \text{displacement} / (\text{gauge length})$ , as given by Equation (1):

$$\begin{aligned} &= \text{displacement} / (10 \text{ inches}) \\ &= \text{output (in volts)} \times 0.00125 \end{aligned} \quad (1)$$

### Load Cell for Measurement of Stress

A load cell was used to measure the force experienced by the concrete specimen during a test. The load cell used was a LCCB-1K by Omega. Figure 2 shows a picture of the load cell. It was a tension and compression "S" type load cell with a maximum capacity of 1000 pounds. The rated output was 3mV/V for the full load of 1000 pounds. A DC voltage source was used to supply an excitation voltage of 10 V. With the 10 V excitation input, the load cell would deliver an output of 30 mV/1000 lbs., or 0.03 mV/lb. The axial force in the concrete sample was computed from the DC output voltage from the load cell, as given by Equation (2):

$$\text{force (in lb.)} = \text{output (in mV)} \times 33.33 \quad (2)$$

The stress in the concrete sample was then calculated from Equations (2) and (3):

$$\begin{aligned} \text{stress} &= \text{force} / (\text{cross-sectional area of concrete}) \\ &= \text{force} / (2.25 \text{ in}^2) \end{aligned} \quad (3)$$



**Figure 2. Picture of the Load cell and LVDT with holder in the CLS test set-up**

## Data Acquisition System (DAS)

The outputs from the LVDT and the load cell were connected to an automatic DAS, which was an Agilent 34970A unit (by Agilent Technologies) with a HP 34901A (20-channel armature multiplexer) plug-in module. The data acquisition unit can be set up to take readings at specified time intervals and for a specified length of time. The HP 34901A multiplexer module can read up to 20 channels of AC or DC voltages with a maximum capacity of 300 V, and has a switching speed of up to 60 channels per second. It also has a built-in thermocouple reference junction for use in temperature measurement by means of thermocouples.

Thus, the Agilent 34970A data acquisition unit with one HP 34901A multiplexer module was adequate for the job of recording load and displacement readings from 10 testing apparatuses. The Agilent 34970A unit can take up to three plug-in modules. Thus, if needed, it can be expanded to take up to 60 channels of output, enough to accommodate 30 testing apparatuses. The stored data was downloaded to a personal computer via an RS232 cable connection. The data files were in CSV format and could be easily read by spreadsheet software such as Excel.

## Preparation of the Constrained Long Specimen and Testing Procedure

The concrete mix to be evaluated was placed in the constrained long specimen apparatus for testing. Figure 3 shows a picture of the mold for the test specimen before a test concrete was placed. Before the fresh concrete was placed into the mold, a thin layer of motor oil was applied on the surface of the plate support and the two sides of the mold to reduce friction. The two gauge studs, which were held in position by two aluminum brackets, were installed at a distance of 10" from each other. The fresh concrete was then placed into the mold and finished with a small hand trowel. After the concrete had sufficiently set, the two side pieces of the mold were removed. The two aluminum brackets, which kept the gauge studs in place, were also removed. The LVDT was installed on one of the studs and the rod holding

the core of the LVDT was connected to the other stud. The position of the rod was adjusted such that the core was placed at the center of the LVDT and the output from the LVDT was zeroed initially. The position of the end grip that was connected to the load cell was adjusted so that the output from the load cell was zero initially. The data acquisition system was then activated to record readings from the load cell and the LVDT from each CLS test apparatus at specified time intervals.



**Figure 3. Picture of the CLS Mold before the Placement of the Concrete**

## Method of Analysis

The analysis consisted of several equations involving three different deformation components in the concrete specimen. The Constrained Long Specimen under tensile force induced by shrinkage of the concrete specimen, exhibiting the change of length of the specimen being measured by the proven ring ( $\delta_{PR}$ ). The first component was the shortening, due to shrinkage ( $\delta_{sh}$ ). The second component was the elastic lengthening, due to induced tensile stress ( $\delta_E$ ). The third one was the creep, due to the induced stresses ( $\delta_{CR}$ ). These three components were related to the total movement of the specimen, as defined by Equation (4):

$$\delta_{PR} = \delta_{CL} = \delta_{sh} - \delta_E - \delta_{CR} \quad (4)$$

In terms of strains ( $\epsilon$ 's), the relationship can be written as shown in Equation (5):

$$\epsilon_{CL} = \epsilon_{sh} - \epsilon_E - \epsilon_{CR} \quad (5)$$

The three different components of strain in the concrete test specimen can be explained further. The first component was the free shrinkage strain, due to drying shrinkage ( $\epsilon_{sh}$ ). The second component was the elastic tensile strain, due to induced tensile stress ( $\epsilon_E$ ). The third component was the tensile creep strain, due to the induced tensile stress ( $\epsilon_{CR}$ ). These three components were related to the total movement of the specimen ( $\epsilon_{CL}$ ), as shown in Equation (5). The elastic strain ( $\epsilon_E$ ) was calculated from the induced stress ( $\sigma_{CL}$ ) and the elastic modulus of the concrete ( $E$ ), as shown in Equation (6):

$$\varepsilon_E = \sigma_{CL}/E \quad (6)$$

The elastic modulus of the concrete ( $E$ ) was measured, in accordance with ASTM Standard Test Method C469, from specimens made of the same concrete and placed under the same conditions. The shrinkage strain ( $\varepsilon_{sh}$ ) was assumed to be equal to the free shrinkage strain measured by the length comparator, in accordance with ASTM Standard Method C157. The creep strain ( $\varepsilon_{CR}$ ) was calculated from the other strains, according to Equation (4), as shown in Equation (7):

$$\varepsilon_{CR} = \varepsilon_{sh} - \varepsilon_E - \varepsilon_{CL} \quad (7)$$

If a concrete member were fully constrained from movement, the induced stress due to drying shrinkage ( $\sigma_{FC}$ ) could be expressed using Equation (8):

$$\sigma_{FC} = (\varepsilon_{sh} - \varepsilon_{CR}) E \quad (8)$$

Substituting Equation (7) into Equation (8),  $\sigma_{FC}$  can be expressed as in Equation (9):

$$\sigma_{FC} = (\varepsilon_E + \varepsilon_{CL}) E = \sigma_{CL} + \varepsilon_{CL} E \quad (9)$$

When the expected shrinkage-induced stress ( $\sigma_{FC}$ ), as computed by Equation (9), exceeds the expected tensile strength of the concrete ( $\sigma_t$ ) at any particular time, the concrete will be likely to crack at that time.

## Concrete Mixtures Evaluated

Concrete mixtures were prepared in the laboratory and tested for their resistance to shrinkage cracking in order to evaluate: 1) the effectiveness of the shrinkage test apparatus used; 2) the shrinkage characteristics of typical concretes used in bridge deck applications in Florida; and, 3) the effects of adding a shrinkage-reducing admixture. A typical mix design for a Florida Class IV concrete with a total cementitious materials content of 700 lbs. per cubic yard (lb./yd<sup>3</sup>) of concrete was selected for use. Various percentages of fly ash and ground blast-furnace slag were incorporated into this basic mix design to form six different mix designs to be evaluated in the laboratory testing program. For each of the concrete mixtures evaluated, a pair of concrete mixes was prepared at the same time—one with the addition of a shrinkage-reducing admixture (SRA) and one without. Since various different test apparatuses were used during different stages of this study, several replicate batches of the same mixes were used, resulting in a total of 15 pairs of concrete mixes tested in this study.

Tables 1 through 15 show the mix proportions for the 15 pairs of concrete mixtures evaluated in this study. The con-

crete mixes were numbered according to the order by which they were prepared and tested. Mixes 1 and 13 had a cement content of 350 lb./yd<sup>3</sup> and a slag content of 350 lb./yd<sup>3</sup> of concrete. Mixes 2 and 3 had a cement content of 210 lb./yd<sup>3</sup> and a slag content of 490 lb./yd<sup>3</sup>. Mixes 4, 7, 8, and 11 had a cement content of 560 lb./yd<sup>3</sup> and a fly ash content of 140 lb./yd<sup>3</sup>. Mixes 5, 9, 10, and 14 had a cement content of 455 lb./yd<sup>3</sup> and a fly ash content of 245 lb./yd<sup>3</sup>. Mixes 6 and 12 had a cement content of 210 lb./yd<sup>3</sup>, a fly ash content of 140 lb./yd<sup>3</sup>, and a slag content of 350 lb./yd<sup>3</sup>. Mix 15 had a cement content of 700 lb./yd<sup>3</sup> and no mineral admixture. The slump of the fresh concrete was targeted to be 8 ± 1.5".

**Table 1. Mix Proportions for Mix 1**

Mix – 1				
Ingredients	Weight (lbs./yd <sup>3</sup> )			
	Standard		Eclipse	
	Design Batch	Actual Batch	Design Batch	Actual Batch
Cement	350	350	350	350
Fly ash	-	-	-	-
Slag	350	350	350	350
Water	287	234	274	219
F.A.	1257	1252	1257	1252
C.A.	1513	1572	1513	1572
Air Entrainer	0.0625	0.0625	0.0625	0.0625
Admixture (WRDA 64)	0.875	0.875	0.875	0.875
Admixture (Adva 120)	1.313	1.313	1.313	1.313
Admixture (Eclipse)	-	-	12	12
Slump (in inches)	6.25	6.25	7.25	7.25
Air (%)	3.75	3.75	3	3
Workability	Good	Good	Good	Good
W/C Ratio	0.41	0.33	0.41	0.33
Unit Weight (pcf)	139.1	139.2	139.1	139.1

**Table 2. Mix Proportions for Mix 2**

Ingredients	Mix – 2			
	Weight (lbs./yd <sup>3</sup> )			
	Standard		Eclipse	
Design Batch	Actual Batch	Design Batch	Actual Batch	
Cement	210	210	210	210
Fly ash	-	-	-	-
Slag	490	490	490	490
Water	224	176	211	165
F.A.	1336	1331	1336	1331
C.A.	1583	1633	1583	1633
Air Entrainer	0.0625	0.0625	0.0625	0.0625
Admixture (WRDA 64)	0.875	0.875	0.875	0.875
Admixture (Adva 120)	2.063	2.063	2.063	2.063
Admixture (Eclipse)			12	12
Slump (in inches)	8	8	9.25	9.25
Air (%)	2.75	2.75	1.75	1.75
Workability	Sticky	Sticky	Sticky	Sticky
W/C Ratio	0.32	0.25	0.32	0.25
Unit Weight (pcf)	142.3	142.2	142.3	142.3

**Table 4. Mix Proportions for Mix 4**

Ingredients	Mix – 4			
	Weight (lbs./yd <sup>3</sup> )			
	Standard		Eclipse	
Design Batch	Actual Batch	Design Batch	Actual Batch	
Cement	56	560	560	560
Fly ash	140	140	140	140
Slag	-	-	-	-
Water	287	244	275	232
F.A.	1250	1246	1250	1246
C.A.	1486	1533	1486	1533
Air Entrainer	0.0625	0.0625	0.0625	0.0625
Admixture (WRDA 64)	1.75	1.75	1.75	1.75
Admixture (Adva 120)	2.188	2.188	2.188	2.188
Admixture (Eclipse)			12	12
Slump (in inches)	7.5	7.5	9	9
Air (%)	3.25	3.25	2.5	2.5
Workability	Good	Good	Good	Good
W/C Ratio	0.41	0.35	0.39	0.33
Unit Weight (pcf)	137.9	137.9	137.4	137.4

**Table 3. Mix Proportions for Mix 3**

Ingredients	Mix – 3			
	Weight (lbs./yd <sup>3</sup> )			
	Standard		Eclipse	
Design Batch	Actual Batch	Design Batch	Actual Batch	
Cement	210	210	210	210
Fly ash	-	-	-	-
Slag	490	490	490	490
Water	287	213	274	200
F.A.	1253	1248	1253	1253
C.A.	1507	1586	1507	1507
Air Entrainer	0.0625	0.0625	0.0625	0.0625
Admixture (WRDA 64)	0.875	0.875	0.875	0.875
Admixture (Adva 120)	1.313	1.313	1.313	1.313
Admixture (Eclipse)			12	12
Slump (in inches)	9	9	8.5	8.5
Air (%)	3.5	3.5	2.5	2.5
Workability	Good	Good	Good	Good
W/C Ratio	0.41	0.30	0.39	0.29
Unit Weight (pcf)	138.8	138.8	138.3	135.5

**Table 5. Mix Proportions for Mix 5**

Ingredients	Mix – 5			
	Weight (lbs./yd <sup>3</sup> )			
	Standard		Eclipse	
Design Batch	Actual Batch	Design Batch	Actual Batch	
Cement	455	455	455	455
Fly ash	245	245	245	245
Slag	-	-	-	-
Water	287	228	275	216
F.A.	1217	1213	1217	1213
C.A.	1469	1533	1469	1533
Air Entrainer	0.0625	0.0625	0.0625	0.0625
Admixture (WRDA 64)	1.75	1.75	1.75	1.75
Admixture (Adva 120)	2.188	2.188	2.188	2.188
Admixture (Eclipse)			12	12
Slump (in inches)	9.25	9.25	8.75	8.75
Air (%)	3.25	3.25	3.25	3.25
Workability	Good	Good	Good	Good
W/C Ratio	0.41	0.33	0.41	0.33
Unit Weight (pcf)	136.0	136.1	136.0	136.1

**Table 6. Mix Proportions for Mix 6**

Ingredients	Mix – 6			
	Weight (lbs./yd <sup>3</sup> )			
	Standard		Eclipse	
Design Batch	Actual Batch	Design Batch	Actual Batch	
Cement	210	210	210	210
Fly ash	140	140	140	140
Slag	350	350	350	350
Water	289	246	275	232
F.A.	1240	1236	1240	1236
C.A.	1475	1522	1475	1522
Air Entrainer	0.0625	0.0625	0.0625	0.0625
Admixture (WRDA 64)	1.75	1.75	1.75	1.75
Admixture (Adva 120)	2.188	2.188	2.188	2.188
Admixture (Eclipse)			12	12
Slump (in inches)	9.25	9.25	9	9
Air (%)	1.75	1.75	2.75	2.75
Workability	Good	Good	Good	Good
W/C Ratio	0.41	0.35	0.41	0.35
Unit Weight (pcf)	137.2	137.2	137.1	137.1

**Table 8. Mix Proportions for Mix 8**

Ingredients	Mix – 8			
	Weight (lbs./yd <sup>3</sup> )			
	Standard		Eclipse	
Design Batch	Actual Batch	Design Batch	Actual Batch	
Cement	560	560	560	560
Fly ash	140	140	140	140
Slag	-	-	-	-
Water	224	264	212	252
F.A.	1453	1449	1455	1451
C.A.	1453	1417	1455	1419
Air Entrainer	0.0625	0.0625	0.0625	0.0625
Admixture (WRDA 64)	0.88	0.88	0.88	0.88
Admixture (Adva 120)	2.06	2.06	2.06	2.06
Admixture (Eclipse)			12	12
Slump (in inches)	2.5	2.5	2.25	2.25
Air (%)	4.5	4.5	3.75	3.75
Workability	Stiff	Stiff	Stiff	Stiff
W/C Ratio	0.32	0.38	0.32	0.38
Unit Weight (pcf)	141.9	141.9	142.0	142.0

**Table 7. Mix Proportions for Mix 7**

Ingredients	Mix – 7			
	Weight (lbs./yd <sup>3</sup> )			
	Standard		Eclipse	
Design Batch	Actual Batch	Design Batch	Actual Batch	
Cement	560	560	560	560
Fly ash	140	140	140	140
Slag	-	-	-	-
Water	254	235	242	223
F.A.	1334	1330	1257	1330
C.A.	1561	1554	1513	1554
Air Entrainer	0.0625	0.0625	0.0625	0.0625
Admixture (WRDA 64)	1.31	1.31	0.88	0.88
Admixture	1.31	1.31	1.31	1.31
Admixture (Eclipse)			12	12
Slump (in inches)	8	8	9	9
Air (%)	2.75	2.75	3.25	3.25
Workability	Good	Good	Good	Good
W/C Ratio	0.36	0.34	0.36	0.34
Unit Weight	142.6	141.4	137.9	141.4

**Table 9. Mix Proportions for Mix 9**

Ingredients	Mix – 9			
	Weight (lbs./yd <sup>3</sup> )			
	Standard		Eclipse	
Design Batch	Actual Batch	Design Batch	Actual Batch	
Cement	455	455	455	455
Fly ash	245	245	245	245
Slag	-	-	-	-
Water	287	324	275	312
F.A.	1351	1347	1351	1347
C.A.	1351	1318	1351	1318
Air Entrainer	0.0625	0.0625	0.0625	0.0625
Admixture (WRDA 64)	0.88	0.88	0.88	0.88
Admixture	1.31	1.31	1.31	1.31
Admixture (Eclipse)			12	12
Slump (in inches)	3.25	3.25	4.5	4.5
Air (%)	2.75	2.75	2.5	2.5
Workability	O.K	O.K	O.K	O.K
W/C Ratio	0.41	0.46	0.41	0.46
Unit Weight	136.6	136.6	136.6	136.6

**Table 10. Mix Proportions for Mix 10**

Ingredients	Mix – 10			
	Weight (lbs./yd <sup>3</sup> )			
	Standard		Eclipse	
Design Batch	Actual Batch	Design Batch	Actual Batch	
Cement	455	455	455	455
Fly ash	245	245	245	245
Slag	-	-	-	-
Water	252	289	240	278
F.A.	1265	1261	1265	1261
C.A.	1513	1480	1513	1480
Air Entrainer	0.0625	0.0625	0.0625	0.0625
Admixture (WRDA 64)	0.88	0.88	0.88	0.88
Admixture (Adva 120)	1.31	1.31	1.31	1.31
Admixture (Eclipse)			12	12
Slump (in inches)	3.25	3.25	4.5	4.5
Air (%)	2.75	2.75	2.5	2.5
Workability	O.K	O.K	O.K	O.K
W/C Ratio	0.36	0.41	0.36	0.41
Unit Weight (pcf)	138.2	138.2	138.1	138.2

**Table 12. Mix Proportions for Mix 12**

Ingredients	Mix – 12			
	Weight (lbs./yd <sup>3</sup> )			
	Standard		Eclipse	
Design Batch	Actual Batch	Design Batch	Actual Batch	
Cement	210	210	210	210
Fly ash	140	140	140	140
Slag	350	350	350	350
Water	224	194	212	183
F.A.	1516	1511	1516	1511
C.A.	1376	1410	1376	1410
Air Entrainer	0.0625	0.0625	0.0625	0.0625
Admixture (WRDA 64)	1.75	1.75	1.75	1.75
Admixture (Adva 120)	2.188	2.188	2.188	2.188
Admixture (Eclipse)			12	12
Slump (in inches)	3	3	6.5	6.5
Air (%)	3.25	3.25	3	3
Workability	Stiff	Stiff	Sticky	Sticky
W/C Ratio	0.32	0.28	0.32	0.28
Unit Weight (pcf)	141.3	141.3	141.3	141.3

**Table 11. Mix Proportions for Mix 11**

Ingredients	Mix – 11			
	Weight (lbs./yd <sup>3</sup> )			
	Standard		Eclipse	
Design Batch	Actual Batch	Design Batch	Actual Batch	
Cement	560	560	560	560
Fly ash	140	140	140	140
Slag				
Water	287	321	275	308
F.A.	1250	1246	1250	1246
C.A.	1486	1456	1486	1456
Air Entrainer	0.0625	0.0625	0.0625	0.0625
Admixture (WRDA 64)	1.75	1.75	1.75	1.75
Admixture (Adva 120)	2.188	2.188	2.188	2.188
Admixture (Eclipse)			12	12
Slump (in inches)	8.5	8.5	9	9
Air (%)	3	3	2.75	2.75
Workability	Good	Good	Good	Good
W/C Ratio	0.41	0.46	0.41	0.46
Unit Weight (pcf)	137.9	137.9	137.9	137.9

**Table 13. Mix Proportions for Mix 13**

Ingredients	Mix – 13			
	Weight (lbs./yd <sup>3</sup> )			
	Standard		Eclipse	
Design Batch	Actual Batch	Design Batch	Actual Batch	
Cement	350	350	350	350
Fly ash				
Slag	350	350	350	350
Water	224	285	212	273
F.A.	1547	1543	1547	1543
C.A.	1405	1348	1405	1348
Air Entrainer	0.0625	0.0625	0.0625	0.0625
Admixture (WRDA 64)	1.75	1.75	1.75	1.75
Admixture (Adva 120)	2.188	2.188	2.188	2.188
Admixture (Eclipse)			12	12
Slump (in inches)	1.75	1.75	7 (Sheared off)	7 (Sheared off)
Air (%)	3.75	3.75	3.25	3.25
Workability	Stiff	Stiff	Stiff	Stiff
W/C Ratio	0.32	0.41	0.32	0.41
Unit Weight (pcf)	143.6	143.5	143.6	143.6

**Table 14. Mix Proportions for Mix 14**

Ingredients	Mix – 14			
	Weight (lbs./yd <sup>3</sup> )			
	Standard		Eclipse	
Design Batch	Actual Batch	Design Batch	Actual Batch	
Cement	455	455	455	455
Fly ash	245	245	245	245
Slag				
Water	224	209	212	197
F.A.	1502	1499	1502	1499
C.A.	1364	1383	1364	1383
Air Entrainer	0.0625	0.0625	0.0625	0.0625
Admixture (WRDA 64)	1.75	1.75	1.75	1.75
Admixture (Adva 120)	2.188	2.188	2.188	2.188
Admixture (Eclipse)			12	12
Slump (in inches)	Sheared off	Sheared off	Sheared off	Sheared off
Air (%)	3.5	3.5	4.5	4.5
Workability	Stiff	Stiff	Stiff	Stiff
W/C Ratio	0.32	0.30	0.32	0.30
Unit Weight (pcf)	140.4	140.4	140.4	140.4

**Table 15. Mix Proportions for Mix 15**

Ingredients	Mix – 15			
	Weight (lbs./yd <sup>3</sup> )			
	Standard		Eclipse	
Design Batch	Actual Batch	Design Batch	Actual Batch	
Cement	700	700	700	700
Fly ash				
Slag				
Water	224	202	212	190
F.A.	1557	1553	1557	1553
C.A.	1415	1441	1415	1441
Air Entrainer	0.0625	0.0625	0.0625	0.0625
Admixture (WRDA 64)	0.875	0.875	0.875	0.875
Admixture (Adva 120)	1.313	1.313	1.313	1.313
Admixture (Eclipse)			12	12
Slump (in inches)	0.25	0.25	0.25	0.25
Air (%)	4.5	4.5	4	4
Workability	Stiff	Stiff	Stiff	Stiff
W/C Ratio	0.32	0.29	0.32	0.29
Unit Weight (pcf)	144.3	144.3	144.3	144.3

## Evaluation of the Effects of a Shrinkage Reducing Admixture

The effects of a shrinkage-reducing admixture on the potential shrinkage-induced stresses in concrete and its potential for shrinkage cracking in service were evaluated using the modified CLS test method. Thirty concrete mixtures, which have been used in bridge decks in Florida and which have a water cement ratio varying from 0.25 to 0.46, were used in this evaluation. Each pair of concrete mixes consisted of a reference mix with no shrinkage-reducing admixture and one with the same mix design but with a shrinkage-reducing admixture added. The amount of shrinkage-reducing admixture added was 12 lbs. per cubic yard of concrete.

The following tests were performed on each of the concrete mixes evaluated:

- 1) Elastic modulus (ASTM C469) and compressive strength (ASTM C39) tests using 4" x 8" specimens at 3, 7, 14, and 28 days. (Two replicates per condition.)
- 2) Splitting tensile strength test (ASTM C496) using 4" x 8" specimens at 3, 7, and 14 days. (Two replicates.)
- 3) Free shrinkage measurement (ASTM C157) using 3" x 3" x 11 $\frac{1}{4}$ " specimens. (Two replicates.)
- 4) CLS test, run at ambient lab conditions, monitored continuously for a minimum of 14 days. (Two replicates.)

Tables 16 through 19 display the following averaged quantities: 1) measured elastic modulus, E; 2) measured induced stress in the CLS test,  $\sigma_{CL}$ ; 3) measured strain in the CLS test,  $\epsilon_{CL}$ ; 4) measured free shrinkage,  $\epsilon_{sh}$ , from ASTM C157 test; and, 5) computed induced tensile stress under a fully constrained condition,  $\sigma_{FC}$ , for the first six pairs of concrete mixes at 3, 7, and 14 days, and for the rest at 3 and 7 days only. The expected induced stresses in the concrete, if it were fully constrained,  $\sigma_{FC}$ , were calculated from the measured induced stress in the CLS test,  $\sigma_{CL}$ , the measured strain in the CLS test,  $\epsilon_{CL}$ , and the measured elastic modulus, E, according to Equation (9).

It can be seen that the free shrinkage,  $\epsilon_{sh}$ , the measured induced stress in the CLS test,  $\sigma_{CL}$ , and the computed induced tensile stress under a fully constrained condition,  $\sigma_{FC}$ , were significantly reduced with the addition of the shrinkage reducing admixture for all of the concrete mixes tested.

**Table 16. Shrinkage Properties of Concrete Mixes 1 to 4**

Time (Days)	E (psi)	Specim. Stress, $s_E$ (psi)	Elastic Strain, $e_E$	Free Shrinkage Strain, $e_{sh}$	Total Specimen Strain, $e_{CL}$	Creep Strain, $e_{CR}$	Computed Shrinkage Stress, $s_{FC}$ (psi)	Splitting Tensile Strength (psi)
Mix - 1								
Standard								
3	4455155	103	0.000023	0.000222	0.000104	0.000094	569*	429
7	5150415	157	0.000030	0.000300	0.000194	0.000076	1151*	594
14	5535946	185	0.000033	0.000380	0.000204	0.000142	1314*	614
Eclipse								
3	4731254	106	0.000022	0.000082	0.000026	0.000033	234	456
7	5404991	164	0.000030	0.000183	0.000043	0.000110	394	603
14	5716239	175	0.000031	0.000262	0.000072	0.000159	588	718
Mix - 2								
Standard								
3	6427326	138	0.000022	0.000189	0.000084	0.000083	682*	492
7	7168223	194	0.000027	0.000320	0.000120	0.000172	1058*	632
14	7285077	192	0.000026	0.000397	0.000154	0.000217	1316*	700
Eclipse								
3	6538004	23	0.000003	0.000092	0.000012	0.000077	95	384
7	6981284	60	0.000009	0.000167	0.000112	0.000047	813*	512
14	7068646	88	0.000012	0.000237	0.000171	0.000054	1290*	600
Mix - 3								
Standard								
3	2905150	28	0.000010	0.000163	0.000115	0.000270	362	354
7	3427850	210	0.000061	0.000323	0.000204	0.000058	908*	661
14	4082624	236	0.000058	0.000395	0.000247	0.000090	1243*	699
Eclipse								
3	3650126	10	0.000003	0.000097	0.000076	0.000018	288	329
7	4185281	138	0.000033	0.000219	0.000153	0.000033	779*	540
14	4193226	168	0.000040	0.000303	0.000215	0.000048	1069*	640
Mix-4								
Standard								
3	3055865	51	0.000017	0.000142	0.000065	0.000060	249	376
7	3462333	108	0.000031	0.000250	0.000147	0.000072	618*	617
14	3901191	139	0.000036	0.000317	0.000195	0.000086	899*	695
Eclipse								
3	3008550	79	0.000026	0.000044	0.000004	0.000013	92	395
7	3343896	151	0.000045	0.000110	0.000034	0.000031	267	607
14	3856788	167	0.000043	0.000181	0.000090	0.000047	507	644

\* Computed stress exceeded splitting tensile strength and the specimen cracked

**Table 17. Shrinkage Properties of Concrete Mixes 5 to 8**

Time (days)	E (psi)	Specim. Stress, $s_E$ (psi)	Elastic Strain, $e_E$	Free Shrinkage Strain, $e_{sh}$	Total Specimen Strain, $e_{CL}$	Creep Strain, $e_{CR}$	Computed Shrinkage Stress, $s_{FC}$ (psi)	Splitting Tensile Strength (psi)
Mix - 5								
Standard								
3	2861518	59	0.000021	0.000114	0.000045	0.000048	187	410
7	3441955	154	0.000045	0.000254	0.000123	0.000087	575	547
14	3619022	180	0.000050	0.000312	0.000167	0.000095	783*	526
Eclipse								
3	2869918	47	0.000016	0.000041	0.000010	0.000014	76	391
7	3336697	102	0.000030	0.000111	0.000057	0.000024	293	457
14	3568982	120	0.000034	0.000181	0.000128	0.000019	576	494
Mix - 6								
Standard								
3	4455155	48	0.000011	0.000045	0.000003	0.000031	1314*	366
7	5150415	70	0.000014	0.000240	0.000132	0.000094	753*	521
14	5535946	76	0.000014	0.000326	0.000188	0.000124	1121*	686
Eclipse								
3	5404263	57	0.000011	0.000013	0.000013	-0.000011	127	321
7	6250985	71	0.000011	0.000141	0.000140	-0.000011	947*	534
14	6457045	76	0.000012	0.000214	0.000225	-0.000023	1530*	615
Mix - 7								
Standard								
3	3606318	51	0.000014	0.000106	0.000069	0.000023	300	467
7	3992038	130	0.000033	0.000206	0.000141	0.000032	696*	561
Eclipse								
3	3388225	35	0.000010	0.000025	0.000008	0.000007	64	365
7	3785151	110	0.000029	0.000085	0.000042	0.000014	269	499
Mix - 8								
Standard								
3	3684585	99	0.000027	0.000103	0.000067	0.000009	346	504
7	4046461	149	0.000037	0.000194	0.000128	0.000029	667*	618
Eclipse								
3	4161028	48	0.000012	0.000032	0.000018	0.000003	122	465
7	4293893	89	0.000021	0.000086	0.000057	0.000008	334	596

\* Computed stress exceeded splitting tensile strength and the specimen cracked

**Table 18. Shrinkage Properties of Concrete Mixes 9 to 12**

Time (Days)	E (psi)	Specim. Stress, $s_E$ (psi)	Elastic Strain, $e_E$	Free Shrinkage Strain, $e_{sh}$	Total Speci- men Strain, $e_{CL}$	Creep Strain, $e_{CR}$	Computed Shrinkage Stress, $s_{FC}$ (psi)	Splitting Tensile Strength (psi)
Mix - 9								
Standard								
3	2820558	51	0.000018	0.000068	0.000024	0.000026	118	314
7	3273363	130	0.000040	0.000204	0.000112	0.000052	497	412
Eclipse								
3	2963033	35	0.000012	0.000022	0.000006	0.000004	53	336
7	3300901	110	0.000033	0.000083	0.000029	0.000021	204	371
Mix - 10								
Standard								
3	3052549	89	0.000029	0.000080	0.000047	0.000004	233	351
7	3280739	154	0.000047	0.000184	0.000109	0.000028	512	468
Eclipse								
3	3114178	55	0.000018	0.000018	0.000005	-0.000005	71	373
7	3298157	101	0.000031	0.000058	0.000035	-0.000007	216	449
Mix - 11								
Standard								
3	3226966	149	0.000046	0.000102	0.000049	0.000007	306	330
7	3666718	158	0.000043	0.000247	0.000164	0.000040	758*	508
Eclipse								
3	3189941	125	0.000039	0.000038	0.000001	-0.000002	127	368
7	3507181	128	0.000037	0.000123	0.000082	0.000004	417	507
Mix - 12								
Standard								
3	3992077	134	0.000034	0.000193	0.000103	0.000055	549*	451
7	4239146	157	0.000037	0.000314	0.000199	0.000079	999*	546
Eclipse								
3	3880440	104	0.000027	0.000083	0.000037	0.000019	246	384
7	4417371	118	0.000027	0.000164	0.000102	0.000035	568	506

\* Computed stress exceeded splitting tensile strength and the specimen cracked

**Table 19. Shrinkage Properties of Concrete Mixes 13 to 15**

Time (Days)	E (psi)	Specim. Stress, $s_E$ (psi)	Elastic Strain, $e_E$	Free Shrinkage Strain, $e_{sh}$	Total Speci- men Strain, $e_{CL}$	Creep Strain, $e_{CR}$	Computed Shrinkage Stress, $s_{FC}$ (psi)	Splitting Tensile Strength (psi)
Mix - 13								
Standard								
3	3861868	119	0.000031	0.000212	0.000138	0.000043	654*	444
7	4539476	139	0.000031	0.000390	0.000281	0.000079	1413*	571
Eclipse								
3	4138054	107	0.000026	0.000086	0.000048	0.000013	304	404
7	4757098	132	0.000028	0.000183	0.000131	0.000025	754*	525
Mix - 14								
Standard								
3	3842707	100	0.000026	0.000094	0.000068	0.000000	361	346
7	3886822	134	0.000034	0.000162	0.000120	0.000008	599*	452
Eclipse								
3	3556466	93	0.000026	0.000037	0.000008	0.000002	122	324
7	4001058	119	0.000030	0.000084	0.000037	0.000017	269	429
Mix - 15								
Standard								
3	4167444	101	0.000024	0.000149	0.000108	0.000017	552*	647
7	4962452	144	0.000029	0.000228	0.000160	0.000039	936*	698
Eclipse								
3	4384647	111	0.000025	0.000075	0.000036	0.000014	266	528
7	4887643	155	0.000032	0.000124	0.000072	0.000020	508	707

\* Computed stress exceeded splitting tensile strength and the specimen cracked

The compressive strength, splitting tensile strength, and the elastic modulus of the 15 pairs of concrete mixtures are shown in Tables 20 through 24.

## Conclusions

From the test data and the analysis results obtained from the 30 concrete mixes tested, the developed CLS method demonstrated that it provided reasonable assessment of expected shrinkage-induced stresses in the concrete. Due to

the creep of concrete at early age, the shrinkage-induced stress in the concrete was much lower than that estimated by multiplying the shrinkage strain by the elastic modulus of the concrete. Using the CLS test method enabled the creep component to be properly considered and a realistic determination of the expected induced shrinkage stresses in concrete in service. It is recommended that further tests may have to be conducted to see if it works with larger sizes of aggregate mixtures as well as for mixtures with fibers in them.

**Table 20. Compressive Strength, Splitting Tensile Strength, and Elastic Modulus of the 15 Pairs of Concrete Mixtures**

Mixes	Time (days)	E (psi)			Compressive Strength (psi)				Splitting Tensile Strength (psi)			
		1	2	Average	1	2	3	Average	1	2	3	Average
Mix - 1  (C-50, S-50), Std (w/c - 0.33)	3	4416855	4493455	4455155	4810	4470	5004	4761	461	396	428	429
	7	5308886	4991944	5150415	6950	7050	6790	6930	654	577	551	594
	14	5640288	5431603	5535946	7700	8160	7740	7867	614	551	676	614
<hr/>												
Mix - 1  (C-50, S-50), Ecl (w/c - 0.33)	3	4584048	4878461	4731254	5030	4830	5020	4960	441	423	504	456
	7	5438242	5371741	5404991	7090	7120	7400	7203	640	613	557	603
	14	5642459	5790019	5716239	8220	8150	8410	8260	788	696	670	718
<hr/>												
Mix - 2  (C-30, S-70), Std (w/c - 0.25)	3	6224478	6630175	6427326	6700	6440	6520	6553	493	486	495	492
	7	7063727	7272718	7168223	8710	8434	8430	8525	658	636	602	632
	14	7271631	7298524	7285077	9370	8760	8560	8897	694	726	680	700
<hr/>												
Mix - 2  (C-30, S-70), Ecl (w/c - 0.25)	3	6445834	6169017	6307425	4710	4810	4960	4827	383	366	403	384
	7	6689849	6790581	6740215	6550	6650	6830	6677	506	516	513	512
	14	6838769	7231382	7035076	7360	7270	7070	7233	607	599	595	600
<hr/>												
Mix - 3  (C-30, S-70), Std (w/c - 0.30)	3	2978144	2832156	2905150	4270	4310	4130	4237	314	384	365	354
	7	3386258	3469441	3427850	5695	5469	5442	5535	709	657	616	661
	14	4044965	4120283	4082624	7450	7570	7560	7527	773	656	667	699
<hr/>												
Mix - 3  (C-30, S-70), Ecl (w/c - 0.29)	3	3618629	3681622	3650126	3590	3530	3570	3563	322	360	304	329
	7	4208640	4161921	4185281	5399	5620	5570	5530	565	555	499	540
	14	4181911	4204542	4193226	7170	6870	6870	6970	610	651	660	640

**Table 21. Compressive Strength, Splitting Tensile Strength, and Elastic Modulus of the 15 Pairs of Concrete Mixtures**

Mixes	Time (days)	E (Psi)			Compressive Strength				Splitting Tensile Strength (psi)			
		1	2	Average	1	2	3	Average	1	2	3	Average
Mix - 4 <i>(C-80, F-20), Std (w/c-0.35)</i>	3	3138865	2972865	3055865	2910	2830	2970	2903	360	403	366	376
	7	3511892	3412774	3462333	6680	6750	6520	6650	604	660	587	617
	14	3881511	3920872	3901191	7870	7910	8100	7960	766	632	688	695
<hr/>												
Mix - 4 <i>(C-80, F-20), Ecl (w/c-0.33)</i>	3	3044235	2906975	2975605	2000	2040	2060	2033	391	400	395	395
	7	3275018	3464325	3369671	6400	6250	6370	6340	571	626	623	607
	14	3792704	3740321	3766512	7900	7940	7920	7920	646	656	630	644
<hr/>												
Mix - 5 <i>(C-65, F-35), Std (w/c-0.33)</i>	3	3000886	2722150	2861518	3440	3460	3430	3443	376	415	439	410
	7	3390959	3492951	3441955	4500	4560	4530	4530	533	590	519	547
	14	3661683	3576361	3619022	5580	5540	5640	5587	566	471	542	526
<hr/>												
Mix - 5 <i>(C-65, F-35), Ecl (w/c-0.33)</i>	3	2880273	2859563	2869918	3230	3300	3320	3283	406	436	331	391
	7	3382939	3290456	3336697	4710	4520	4510	4580	489	390	491	457
	14	3616783	3521181	3568982	5540	5540	5550	5543	529	487	464	494
<hr/>												
Mix - 6 <i>(C-30, S-50 &amp; F-20), Std (w/c-0.35)</i>	3	2618982	2622861	2620921	2450	2410	2380	2413	381	345	372	366
	7	3120751	3162391	3141571	4690	4790	4620	4700	574	496	492	521
	14	3514496	3510558	3512527	6669	6465	6903	6679	669	726	664	686
<hr/>												
Mix - 6 <i>(C-30, S-50 &amp; F-20), Ecl (w/c-0.35)</i>	3	2535208	2548807	2542007	2280	2210	2400	2297	376	303	284	321
	7	3349643	3362484	3356063	4720	4780	4690	4730	481	542	578	534
	14	3495439	3537646	3516542	6030	6450	6365	6282	649	588	607	615

**Table 22. Compressive Strength, Splitting Tensile Strength, and Elastic Modulus of the 15 Pairs of Concrete Mixtures**

Mixes	Time (days)	E (Psi)			Compressive Strength				Splitting Tensile Strength (psi)			
		1	2	Average	1	2	3	Average	1	2	3	Average
Mix - 7 <b>(C-80, F-20), Std (w/c - 0.34)</b>	3	3606318	3606318	3606318	4463	4439	4455	4452	465	467	467	467
	7	4076555	3900563	3988559	5855	6324	6006	6061	644	499	539	561
	14	4525851	4304663	4415257	7533	7509	7239	7427	581	478	606	555
	28	4537320	4525331	4531325	8002	8328	8265	8198	576	684	551	604
<hr/>												
Mix - 7 <b>(C-80, F-20), Ecl (w/c - 0.34)</b>	3	3388225	3388225	3388225	3516	3548	3572	3545	376	366	354	365
	7	3729430	3840872	3785151	5194	5417	5314	5308	493	447	557	499
	14	3983873	3991834	3987853	6356	6197	6339	6297	552	514	523	530
	28	4138115	4332631	4235373	7636	7422	7517	7525	616	598	676	630
<hr/>												
Mix - 8 <b>(C-80, F-20), Std (w/c - 0.38)</b>	3	3631600	3737570	3684585	4733	4781	4789	4767	483	512	516	504
	7	4056772	4036149	4046461	6539	6491	6658	6563	611	634	611	618
	14	4314802	4203692	4259247	7453	7557	7350	7453	718	718	704	713
	28	4497366	4609553	4553460	8178	8399	8341	8306	1970	2057	2100	2043
<hr/>												
Mix - 8 <b>(C-80, F-20), Ecl (w/c - 0.38)</b>	3	4019694	4260053	4139874	4964	4805	4932	4900	413	520	463	465
	7	4281844	4305943	4293893	6722	6499	6451	6557	616	611	561	596
	14	4728351	4441247	4584799	7525	7636	7366	7509	628	734	595	652
	28	4724886	4831122	4778004	7881	8227	8402	8170	693	745	610	683
<hr/>												
Mix - 9 <b>(C-65, F-35), Std (w/c - 0.46)</b>	3	2847699	2793418	2820558	2426	2490	2498	2471	326	290	326	314
	7	3230478	3316248	3273363	3651	3611	3611	3625	457	446	334	412
	14	3446445	3625646	3536046	4789	4653	4797	4746	479	557	563	533
	28	3599945	3822791	3711368	5878	5688	5823	5796	636	636	545	606
<hr/>												
Mix - 9 <b>(C-65, F-35), Ecl (w/c - 0.46)</b>	3	2997575	2928491	2963033	2538	2649	2561	2583	358	318	332	336
	7	3223592	3378211	3300901	3802	3938	3985	3908	369	377	368	371
	14	3607691	3715169	3661430	4828	4868	4852	4850	561	519	416	498
	28	3864973	3711668	3788320	5727	5759	5664	5717	531	614	601	582

**Table 23. Compressive Strength, Splitting Tensile Strength, and Elastic Modulus of the 15 Pairs of Concrete Mixtures**

Mixes	Time (days)	E (psi)			Compressive Strength (psi)				Splitting Tensile Strength (psi)			
		1	2	Average	1	2	3	Average	1	2	3	Average
Mix - 10 <b>(C-65, F-35), Std (w/c - 0.41)</b>	3	2936739	3168360	3052549	2657	2792	2919	2789	360	364	328	351
	7	3295355	3266124	3280739	3651	3699	3906	3752	457	461	485	468
	14	3466569	3496266	3481417	4598	4765	4741	4701	523	523	463	503
	28	3702587	3719864	3711225	5759	5775	5743	5759	573	602	507	561
<hr/>												
Mix - 10 <b>(C-65, F-35), Ecl (w/c - 0.41)</b>	3	3161160	3067196	3114178	2681	2705	2832	2739	360	382	378	373
	7	3240103	3356210	3298157	3866	3874	3930	3890	469	497	380	449
	14	3601638	3626390	3614014	5003	4860	4988	4950	507	459	581	516
	28	3712301	3959791	3836046	5839	5950	6157	5982	403	541	499	481
<hr/>												
Mix-11 <b>(C-80, F-20), Std (w/c - 0.46)</b>	3	3258290	3195641	3226966	3691	3683	3747	3707	322	326	344	330
	7	3720572	3612864	3666718	5520	5409	5345	5425	464	612	447	508
	14	3862169	3827133	3844651	6064	6006	5979	6016	490	555	477	507
	28	4145363	4255670	4200516	7151	7199	7247	7199	542	441	537	506
<hr/>												
Mix-11 <b>(C-80, F-20), Ecl (w/c - 0.46)</b>	3	3143982	3235900	3189941	3524	3516	3675	3572	346	439	320	368
	7	3498332	3516031	3507181	4956	5051	4972	4993	490	470	562	507
	14	3610294	3660458	3635376	5688	5823	5611	5707	549	542	604	565
	28	3834219	3949312	3891766	7151	7366	6889	7135	667	687	688	681
<hr/>												
Mix-12 <b>(C-30, S-50, F-20), Std (w/c - 0.28)</b>	3	3550043	4434111	3992077	4844	4645	5019	4836	414	414	527	451
	7	4203387	4274906	4239146	6618	6411	6634	6555	577	501	560	546
	14	4369976	4487084	4428530	7485	7533	7453	7491	594	543	652	596
	28	4591187	4564588	4577888	7803	8130	8225					
<hr/>												
Mix-12 <b>(C-30, S-50, F-20), Ecl (w/c-0.28)</b>	3	4100167	3660713	3880440	3810	3922	3961	3898	362	430	360	384
	7	4442825	4391918	4417371	5727	5791	5759	5759	505	505	506	506
	14	4542769	4575835	4559302	6364	7016	6698	6692	593	577	614	595
	28	4794909	4926751	4860830	7247	7207	7151	7202	524	579	553	552

**Table 24. Compressive Strength, Splitting Tensile Strength, and Elastic Modulus of the 15 Pairs of Concrete Mixtures**

Mixes	Time (days)	E (Psi)			Compressive Strength				Splitting Tensile Strength			
		1	2	Average	1	2	3	Average	1	2	3	Average
Mix-13 <b>(C-50, S-50), Std (w/c - 0.41)</b>	3	3735773	3987963	3861868	6189	6491	6523	6401	414	507	412	444
	7	4570450	4508502	4539476	8114	8193	8201	8169	556	498	659	571
	14	4747266	5123076	4935171	9259	9378	9514	9384	755	671	729	718
	28	4781950	5146989	4964470	9657	9736	9553	9649	911	656	867	811
Mix-13 <b>(C-50, S-50), Ecl (w/c - 0.41)</b>	3	4111928	4164180	4138054	5497	5314	5417	5409	406	410	396	404
	7	4658387	4855809	4757098	7398	7278	7613	7430	483	515	576	525
	14	5001046	5001046	5001046	8543	8519	8710	8591	509	562	646	572
	28	5177606	5134069	5155838	9044	9148	9108	9100	789	599	629	672
Mix-14 <b>(C-65, F-35), Std (w/c - 0.30)</b>	3	3858952	3826463	3842707	3475	3523	3378	3459	287	383	367	346
	7	3886822	2911755	3886822	4542	4470	4311	4441	467	436	453	452
	14	4423983	4366718	4395351	5505	5377	5170	5351	515	533	545	531
	28	5580151	4812471	5196311	7239	7382	6928	7183	611	509	723	615
Mix-14 <b>(C-65, F-35), Ecl (w/c - 0.30)</b>	3	3556466	3341947	3449206	3043	2954	2980	2993	313	327	331	324
	7	3965263	4036854	4001058	4176	4073	4120	4123	475	416	396	429
	14	4441069	4218399	4329734	5003	5338	4828	5056	481	515	561	519
	28	4592010	4711529	4651769	6618	6570	6284	6491	526	508	507	514
Mix-15 <b>(C-100), Std (w/c - 0.29)</b>	3	3803863	4510687	4157275	7764	8082	7835	7894	618	622	702	647
	7	5039900	5039900	5039900	10047	9561	9713	9773	651	722	722	698
	14	5315464	5123516	5219490	11192	10595	10206	10664	769	768	611	716
	28	5322837	5471778	5397307	11089	11526	11574	11396	597	692	716	668
Mix-15 <b>(C-100), Ecl (w/c - 0.29)</b>	3	4408573	4323830	4366202	6109	6173	6109	6130	528	472	585	528
	7	3366304	4917633	4917633	7692	7589	7772	7684	696	679	745	707
	14	5035781	5669101	5352441	9052	8480	8480	8670	627	504	532	554
	28	5234741	5439419	5337080	9076	9386	9593	9352	730	678	571	660

---

## References

- [1] Wiegrink, K., Marikunte, S., & Shah, S. P. (1996). Shrinkage Cracking of High-Strength Concrete, *ACI Materials Journal*, 93(2), 409-415.
- [2] Bloom, B., & Bentur, A. (1995). Free and Restrained Shrinkage of Normal and High-Strength Concretes, *ACI Materials Journal*, 92(2), 211-217.
- [3] Samman, T. A., Mirza, W. H., & Wafa, F. F. (1996). Plastic shrinkage cracking of normal and high-strength concrete: a comparative study, *ACI materials journal*, 93(1), 36-40.
- [4] Tia, M., Leung, T. M., Darku, D., Richardson, D., & Brown, D. (1998). Development of a Laboratory Procedure for Evaluating Concrete Mixes for Resistance to Shrinkage Cracking in Service, *Research Report, University of Florida*.
- [5] Grzybowski, M., & Shah, S. P. (1990). Shrinkage Cracking of Fiber Reinforced Concrete, *ACI Materials Journal*, 87(2), 138-148.
- [6] Shaeles, C. A., & Hover, K. C. (1988). Influence of Mix Proportions and Construction Operations on Plastic Shrinkage Cracking in Thin Slabs, *ACI Materials Journal*, 85(6), 495-504.
- [7] Pigeon, M., Toma, G., Delagrange, A., Bissonnette, B., Marchand, J., & Prince, J. C. (2000). Equipment for the Analysis of the Behavior of Concrete under Restrained Shrinkage at Early Ages, *Magazine of Concrete Research*, 52(4), 297-302.
- [8] Altoubat, S. A., & Lange, D. A. (2001). Creep, Shrinkage and Cracking of Restrained Concrete at Early Age, *ACI Materials Journal*, 98(4), 323-331.
- [9] Subramanian, R., Mang, T., Bergin, M. J., & Ishee, C. (2004). Evaluation of the effects of a Shrinkage reducing admixture on the Potential Shrinkage induced stresses in concrete, *Transportation Research Board, 83<sup>rd</sup> Annual Meeting Proceedings*, Washington D.C, January 11 – 14, 2004.

## Biographies

**RAJARAJAN SUBRAMANIAN** is a lecturer in the Civil Engineering Department at the Pennsylvania State University at Harrisburg. Dr. Subramanian graduated with a bachelor's degree in Civil and Structural Engineering from Annamalai University in India. He obtained his master's and doctoral degrees from the University of Florida. He has over 25 years of experience working for government, industry, and academia. Dr. Subramanian may be reached at [rus30@psu.edu](mailto:rus30@psu.edu)

**MANG TIA** is a professor of Civil Engineering at the Engineering School of Sustainable Infrastructure and Environment, University of Florida. Dr. Tia has more than 30 years of experience as an academician. His research interests include Portland cement concrete and asphalt concrete. He has published more than 50 technical journal and conference papers and currently is the Graduate Coordinator of the Civil and Coastal Engineering Department at the University of Florida. Dr. Tia may be reached at [tia.ce@ufl.edu](mailto:tia.ce@ufl.edu)

**MICHAEL J. BERGIN** has 25 years of working experience with the Florida Department of Transportation as a Materials Engineer. Prior to his working at FDOT, Mr. Bergin was working residential and commercial construction for 10 years. He graduated with a bachelor's degree in Civil Engineering from the University of Florida. At the national level, he is actively involved in the FHWA High Performance Concrete Technical Delivery Team, and serves as a member of a task team harmonizing the AASHTO and ASTM Cement Specifications. Within the Department, he is a member of the Construction Technical Review Team for concrete qualifications required for testing and inspection. Mr. Bergin may be reached at [michael.bergin@dot.state.fl.us](mailto:michael.bergin@dot.state.fl.us)

**CHARLES A. ISHEE** is currently working with Applied Research Associates, Inc., as a materials engineer. Prior to his working at ARA, he worked as a concrete materials engineer at the Florida Department of Transportation for more than 10 years. Mr. Ishee may be reached at [charles.ishee@ara.com](mailto:charles.ishee@ara.com)

# A MULTI-AGENT-BASED APPROACH TO DYNAMIC SCHEDULING OF MACHINES AND AUTOMATED GUIDED VEHICLES (AGV) IN MANUFACTURING SYSTEMS BY CONSIDERING AGV BREAKDOWNS

Vahit Kaplanoğlu, University of Gaziantep; Cenk Şahin, Cukurova University; Adil Baykasoğlu, Dokuz Eylül University; Rızvan Erol, Cukurova University; Alper Ekinci, University of Gaziantep; Melek Demirtaş, Cukurova University

## Abstract

In a competitive business environment, producing goods on time plays a very important role. In addition to regular control complexities in manufacturing environments, some unforeseen technical problems may affect the efficiency of production. The breakdown of automated guided vehicles (AGV) during manufacturing is one of these problems. This problem generally requires an instantaneous solution while the system is operating. However, traditional production control systems and algorithms handle this kind of problem centrally and usually are not able to provide effective solutions promptly. One possibility is to use a multi-agent-based scheduling approach for AGVs and machines within a manufacturing system that takes into consideration AGV breakdowns. After implementation, this approach is designed to work in a real-time manufacturing environment and feasible schedules should emerge from negotiation/bidding mechanisms between agents.

## Introduction

Producing goods on time plays a very important role in manufacturing control and planning. Production plans and schedules are generally interrupted with unexpected events around or within the system. These problems may affect the efficiency of production planning or they may collapse all the plans of operations. The breakdown of automated guided vehicles (AGV) in flexible manufacturing systems is one of those problems. AGV systems are industrial transportation systems used in various industrial contexts: container terminals, parts transportation in heavy industry, and manufacturing systems [1-3]. They have considerable functionality in manufacturing systems and container terminals may be the source of unexpected events within a manufacturing or logistics system.

The operational decisions of AGVs especially attracted researchers to design and implement cost-effective operating decisions. However, the complexity of the problem has led the researchers to use distributed methods other than

central optimization approaches. Distributed artificial intelligence, such as multi-agent-based systems, can allow for effective management of dynamic manufacturing operations. As is expected from a fairly young area of research, there is not yet universal consensus on the definition of an agent [4]. However, the Wooldridge and Jennings' definition is increasingly adopted in this field: "An agent is a computer system that is situated in some environment, and that is capable of autonomous action in this environment in order to meet its design objectives" [5]. An agent is a component that can exhibit reasoning behavior under both proactive (goal-directed) and reactive (event-driven) stimuli. When an agent is instantiated, it will wait until it is given a goal to achieve or experiences an event that requires a response [6].

Some of the authors of this study have previously addressed a multi-agent-based simultaneous AGV and machine scheduling approximation and tested it on test-bed problems [7]. Multi-agent-based approximation has proven its success in dynamic and volatile business environments. However, AGV breakdown occurrences were not considered in previous studies. The AGVs were assumed to be operational without breaking down throughout the entire manufacturing process. In this current study, the breakdowns of AGVs were considered to extend the scope of the previous studies. The intention of this study is to get closer to real manufacturing environments.

## Literature Review

Previous studies on AGV control have a wide scope in the literature and range from traffic control on the AGV paths to AGV deadlock prevention [8], [9]. The application areas range from manufacturing floors to container terminals [7], [10]. The solution approximation for AGV control also encompasses a wide research domain, from integer programming to meta-heuristics, and from Petri-net to multi-agent systems [7], [8], [10-13]. However, this current literature review focused on AGV breakdown during real-time manufacturing operations, of which few studies were found. Of

those reviewed, AGV failures on automated transportation systems were neglected. According to Ebben [14], when an AGV breaks down, it may stop other AGVs. There are two options when the AGV breaks down: it can be fixed on the system or removed from the system to the repair section; the choice generally depends on repair time.

Taghaboni-Dutta and Tanchoco [15] noted that routing flexibility allows a quick recovery to breakdowns and other disruptive events, but their study does not examine failures. According to their study, failures can be neglected in AGV systems when the AGV workload is low and failures can be resolved quickly. Another study about AGV control that considered disturbances was by Badr et al. [16]. They presented five steps to clarify disturbance handling during dynamic scheduling: disturbance detection, disturbance analysis, action selecting, action announcement, and schedule repair. Merdan et al. [17] proposed an approximation for conveyor and machine failures in workflow scheduling by using a multi-agent system. They tested dispatching rules in combination with the all re-routing re-scheduling policies under machine and conveyor failures. They then ranked the rules based on their performance results from the simulation.

## Design of an AGV Resource Agent during Breakdown

In this current study, an AGV breakdown situation was modeled under a multi-agent-based system approach. The system was designed using the Prometheus methodology that defines a detailed process for specifying, designing, implementing, and testing/debugging agent-oriented software systems. This methodology was developed for specifying and designing agent-oriented software systems, and is considered general purpose in that it is not tied to any specific software platform. Unlike other methods, Prometheus supports the development of intelligent agents, provides start-to-end support, evolved out of practical industrial and pedagogical experience, is used in both industry and academia, and is detailed and complete [4]. Figure 1 presents the phases of the Prometheus design methodology.

## System Specification

The agent types are decided and designed through the stages of this design methodology. Here are the agent types in the proposed system: Machine Resource Agent, Machine Scheduler Agents, AGV Resource Agent, AGV Scheduler Agents, and Operation Agent. In the system specification stage of Prometheus, negotiations between agent types, system goals, agent roles in the system, and scenarios are iden-

tified. Figure 2 shows the system specification stage of the Prometheus methodology. There are four main roles in the system: AGV management, machine management, system management, and negotiation management.

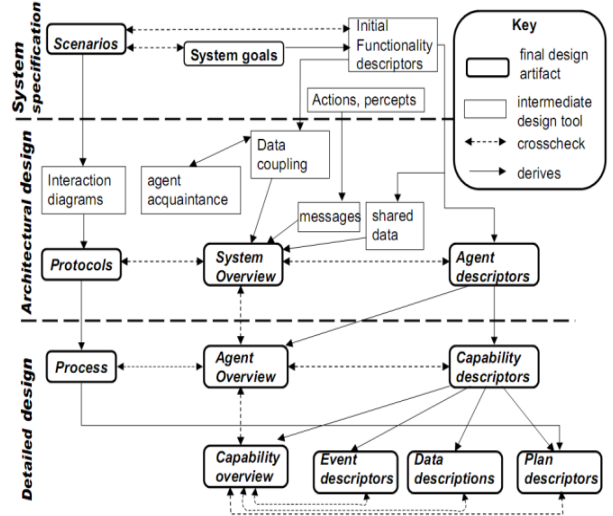


**Figure 1. Phases of the Prometheus Methodology [4]**

This study focused on the AGV management role in the system specification stage. The ovals in Figure 2 show the goals of the system elements. One of the goals of the AGV management role for the proposed system was “AGV Scheduling after AGV Breakdown” (see Figure 2). The sub-goal is also designed in the system specification stage. Three sub-goals of the “AGV Scheduling after AGV Breakdown” goal are given in Figure 3:

1. AGV that is loaded and has a task in its blackboard.
2. AGV that is free and has a task in its blackboard.
3. AGV that is loaded and has no task in its blackboard.

## Architectural Design

The negotiation protocols between agent types were designed in this stage of the Prometheus methodology. A system overview diagram is given in Figure 4. The AGV scheduler agent negotiates with operation agents in order to find real-time operation transportation and processing schedule. Figure 4 also shows an example negotiation protocol between operation agents and scheduler agents. When an operation agent enters into the proposed multi-agent-based system then it calls for proposals for the machine and scheduler agents that are available in the system. When the order agent finds a proper machine agent to be processed, it then calls for a proposal to a scheduler agent to be transported to the machine.

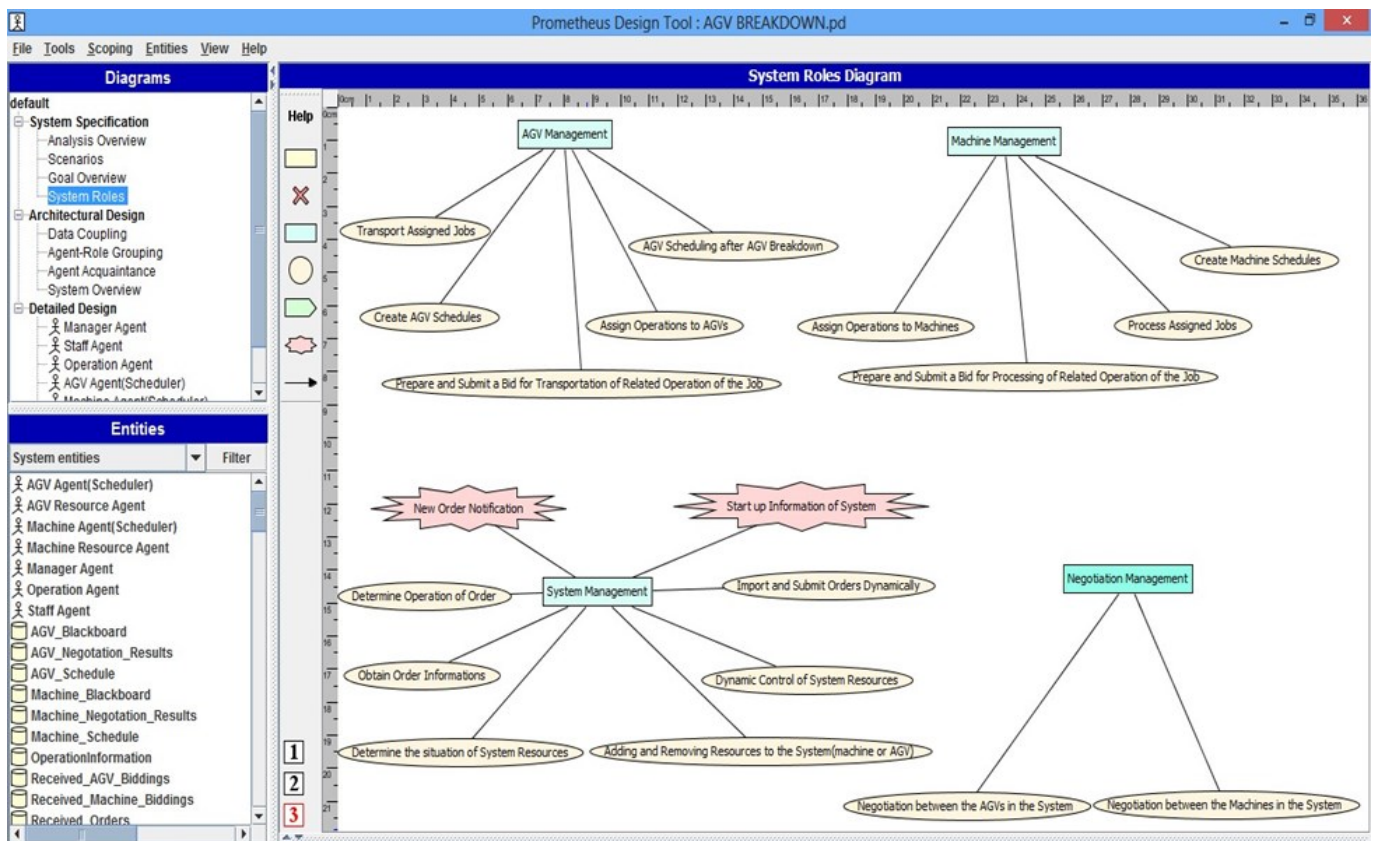


Figure 2. System Roles in PDT

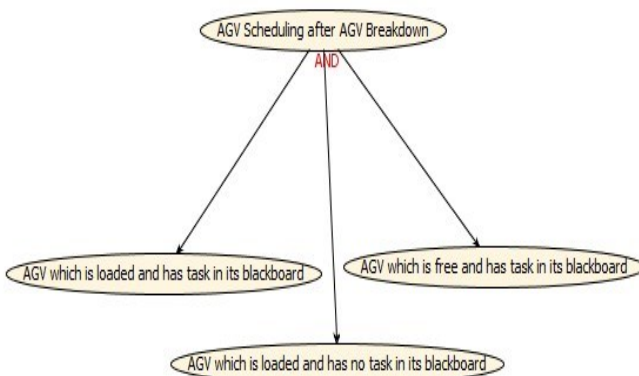


Figure 3. Sub-goals of the “AGV Scheduling after AGV Breakdown” Goal

## Detailed Design

In the detailed design stage, the capabilities of the scheduler agent type are defined by the breakdown condition. A resource agent could be in any of the following states in a flexible manufacturing system:

1. Idle and ready
2. Transportation of an operation
3. Deadheading trip (going to take a job from a machine)

While the AGV resource agent is operating, it can break down. The AGV resource agent has an attribute of working status of either “in working condition” or “broken down”; its status changes from “in working condition” to “broken down” when it breaks down. In all three states, the resource agent updates its status attribute. The resource agent sends the breakdown information to the scheduler agent after updating its attribute. Figure 5 shows the detailed design for the resource agent. Figure 6 shows the negotiation protocol of resource and scheduler agents. When the scheduler agent receives the breakdown message, it reasons in one of three ways by controlling the blackboard. Figure 7 shows a detailed design for the scheduler agent. When the scheduler agent takes the breakdown message from the resource agent, it sends the message to the operation agents in its blackboard, which then start a new negotiation with the scheduler agents in order to be transported. Figure 8 shows the standard negotiation protocol between operation and scheduler agents.

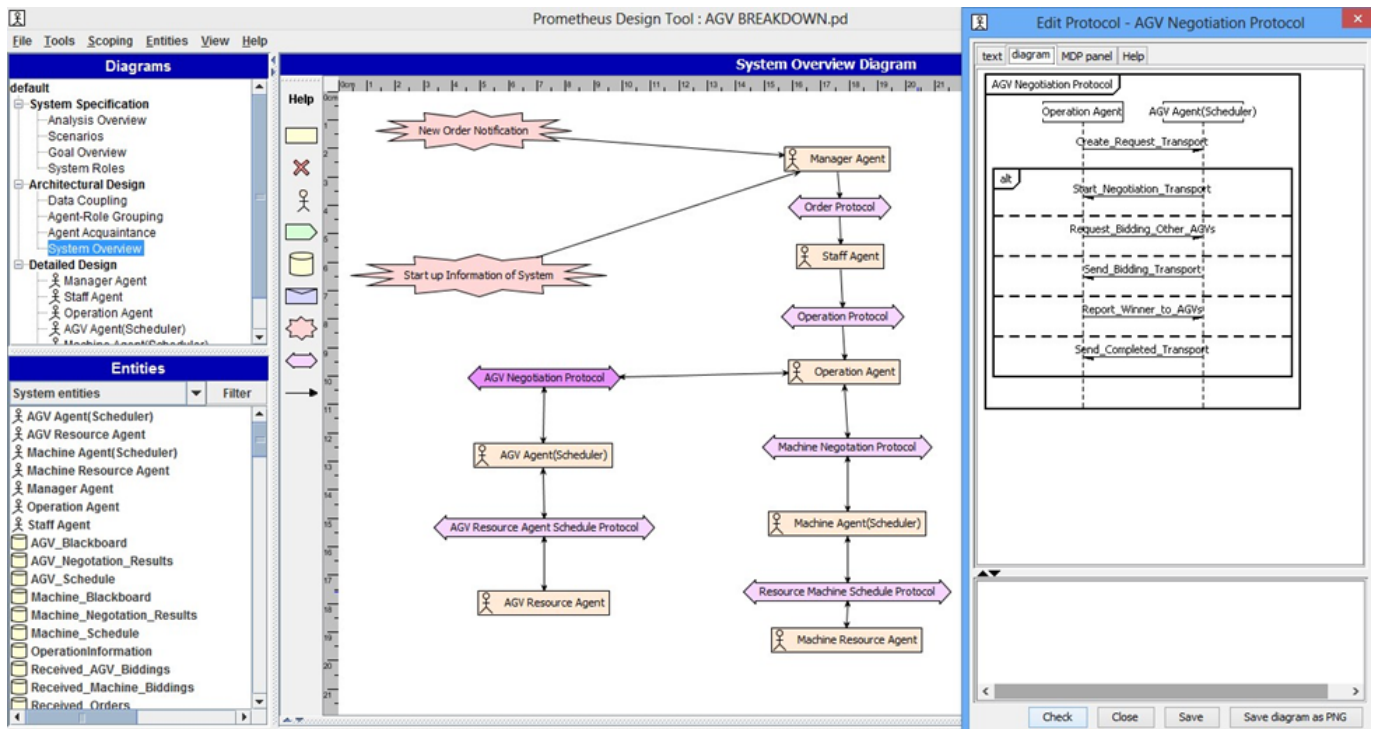


Figure 4. System Overview

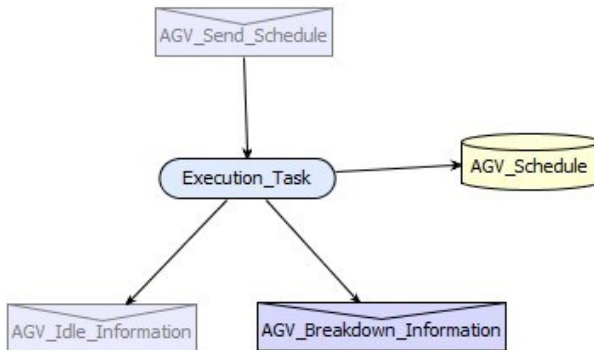


Figure 5. Detailed Design of an AGV Resource Agent

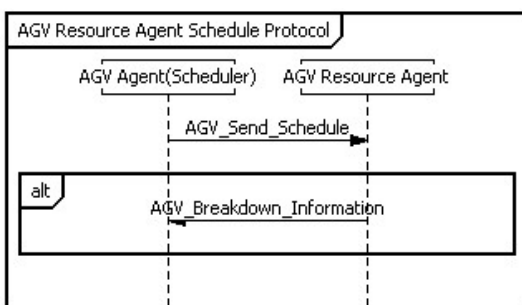


Figure 6. Negotiation Protocol of AGV Resource and AGV Scheduler Agents

## Algorithm for AGV Breakdown Conditions

This section details the scheduler agent's decision making. The operation agent informs the scheduler agents when the AGV breaks down. The scheduler agent then assesses the coordination information inside the messages and performs a reward. Scheduler agents consider the proposal of machine operations as “broken down” AGV, according to Equation (1). After the AGV breaks down and the blackboard resets, the current time must be equal to the earliest pickup time of operation  $i$ :

$$t = EPT_i, \text{ so } ELT_i = \{t + \Delta t(CL, AGVBDP_i)\} \quad i = 1 \dots n \quad (1)$$

where,  $ELT_i$  denotes the earliest loading time of operation  $i$ ; CL is the current location of the AGV resource agent;  $AGVBDP$  is AGV's breakdown point for operation  $i$ ;  $t$  is the current time;  $\Delta(.,.)$  is the required time between two locations; and,  $EPT_i$  is the earliest pickup time of operation  $i$ .

Scheduler agents evaluate the proposal according to Equation (2):

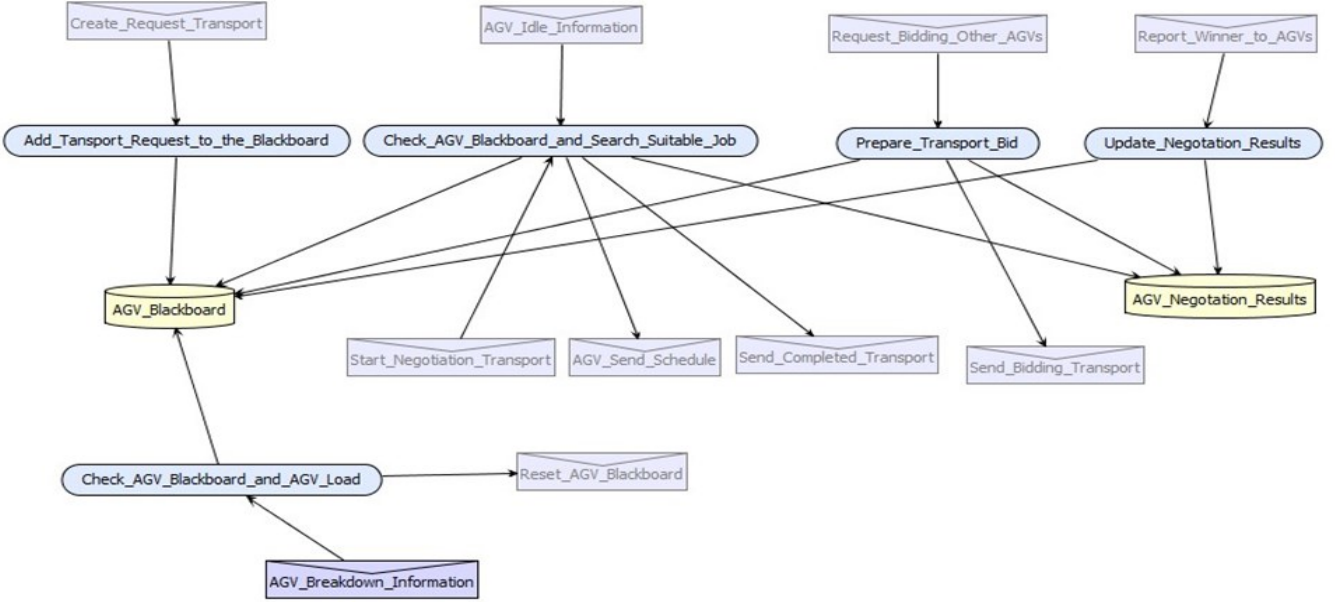


**Figure 7. AGV Scheduler Agent with Details**

$$ELT_i = \begin{cases} t + \Delta t(CL, PCP_i), & t > EPT_i, \\ t + \max\{\Delta t(CL, PCP_i), (EPT_i - t)\}, & t \leq EPT_i, \end{cases} \quad i=1 \dots n \quad (2)$$

where,  $ELT_i$  denotes the earliest loading time of operation  $i$ ;  $CL$  is the current location of the AGV resource agent;  $PCP_i$  is the pickup point of operation  $i$ ;  $t$  is current time;  $\Delta t(.,.)$  is the required time between two locations; and,  $EPT_i$  is the earliest pickup time of operation  $i$ .

Then, an operation is selected from the AGV blackboard by using Equation (3):

$$ELT_s = \min\{ELT_i\}, \quad i=1 \dots n \quad (3)$$

The scheduler agent then proposes a time to the respective operation agents by adding  $ELTs$  to the related loaded trip time, as shown in Equation (4):

$$PR = ELT_s + \Delta t(PCP_s, DP_s) \quad (4)$$

After the start of the negotiations, operation agents call to all scheduler agents to submit a proposal. This plan first checks whether an operation has already been rewarded. If there is not a rewarded operation, then it prepares an offer. When preparing a proposal, the scheduler agent finds the operation that has the minimum  $ELT$ , using Equations (5) and (6), where  $EFT$  and  $NL$  denote the earliest free time and the next location of the AGV resource agent, respectively.

$$ELT_i = \begin{cases} EFT + \Delta t(NL, PCP_i), & EFT > EPT \\ EFT + \max\{\Delta t(NL, PCP_i), (EPT_i - EFT)\}, & EFT \leq EPT \end{cases} \quad i=1 \dots n \quad (5)$$

$$ELT_s = \min\{ELT_i\}, \quad i=1 \dots n \quad (6)$$

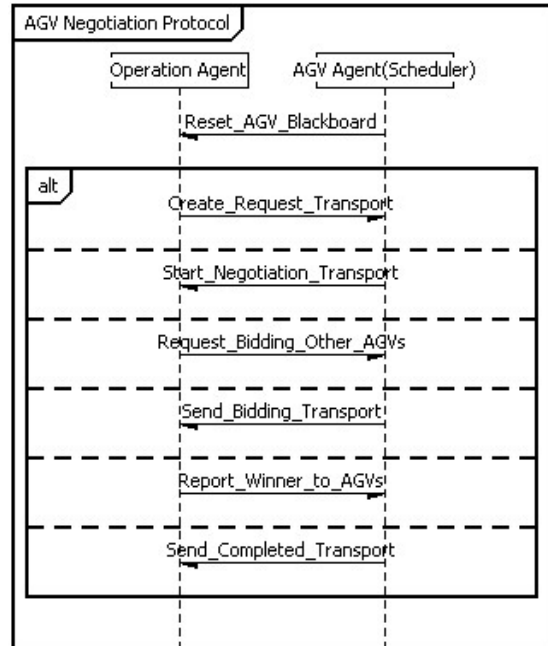


**Figure 8. Negotiation of Operation and AGV Scheduler Agents**

If the operation in the current negotiation matches the selected operation in the scheduler agent's blackboard belief set, the scheduler agent proposes operations by adding *ELTs* the related loaded trip time, as given by Equation (7):

$$PR = ELT_s + \Delta t(PCP_s, DP_s) \quad (7)$$

## Conclusions and Future Research

Resources that are used in flexible manufacturing systems pose unforeseen technical problems in addition to regular control and maintenance complexities. The breakdown of AGVs during real-time manufacturing affects many related schedules of operations and machines. This problem generally requires an instantaneous solution, while the system is operating. The proposed multi-agent-based design was developed in order to solve these complexities during the manufacturing process. The design uses the capabilities of multi-agent systems in order to solve real-time scheduling complexities. Feasible and effective schedules were expected to emerge from negotiation/bidding mechanisms between agents. Future research directions include

- Implementing the proposed design on a multi-agent programming language.
- Finding test-bed studies in order to compare the results of multi-agent systems with other approximations.
- Developing multi-agent-based simulation models in order to test the effectiveness of the proposed model.

## Acknowledgment

The current study was supported by The Scientific and Technological Research Council of Turkey (TUBITAK); grant number: 111M279.

## References

- [1] Le-Anh, T., & De Koster, M. B. M. (2006). A Review of Design and Control of Automated Guided Vehicle Systems. *European Journal of Operational Research*, 171(1), 1-23.
- [2] Lin, L., Shinn, S. W., Gen, M., & Hwang, H. (2006). Network Model and Effective Evolutionary Approach for AGV Dispatching in Manufacturing System. *Journal of Intelligent Manufacturing*, 17(4), 465-77.
- [3] Vis, I. F. A. (2006). Survey of Research in the Design and Control of Automated Guided Vehicle Systems. *European Journal of Operational Research*, 170 (3), 677-709.
- [4] Padgham, L., & Winikoff, M. (2004). *Developing Intelligent Agent Systems: A Practical Guide*. Melbourne, Australia: John Wiley & Sons.
- [5] Wooldridge, M., & Jennings, N. R. (1995). Intelligent Agents: Theory and Practice. *The Knowledge Engineering Review*, 10(2), 115-52.
- [6] Hahn, C., Madrigal-Mora, C., & Fischer, K. (2009). A Platform-Independent Metamodel for Multiagent Systems. *Autonomous Agents and Multi-Agent Systems*, 18(2), 239-66.
- [7] Erol, R., Sahin, C., Baykasoglu, A., & Kaplanoglu, V. (2012). A Multi-Agent Based Approach to Dynamic Scheduling of Machines and Automated Guided Vehicles in Manufacturing Systems. *Applied Soft Computing*, 12(6), 1720-32.
- [8] Herrero-Perez, D., & Martinez-Barbera, H. (2011). Decentralized Traffic Control for Non-Holonomic Flexible Automated Guided Vehicles in Industrial Environments. *Advanced Robotics*, 25(6-7), 739-63.
- [9] Kim, K. H., Jeon, S. M., & Ryu, K. R. (2006). Deadlock Prevention for Automated Guided Vehicles in Automated Container Terminals. *OR Spectrum*, 28 (4), 659-79.
- [10] Gelareh S, Merzouki R, McGinley K, Murray R. (2013). Scheduling of Intelligent and Autonomous Vehicles under Pairing/Unpairing Collaboration Strategy in Container Terminals. *Transport Research Part C: Emerging Technologies*, 33, 1-21.
- [11] Farahani, R. Z., Pourakbar, M., Miandoabchi, E. (2007). Developing Exact and Tabu Search Algorithms for Simultaneously Determining AGV Loop and P/D Stations in Single Loop Systems. *International Journal of Production Research*, 45(22), 5199-222.
- [12] Wallace, A. (2001). Application of AI to AGV Control-Agent Control of AGVs. *International Journal of Production Research*, 39(4), 709-26.
- [13] Rajotia, S., Shanker, K., & Batra, J. L. (1998). An Heuristic for Configuring a Mixed Uni/Bidirectional Flow Path for an AGV System. *International Journal of Production Research*, 36(7), 1779-99.
- [14] Ebben, M. J. R. (2001). *Logistic Control in Automated Transportation Networks*. Enschede, The Netherlands: Universiteit Twente.
- [15] Taghaboni-Dutta, F., & Tanchoco, J. (1995). Comparison of Dynamic Routing Techniques for Automated Guided Vehicle System. *International Journal of Production Research*, 33(10), 2653-69.
- [16] Badr, I., Schmitt, F., & Gohner, P. (2010) Integrating Transportation Scheduling with Production Scheduling for FMS: An Agent-Based Approach. *IEEE International Symposium on Industrial Electronics*, 3539-44.

- 
- [17] Merdan, M., Moser, T., Sunindyo, W., Biffl, S., & Vrba, P. (2013). Workflow Scheduling Using Multi-Agent Systems in a Dynamically Changing Environment. *Journal of Simulation*, 7(3), 144-58.

## Biographies

**VAHİT KAPLAÑOĞLU** received his B.Sc. degree in Industrial Engineering from the University of Marmara, Department of Industrial Engineering, in 2004. He received his M.Sc. and Ph.D. degrees in Industrial Engineering from the University of Gaziantep, Department of Industrial Engineering, in 2007 and 2011, respectively. He is currently working at the University of Gaziantep as an assistant professor. His research interests include logistics and supply chain management, multi-agent systems, and distributed artificial intelligence. Dr. Kaplanoğlu may be reached at [kaplano glu@gantep.edu.tr](mailto:kaplano glu@gantep.edu.tr)

**CENK ŞAHİN** received his B.Sc., M.Sc., and Ph.D. degrees in Industrial Engineering from Cukurova University, Department of Industrial Engineering, in 2001, 2004, and 2010, respectively. He is currently working at the Cukurova University as an assistant professor. His research interests include production scheduling, artificial neural networks, logistics and supply chain management, and multi-agent systems. Dr. Şahin may be reached at [sahin.cenk@gmail.com](mailto:sahin.cenk@gmail.com)

**ADIL BAYKASOĞLU** received his B.Sc., M.Sc., and Ph.D. degrees in mechanical and industrial engineering in Turkey and the UK. From 1993 to 1996, he worked in the Department of Mechanical Engineering and Industrial Engineering at the University of Gaziantep, first as a research assistant then as an instructor. He is presently a full professor in the Industrial Engineering Department at the Dokuz Eylül University. He has published more than 260 academic papers, three books, and edited several conference books on operational research, computational intelligence, fuzzy logic, quality, and manufacturing systems design. He is also editor of the *Turkish Journal of Fuzzy Systems* and serving on the board of several academic journals. Dr. Baykasoğlu may be reached at [adil.baykasoglu@deu.edu.tr](mailto:adil.baykasoglu@deu.edu.tr)

**RİZVAN EROL** received his Ph.D. degree in Industrial and Management Systems Engineering from Arizona State University in 1996. He is currently professor and chairperson of Industrial Engineering at Cukurova University in Turkey. His main research areas are applied operations research, supply chain management, and health systems. Dr. Erol may be reached at [rerol@cu.edu.tr](mailto:rerol@cu.edu.tr)

**ALPER EKİNCİ** received his B.Sc. degree in Industrial Engineering from the University of Gaziantep in 2012. He is currently studying towards the Master of Science Workflow Scheduling Using Multi-Agent Systems in a Dynamically Changing Environment under the supervision of Vahit Kaplanoğlu. His research interests include artificial intelligence and its applications in multi-agent-based machine scheduling. Mr. Ekinci may be reached at [alper ekinci-ae@gmail.com](mailto:alper ekinci-ae@gmail.com)

**MELEK DEMIRTAŞ** received her B.Sc. and M.Sc. degrees in Industrial Engineering from Cukurova University, Department of Industrial Engineering, in 2010 and 2013, respectively. She is currently studying towards her Ph.D. under the supervision of Cenk Sahin. Her research interests include multi-agent-based machine scheduling and supply chain management. Ms. Demirtaş may be reached at [demirtasm@cu.edu.tr](mailto:demirtasm@cu.edu.tr)

# INTRODUCING KINEMATICS INTO ROBOTIC OPERATING SYSTEMS

Asad Yousuf, Savannah State University; William Lehman, Bill's Robotic Solutions; Mir Hayder, Savannah State University; Mohamad Mustafa, Savannah State University

## Abstract

The study of kinematics is essential to robotics. A robot, to perform most applications, needs to process positional data and transform data from one frame of reference to another. Robots have sensors, links, and actuators, each with its own frame of reference; so transformations between reference frames can be quite tedious. Traditionally, kinematics for robots is introduced to students using MATLAB and the Robotic Toolbox. In this study, the authors examined the introduction of kinematics for robotics with the features and tools available in the open source Robot Operating System (ROS). ROS implements tools for kinematics transforms (`tf`) as a key part of the ROS core libraries.

ROS defines robots with the unified robot description format (URDF) standard based upon extensible markup language (XML). URDF is, in many respects, similar to the Denavit-Hartenberg (D-H) convention but with significant additional enhancements. Students in electronic engineering technology (EET) were introduced to kinematics and ROS so they would have greater insight into engineering projects involving robotics. It was discovered that using ROS in robotics projects not only makes the projects more interesting to students, but also gives students an authentic experience with distributive systems and odometry sensors. Kinematics for robots uses linear algebra, matrices, natural logarithms (Euler's equation), imaginary numbers and trigonometry. The areas of mathematics were used to introduce kinematics for robotics to EET students to understand electricity, electric fields, and circuit theory. Emphasis was placed on matrix operations, operations involving trigonometry functions and imaginary numbers. The authors summarize here the results of this approach.

## Introduction

The study of kinematics is a key tool in both industrial and mobile robotics. Robots have sensors, links, and actuators, each with its own frame of reference; so transformations between reference frames can be quite tedious. Software makes transforms easy to perform and automatic, but students need to understand kinematics to use the software [1]. Labs were designed for EET students to give them basic kinematic concepts, while gaining experience with ROS. In this paper, kinematic theory is presented to give the

reader a good idea of what kinematic concepts were presented in the lab. Also in the labs were detailed descriptions of how ROS can be used to learn kinematics.

The topics covered for the kinematic labs are depicted in Figure 1. Euler angles tend to be intuitive to describe robot motion, but have issues when angles approach 90°. Quaternions are an alternative to Euler angles but are not intuitive to use. Quaternions were treated as black boxes and Euler angles were used for inputs to the robot model to have the best of both descriptions of rotation [2]. Joints used in labs were revolute or prismatic. Other joint types were approximated in ROS using combinations of revolute and prismatic joints. The joint types were limited to keep the introduction to kinematics simple.

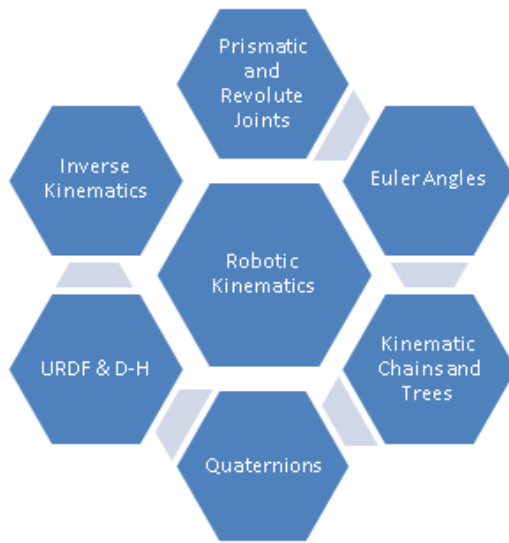
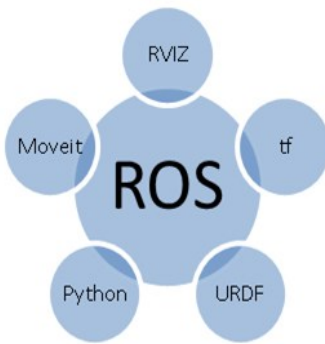


Figure 1. Robotic Kinematic Topics for Labs

Joints in robots are usually combined in a series to form chains. The robot modeling software allowed for chains to be combined into tree-like structures. A good example of a kinematic tree would be a robot with two or more arms. Forward kinematics determines the position of the robot, given the joint rotations or distance for prismatic sliding joints. Inverse kinematics is more difficult than forward kinematics since it is needed to find one or more ways to move a robot to a given point in space. Where there is usually a solution in forward kinematic problems, there may be multiple or no solutions in an inverse kinematic problem.

# Robotic Operating System

Kinematics was explored using software packages. ROS has a number of software packages that deal with kinematics (see Figure 2). To demonstrate the kinematic concepts from Figure 1, more than one software package was used from Figure 2. RVIZ is a robot simulator that can display a URDF robot model in 3D along with data from other sensors such as cameras. All the labs take advantage of RVIZ to demonstrate the six kinematic concepts in Figure 1.



**Figure 2. Software Packages in ROS for Labs**

The tf software package provides a library of kinematic routines that provide all of the mathematical functions needed to transform kinematic data from one frame of reference to another in robot manipulators. Transforms in ROS are made on positional data in both space and time. There are good tutorials in ROS on how data are transformed in the temporal domain. In this study, examples and labs were based on positional data that were constant so that extrapolation in time could be ignored. Time was important but could be ignored to “keep it simple” for students [3]. URDF is a XML modeling language capable of modeling most robots. Python is a programming language with interfaces to the ROS system. Software packages in ROS are written mainly in Python, Lisp, and C++. Python interpreter was used much like a calculator. RVIZ GUI will display robot information and the results will be confirmed using calculations made in Python. MoveIt is a fascinating software package for controlling robot arms and manipulators. The labs developed to introduce students to robot kinematics are listed in Table 1.

Lab 1 dealt with analyzing views of robots from different frames of reference and converting quaternions to and from axis angle representation. In Lab 2, the students converted quaternions to and from Euler angles using the Python programming language. In Lab 3, students learned to read and write URDF files with the Linux Ubuntu screen editor gedit. The extension to Lab 3 exposed students to converting D-H

tables to URDF files. Finally, students confirmed whether the URDF model was correct with the RVIZ robot simulator. Lab 4 offered the opportunity to run a number of inverse algorithms from OMPL using both the Willow Garage PR2 and 6R robot [4]. Of all the labs in Table 1, Labs 1–3 dealt with concepts in forward kinematics and Lab 4 in inverse kinematics.

**Table 1. Titles of Labs**

Lab	Title
1	RVIZ and PYTHON with simple robot manipulator model
2	RVIZ, TF, and PYTHON with aircraft robot model
2A	Finding position and interpolation with quaternions
3	URDF and hydra robot models
3A	Converting D-H tables to URDF models
4	MoveIt and inverse kinematics
4A	Evaluating student designed robot

## Lab 1: RVIZ and PYTHON with a Simple Robot Manipulator Model

In this lab, students learned how to use the RVIZ robot simulator and convert quaternions to/from an axis angle representation. Python programming language was used to make the manual calculations and confirm whether ROS was working as expected (see Figure 3). Python is an interpreted language and supported by the ROS.

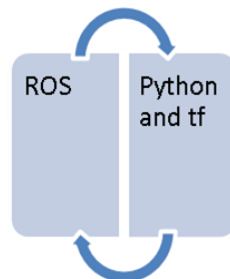


**Figure 3. Setup for Lab 1**

There were four sections in this lab:

1. Setup and RVIZ features
2. Converting from quaternion to axis angle representation
3. Frames of reference
4. Robot arm movement sequence

Setup guided the students through the startup of RVIZ, Robot State Publisher, and terminals. Features of the RVIZ display were explored. Quaternions to axis angle representation were converted to get useful information from the quaternion. The frames of reference in the chain of links was also changed to take different measurements. Finally, the sequences of moving arm joints were explored to set the robot to different positions in 3D space. Figure 4 represents the RVIZ robot simulator showing the robot arm. The position is shown on the RVIZ screen along with relative position using quaternions for the orientation. The robot state publisher screen is also displayed with sliders to control the robot arm [5]. Figure 5 represents the RVIS robot simulator showing the robot arm visuals turned off to reveal the axis systems of each frame.

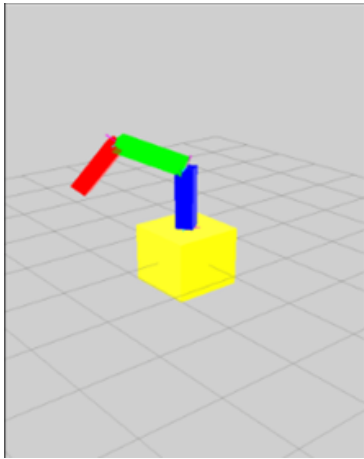


**Figure 4. RVIZ Simulator and State Publisher Window**

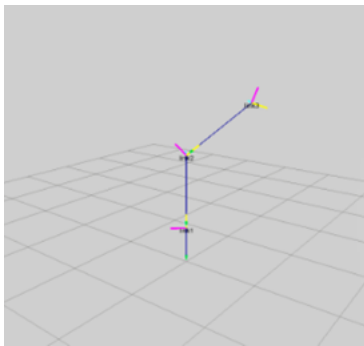


**Figure 5. Joint Conventions and 3D Axis**

## Quaternions

Axis angle is somewhat intuitive and similar to quaternions but in 3D. Axis angle can be converted to and from Euler angles and to and from quaternions. Equations (1)-(11) convert the axis angle vector to a quaternion [6]:

$$q1 = \sin\left(\frac{\alpha}{2}\right)\cos\beta_x \quad (1)$$

$$q2 = \sin\left(\frac{\alpha}{2}\right)\cos\beta_y \quad (2)$$

$$q3 = \sin\left(\frac{\alpha}{2}\right)\cos\beta_z \quad (3)$$

The quaternion was normalized, so Equation (4) was applied.

$$q1^2 + q2^2 + q3^2 + q4^2 = 1 \quad (4)$$

Equations (5)-(8) convert a quaternion to an axis angle vector.

$$\alpha = 2\cos^{-1}(q4) \quad (5)$$

$$x = \frac{q1}{\sqrt{1-q4^2}} \quad (6)$$

$$y = \frac{q2}{\sqrt{1-q4^2}} \quad (7)$$

$$z = \frac{q3}{\sqrt{1-q4^2}} \quad (8)$$

The direction cosine angles can be found using Equations (9)-(11):

$$\beta_x = \cos^{-1} x \quad (9)$$

$$\beta_y = \cos^{-1} y \quad (10)$$

$$\beta_z = \cos^{-1} z \quad (11)$$

Example:

Given the quaternion

$$q1 = 0.293802$$

$$q2 = -0.0957684$$

$$q3 = -0.294745$$

$$q4 = 0.904231$$

The quaternion is normalized

$$1 = q1^2 + q2^2 + q3^2 + q4^2 = 0.999999518$$

$$a = 0.427043673$$

$$\alpha = 2\cos^{-1}(q4) = 0.8824416 = 50.56^\circ$$

$$x = 0.6829905$$

$$y = -0.2242590$$

$$z = -0.6901987$$

It should be noted that  $x^2 + y^2 + z^2 = 1$ , and is thus normalized.

$$\beta_x = \cos^{-1} x = 46.5^\circ$$

$$\beta_y = \cos^{-1} y = 77.4^\circ$$

$$\beta_z = \cos^{-1} z = 133.6^\circ$$

distances from one point in the environment to another. The tf library is used in ROS to perform this task.

## Lab 2: RVIZ, TF, and PYTHON with an Aircraft Robot Model

In this lab, students learned how to use the RVIZ robot simulator, Python programming interpreter, and ROS tf library to study Euler angles. The robot state publisher allows for the robot model in RVIZ to be controlled with sliders (see Figure 6). There were three sections in this lab:

1. Euler angles and gimbal lock
2. Converting quaternions to and from Euler angles
3. Frames of reference and the tf transform

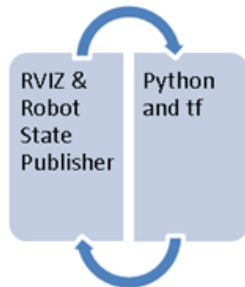
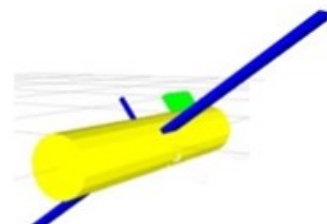


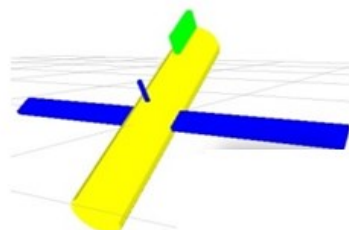
**Figure 6. Setup for Lab 2**

Euler angles are expressed in terms of roll, pitch, and yaw to specify the orientation of an aircraft. In ROS, roll is a rotation about the x axis, pitch is a rotation about the y axis, and yaw is a rotation about the z axis (see Figure 7). All rotations in ROS follow the right-hand rule for direction of rotation [7].

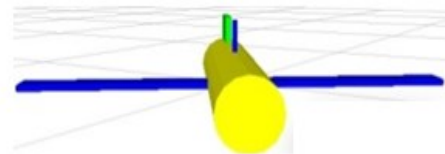
Table 2 shows the combinations of possible Euler angles. It should be noted that Tait-Bray angles are also referred to as Euler angles. The tf library provides two ways to convert Euler angles to quaternions with any of the combinations in Table 2. The tf library can also provide a convenient conversion from quaternions to Euler angles [8]. Euler angles are intuitive to use except that there are issues with Gimbal Lock. Quaternions avoid the issues of Euler angles, but are difficult to visualize. This dilemma can be solved by converting to and from Euler angles [9]. Using multiple frames of reference for a robot makes it easy to calculate angles and



(a) Roll



(b) Pitch



(c) Yaw

**Figure 7. Roll, Pitch, and Yaw of an Aircraft**

**Table 2. Euler Angle Combinations**

Proper Euler Angles	Tait-Bray Angles
RYR	RYP
RPR	RPY
PRP	PRY
PYP	PYR
YPY	YPR
YRY	YRP

---

## Lab 2A: Finding Position and Interpolation with Quaternions

In this extension to Lab 2, position was determined from Equation (12) and interpolation between two quaternions was found with the SLERP algorithm of Equation (12):

$$Q P_1 Q^* = P_2 \quad (12)$$

where,  $Q$  is the quaternion;  $Q^*$  is the conjugate of the quaternion,  $Q$ ;  $Q$  and  $Q^*$  are both normalized quaternions; and,  $P_1$  is a vector in the form  $[x, y, z, 0]$  and is not normalized. The first half of the calculation is a quaternion multiplied between  $Q$  and  $P_1$ . The results of the multiplication are a quaternion, which in turn is multiplied by the  $Q^*$  quaternion. Position 2 is also a vector in the form  $[x, y, z, 0]$ . Interpolation between two quaternions was found with the SLERP algorithm, which was implemented in Python [10]. Students determined the change in position between successive frames using Equation (12).

## Lab 3: URDF and Hydra Robot Models

In this lab, students learned how the Unified Robot Description Format (URDF) describes robots and could use it to design their own robot. The Ubuntu Linux editor, gedit, was used to modify and create URDF text files. RVIZ, a robot simulator, and the robot state publisher in ROS, were used to display and control the robot models [11]. There were five sections in this lab:

1. URDF format and simple robot model
2. Ubuntu Linux graphical screen editor gedit
3. Hydra robot example
4. Hydra robot URDF models
5. Design a robot URDF model

URDF can be used to model a robot with links (members) connected by joints in a chain or tree. Most industrial robots can be modeled by chains of joints offset by links. Multi-arm robots can be modeled with a tree data structure of joints connected by links to a base link. The transmission element will not be covered in this lab at this point, since all the robots needed are created by chains or trees. Other elements of URDF such as sensors are also not used. There are two main types of URDF XML elements that were needed to create robot links and joints. Link elements (or blocks) can contain elements for inertial properties, visual properties, and collision properties. Joint elements can contain elements for origin, parent link name, child link name, axis of rotation/translation, calibration, dynamics, limit, mimic another joint, and safety controller information. The kine-

matic chain or tree of Figure 8 can be represented by a graph of links connected though joints between each link and other links.

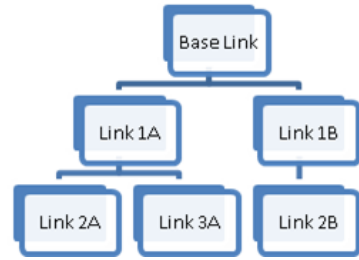


**Figure 8. Kinematic Tree**

Link 1A is moved by the joint between the base link and Link 1A. Link 1A is connected to a joint between Link 1A and Link 2A that moves Link 2A. Link 1A is also connected to a joint between Link 1A and Link 3A, which moves Link 3A. Each Link is moved by a single joint but may be connected to a number of joints that move other links. In URDF terminology, multiple joints can be connected to one link, but the link can only be a child in one of the joints connected to it and must be a parent to all the other joints connected to it. The base link is the first link in the tree and is special. The origin of the axis system to world coordinates  $x$ ,  $y$ , and  $z$  was determined from the odometry frame (/odom) and map. In the next example, the robot arm axis origin was located at world coordinate 0, 0, 0. It should be noted the students received a graph of the kinematic tree or chain with the urdf\_graphviz command entered into the terminal [12].

Link elements must have the “name” attributes for the link. The inertial and collision properties for the link are not included, except where it will be connected to a prismatic type joint. The visual information can be provided by specifying a rectangle, sphere, or cylinder shape for the link or a mesh. Although the mesh produced by a computer aided design (CAD) program can be very pleasing to the eye, it was kept simple with a rectangle or cylinder shape. As a convention in the design of the robots for the labs, all of the link and joint elements were grouped together for readability of the URDF file [13], see Figure 9. The joint element had a name and an attribute for the type of joint. Only a revolute, continuous, or prismatic type was selected for the joint. The ROS continuous joint type in actuality is a revolute. In URDF, a continuous joint is a revolute joint with the angle of rotation of 360°, where the revolute joint limits of rotation must be specified. The joint attaches a parent link to a child link. The child link can be a parent link to one or more other links in a chain or tree. The child link, however, can never be connected through a series of joints and links back to its parent link making a loop [14].

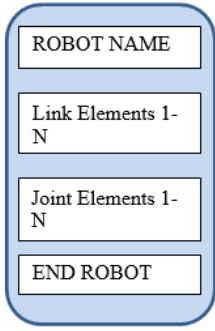


**Figure 9. Types of URDF XML Blocks**

An example link element can be found in Figure 10. The link could have been named anything to identify it, but it was named “link2” as it was the second link in the chain. The inertial and collision information was skipped, not because it was not useful but rather to keep the example simple. The visual element contained the geometry element, which set the type of display using the geometry element. The box element was inside the geometry element. The box element set the x, y, z sizes of the rectangle. The visual also contained the material element, which set the color of the rectangle link. This link was set to an arbitrary color to distinguish it from other links in the RVIS simulator display.

```
<link name="link2">
<visual>
  <geometry>
    <box size="1 0.25 0.25"/>
  </geometry>
  <origin rpy="0 1.571 0" xyz="0 0 0.5"/>
  <material name="linkc2">
    <color rgba="1 0 1 1"/>
  </material>
</visual>
</link>
```

**Figure 10. URDF XML Element Link Block**

The visual also has the origin element inside it. The origin rotates the linkage visual display using roll, pitch, and yaw angles. Roll is about the x axis, pitch is rotation about the y axis, and yaw is rotation about the z axis. In the above example, the rectangle was rotated 90° from the long side on the x axis to now point along the z axis. The link was offset 0.5 meters above the origin of the base link. The robot was actually buried in the floor in a hole with 0.5 meters deep. Syntax of the XML elements had the form “<label parameters>” followed by other elements and a “/>” or “</label>” [15].

Next, a joint XML element was examined (see Figure 11). The joint must have some name, which should make

sense to identify where on the robot it resides. In this example, it was labeled as “link1\_link2”, since the link named link1 was connected to the link named link2. The joint was a revolute type with no limits on rotation angle, so a continuous type was chosen. The parent link was link1 and the child link was link2.

```
<joint name="link1_link2"
type="continuous">
<parent link="link1"/>
<child link="link2"/>
<axis xyz="1 0 0" />
<origin rpy="0 0 0" xyz="0 0
1.0"/>
</joint>
```

**Figure 11. URDF XML Joint Element Example**

The axis element specified the axis that the joint would revolve around, which in this case was x. The origin xyz attribute was an offset of the joint from the parent joint origin to the child’s joint origin. The origin rpy parameter was a roll, pitch, and yaw rotation on the child’s joint frame of reference. The robot URDF examples with prismatic joints were slightly more complex since prismatic joints require limit and safety parameters not required for continuous joint types. The following command in the terminal window can be used in ROS to check the syntax of the URDF file.

```
rosrun urdfdom check_urdf filename.urdf
```

### Lab 3A: Converting a D-H Table to a URDF Model

Denavit-Hartenberg (D-H) conventions ease the process of calculating the position and orientation of frames in a kinematic chain [16]. As noted earlier, URDF can be used to model robots that are kinematic trees. URDF does not require axis systems for frames to only rotate about the z axis. URDF actually uses an arbitrary axis for revolute or prismatic joints. However, the parameters of the URDF joint variables can be shown in a table analogous to D-H parameters. To demonstrate, the axis system was used in Figure 12 in order to make the D-H table for the 3R robot similar to the 3R robot introduced earlier. The  $\theta$  variable represents rotation about the z axis of the joint. The  $d$  parameter is the distance along the z axis to the next joint. The  $d$  parameter is also a variable in the case of prismatic joints. The “ $a$ ” parameter is the distance of each common normal or the offset between joints. Finally, the  $\alpha$  parameter is the angle between the current joint,  $i$ , and the next joint  $i+1$ .

The parameters in the D-H table can be translated to parameters in the URDF joint element [17]. Figure 12 has the y axis going into the page for Joint 1 and the z axis coming out of the page for Joints 2 and 3. The parameters of the URDF joint elements can be enumerated in a table similar in concept to the D-H table (see Table 3). For a simple kinematic chain, there would be a single corresponding table to model the joints in the robot. For a kinematic tree, multiple joint element parameter tables can be used to represent each kinematic chain in the tree. The  $d_i$  parameters will always be placed in the corresponding Joint + 1 z axis offset between Joint i and Joint i+1. The  $\alpha_i$  parameter is the offset between Joint i and Joint i+1 along the x axis of Joint I and joint i+1.

The robot has to be placed in world coordinates in ROS for a convenient orientation and to simplify calculations. The 3R robot is placed at the origin of the world axis system and aligned with that axis system. This means that instead of rotating Joint 2 by 90°, Joint 2 will be rotated so that the z axis comes out of the page. Joints 3 and 4 will also be rotated since Joint 2 is attached to Joint 3, which is attached to Joint 4. Joint 4 is a fixed type joint and does not move. Joint 4 is included to show the  $a_3$  parameter in the D-H table. Dummy URDF link elements are set up with simple names such as Link\_1, Link\_2, etc. No information is needed in the URDF link element since visual elements of the robot model are not being displayed in the lab. A base link (not included in D-H table) is needed to attach the robot model to the world coordinates. The parameters from the table to the URDF joint element are also straightforward (see Table 4). The x, y, z parameters correspond to the origin xyz parameter in the URDF joint element. The roll, pitch, and yaw parameters corresponds to the origin rpy parameter in the URDF joint element. Finally, the axis parameters define a unit vector pointing along the z axis. Since this is a revolute joint, the joint will rotate around the z axis.

After students create the URDF joint element parameter, given the D-H table they perform, they convert it to URDF and display the results in RVIZ to confirm that it matches the axis system orientation of Figure 12. The  $a_3$  parameter is between Joints 3 and 4. In Figure 13, the red axis is x, the green axis is y, and the blue axis is z.

**Table 4. URDF Joint Elements Parameters**

#	Joint Type	Joint Link #	Joint+1 Link #	x	y	z	Joint+1 Roll	Joint+1 Pitch	Joint+1 Yaw	Joint+1 Axis x	Joint+1 Axis y	Joint+1 Axis z
1	R	Base	1	0	0	$d_I$	0	0	0	0	0	1
2	R	1	2	$\alpha_2$	0	0	90°	0	0	0	0	1
3	R	2	3	$\alpha_3$	0	0	0	0	0	0	0	1
4	Fixed	3	4	0	0	0	0	0	0	-	-	-

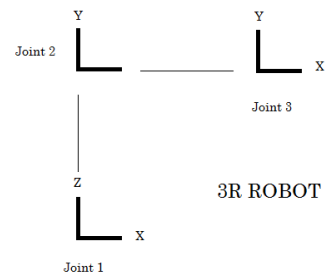


**Figure 12. Axis 3R Robot**

**Table 3. D-H Parameters for 3R Robot**

Link	$\theta_i$	$d_i$	$\alpha_i$	$a_i$
1	$\theta_1$	$d_I$	0	90°
2	$\theta_2$	0	$\alpha_2$	0
3	$\theta_3$	0	$\alpha_3$	0

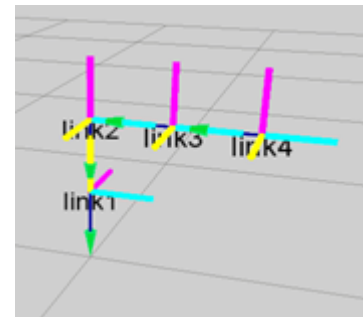


**Figure 13. D-H 3R Robot Displayed in RVIZ**

## Lab 4: MoveIt and Inverse Kinematics

There were two sections in this lab:

1. Setup MoveIt
2. Students record benchmark information for each configuration including planning time [18-20]
3. Smoothness of trajectory is noted

In this lab, the advantage of existing demonstration software that uses the PR2 and 6R robot was taken. Students set the robots to different start and end states for the PR2 and 6R robots. Students then watched the robot perform each motion using the planning algorithm from the OMPL library and recorded the time it took to calculate a solution. There is an excellent tutorial that walks the students through the setup and use of the demo software [21]. In the lab, students selected from among the following planners to perform the path selected for the PR2 or 6R robot [22]:

1. Bi-directional kinematics planning by interior-exterior cell exploration (BKPIECE)
2. Kinematics planning by interior-exterior cell exploration (KPIECE)
3. Lazy bi-directional kinematics planning by interior-exterior cell exploration (LBKPIECE)
4. Expansion space trees (EST)
5. Probabilistic roadmap method (PRM)
6. Transition-based rapidly-exploring random trees

Building upon the RVIZ plugin tutorial, the students were presented with a problem requiring building a table for the selected algorithm using different planning groups and other planning parameters. The students then recorded the results of the test in a table of planning parameters versus time and evaluated the results. Objects were inserted into the scene to demonstrate and test planning with obstacles [23]. The goal of the lab was to give them some insight into the complexity of inverse kinematics (see Figure 14).

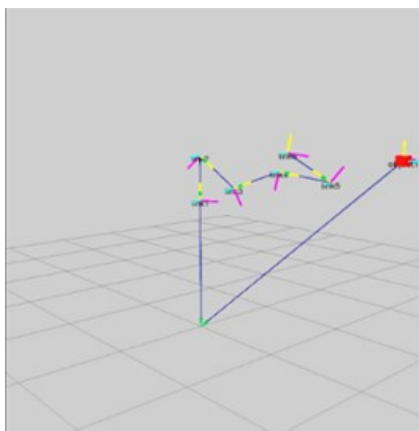


**Figure 14. Demo Software Screen with 6R Robot**

### Lab 4A: Evaluating the Student-designed Robot

The students evaluated the robot that they designed in Lab 3. They used MoveIt setup assistant to configure their robot. The students set up pre-configured poses for their

robot and followed a procedure similar to Lab 4 to evaluate the robot [24].

## Conclusion

In this paper, the authors presented the major features of the seven labs developed to introduce students to kinematics using ROS. Labs were developed for students to use accelerometers and gyros to track real robots using ROS. The introduction to robotic kinematics should provide the background to understanding kinematic aspects of these labs. The robot toolbox provides a powerful system for introducing students to robotic kinematics [25]. Given the limited classroom time available for kinematics, the study focused on forward kinematics and ROS. Given more time in the robotics course, the authors would have included both MATLAB and ROS. MATLAB has recently developed a robot toolbox that allows MATLAB to connect to ROS. Although MATLAB can connect to a ROS system, there is a definite value to introducing kinematic concepts in ROS to lower the ROS learning curve and re-enforcing kinematic concepts. The labs were tested with the Hydro and Indigo versions of ROS, but future plans are to include Jade. Information on how to obtain the free open source labs outlined in this paper can be found at the website for Brazen Head Automation [26].

## References

- [1] Tully, F. (2013). Technologies for Practical Robot Applications (TePRA). *Proceedings of 2013 IEEE International Conference on Open-Source Software workshop*. ISSN 2325-0526, pages 1-6. doi 10.1109/TePRA.2013.6556373.
- [2] James, D. (2006). Representing Attitude: Euler Angles, Unit Quaternions, and Rotation Vectors. *Matrix*, Citeseer.
- [3] Robot Operating System (n.d.). Retrieved October 25, 2015, from [www.wiki.ros.org/tf](http://www.wiki.ros.org/tf)
- [4] Open Motion Planning Library: A Primer. <http://ompl.kavrakilab.org>
- [5] Bruno, S., & Oussama, K. (2008). Handbook of Robotics, *Digital Design*. Springer.
- [6] Maths-Rotation Conversions (n.d.). Retrieved on October 25, 2015, from [www.euclideanspace.com/maths/geometry/rotations/conversions/](http://www.euclideanspace.com/maths/geometry/rotations/conversions/)
- [7] Coordinate Frames for Mobile Platforms (n.d.). Retrieved on October 25, 2015, from <http://www.ros.org/reps/rep-0105.html>
- [8] Standard Units Measure and Coordinate Conventions (n.d.). Retrieved on October 25, 2015, from <http://www.ros.org/reps/rep-0103.html>

- 
- [9] Robot Operating System (n.d.). Retrieved October 25, 2015, from [wiki.ros.org/geometry/CoordinateFrameConventions](http://wiki.ros.org/geometry/CoordinateFrameConventions)
- [10] van Oosten, J. (2012). Understanding Quaternions. *3D Game Engine Programming*.
- [11] Robot Operating System (n.d.). Retrieved October 25, 2015, from <http://wiki.ros.org/urdf/Tutorials>
- [12] Robot Operating System (n.d.). Retrieved October 25, 2015, from [wiki.ros.org/urdfoveit.ros.org/urdf](http://wiki.ros.org/urdfoveit.ros.org/urdf)
- [13] Robot Operating System (n.d.). Retrieved October 25, 2015, from [wiki.ros.org/urdf/XML/link](http://wiki.ros.org/urdf/XML/link)
- [14] Robot Operating System (n.d.). Retrieved October 25, 2015, from [wiki.ros.org/urdf/XML/joint](http://wiki.ros.org/urdf/XML/joint)
- [15] Robot Operating System (n.d.). Retrieved October 25, 2015, from [en.wikipedia.org/wiki/XML](http://en.wikipedia.org/wiki/XML)
- [16] Spong, M. W., Hutchinson, S., & Vidyasagar, M. (2004). Robot Dynamics and Control. Second Edition, *Chapter 3 Forward Kinematics: The Denavit-Hartenberg Convention*. Wiley.
- [17] Thomas, F. (2012). Solved Problems in Robot Kinematics Using the Robotic Toolbox. *Universitat Politecnica DE Catalunya Barcelona Tech*. Barcelona, Spain.
- [18] Corke, P. (2013). Robotics, Vision and Control. Edition 1, *Section 8.1.4 Jacobian and Manipulability*. Springer.
- [19] Tsai, T. (1986). Workspace Geometric Characterization and Manipulability of Industrial Robots. *PhD thesis, the Graduate School of Ohio State University*.
- [20] Vahrenkamp, N., Asfour, T., Metta, G., Sandini, G., & Dillmann, R. (2012). Manipulability Analysis. *Proceedings of IEEE-RAS International Conference on Humanoid Robots (Humanoids)*. Osaka, Japan.
- [21] Robot Operating System (n.d.). Retrieved Oct 25, 2015, from <http://moveit.ros.org/documentation/tutorials/>
- [22] Sucan, I. A., Moll, M. & Kavraki, L. E. (2012). The Open Motion Planning Library. *IEEE Robotics and Automation Magazine*.
- [23] Prats, M, Sucan, I., & Chitta, S. (n.d.). Workspace Analysis. (n.d.). Retrieved October 25, 2015, from <http://moveit.ros.org/assets/pdfs/2013/icra2013tutorial/ICRATutorial-MoveIt.pdf>
- [24] Chitta, S., & Sucan, I. (2013). MoveIt. *ROS Devel-oper Conference*. Stuttgart, Germany.
- [25] Corke, P. (2014). Robotic Toolbox for Matlab. *Release 9*. Retrieved October 25, 2015, from <http://www.petercorke.com/robot>
- [26] Brazen Head Automation (n.d.). Retrieved October 25, 2015, from <http://www.brazenbot.com>

## Biographies

**ASAD YOUSUF** is a professor at Savannah State University. He earned his B.S. degree from N.E.D University, M.S. degree from the University of Cincinnati, and doctoral degree from the University of Georgia. Dr. Yousuf is a registered professional engineer in the state of Georgia. He is also a Microsoft Certified Systems Engineer. Dr. Yousuf may be reached at [yousufa@savannahstate.edu](mailto:yousufa@savannahstate.edu)

**WILLIAM LEHMAN** is president of Bill's Robotic Solutions, which he started in 2013. He has over 20 years of experience in software and hardware development. He has worked on numerous projects in digital communication systems, robotics, and aerospace applications. Mr. Lehman received his B.S. degree in Electrical Engineering from the Catholic University of America. Mr. Lehman may be reached at [tec.teacher.lehman@gmail.com](mailto:tec.teacher.lehman@gmail.com)

**MIR HAYDER** is an assistant professor in the Department of Engineering Technology at Savannah State University. He received his Ph.D. in mechanical engineering from McGill University. His research interests include robotics, fluid-structure interaction, syngas and blended fuel combustion, and flow and structural simulations. Dr. Hayder may be reached at [hayderm@savannahstate.edu](mailto:hayderm@savannahstate.edu)

**MOHAMAD MUSTAFA** is a professor of civil engineering technology at Savannah State University. He had six years' of industrial experience prior to teaching at SSU. He received his B.S., M.S., and Ph.D. degrees in civil engineering from Wayne State University. His research interests include sensors applications in civil engineering. Dr. Mustafa may be reached at [mustafam@savannahstate.edu](mailto:mustafam@savannahstate.edu)

# FUZZY LOGIC CONTROL OF A QUADROTOR

Ming Li, University of Michigan-Flint

## Abstract

Quadrrotors have attracted considerable research interests because they are highly maneuverable. Quadrrotors can achieve quasi-stationary flight as well as vertical take-off and landing, which enable them to be utilized for various applications such as surveillance and reconnaissance, search and rescue, environment monitoring and so on. However, since quadrrotors are often utilized in complicated environments, damage to the structure of the quadrrotors may occur; for example, the tip of the blades may be broken. In this study, the author developed a fuzzy logic controller to provide fault accommodations under different structural health conditions for quadrrotors systems. The integration of health information and control strategies can optimize the performance of quadrrotors. The proposed method was tested on the simulated model of the Draganflyer. The simulation results of the quadrrotor operated under normal conditions and with component failure are presented here.

## Introduction

Small four-rotor helicopters have gained popularity in unmanned aerial vehicle applications. They can achieve quasi-stationary hovering in addition to vertical take-off and landing (VTOL) in limited space. Unlike regular helicopters, they are under actuated dynamic vehicles with four fixed-pitch-angle rotors. The motion of a quadrrotor is controlled by rotating the front and rear rotors counterclockwise and the left and right rotors clockwise. Using four rotors increases the payload capacity and maneuverability of the helicopter. But control of the system is very complicated, since all movements are highly dependent upon each other. Many studies have been carried out to optimize the control of quadrrotors. Gao et al. [1] designed a fuzzy adaptive PD (proportional-derivative) controller for a quadrrotor. Choi and Ahn [2] utilized a back-stepping-like feedback linearization method to control and stabilize a quadrrotor. Li et al. [3] adopted time-optimal control by using a genetic algorithm.

In this paper, the author presents a fuzzy logic control system for the quadrrotor under different health conditions. Fuzzy logic is based on the mathematical theory of fuzzy sets. It performs reasoning approximately rather than accurately with a series of if-then rules. With prior knowledge and experience turned into rules, fuzzy logic can simplify modeling and control of a complex nonlinear system reliably and efficiently. In several studies, fuzzy logic was ap-

plied in order to actively reconfigure the control scheme to maintain operations of the system when faults occur [4].

The approach in this current study was tested on the simulated model of the Draganflyer manufactured by RCToys [5], which is shown in Figure 1. With a structure assembled from low-cost components, the possibility of component failure may increase. It is necessary to identify and evaluate the health conditions of the system in order to optimize the control strategies of a quadrrotor. In the proposed approach, the possible structural health conditions of a quadrrotor were classified and the reconfiguration of the controller was automatically achieved so that stable and acceptable performance of the system could be maintained.



Figure 1. Draganflyer V Ti Quadrrotor

## Dynamic Model

The propulsion of the quadrrotor comes from four electric motors. The lift forces vary with the rotor speed. The difference in the lift forces tilts the quadrrotor and the quadrrotor accelerates along that direction. By increasing/reducing the speed of the front rotor while at the same time reducing/increasing the speed of the rear rotor, the pitch movement can be obtained [6]. By changing the speed of the lateral rotors with a similar approach, the roll movement can be obtained. By varying the speed of the two pairs of rotors together, the yaw movement can be obtained. Figure 2 shows the simplified model of the quadrrotor:

where,  $I = \{e_x, e_y, e_z\}$  denotes the inertial frame attached to the earth;  $A = \{e_1, e_2, e_3\}$  is a body fixed frame attached at

the center of mass of the quadrotor; and  $\phi$ ,  $\theta$ ,  $\psi$  are Euler angles, which denote roll, pitch, and yaw, respectively.

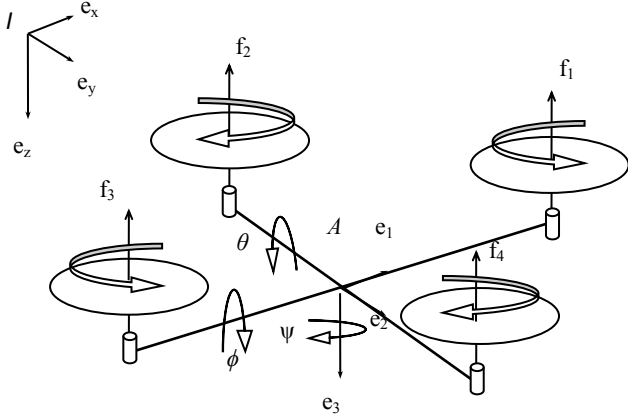


**Figure 2. Schematic Diagram of the Quadrotor**

The dynamic model of the helicopter was derived using Equations (1)-(5) [6], [7]:

$$\dot{\xi} = v \quad (1)$$

$$\dot{v} = ge_z - \frac{1}{m} TRe_z \quad (2)$$

$$\dot{R} = Rsk(\Omega) \quad (3)$$

$$I_f \dot{\Omega} = -\Omega \times I_f \Omega - G_a + \tau_a \quad (4)$$

$$I_r \dot{\omega}_i = \tau_i - Q_i \quad (5)$$

where,  $\xi = [x \ y \ z]^T$  and  $v = [v_x, v_y, v_z]^T$  denote the position and velocity of the origin of  $A$  with respect to  $I$ , respectively.

Equations (6) and (7) give the total thrust,  $T$ , and the rotational transformation matrix,  $R$ :

$$T = \sum_{i=1}^4 |f_i| \quad (6)$$

$$R = \begin{bmatrix} C_\theta C_\psi & C_\psi S_\theta S_\phi - S_\psi C_\theta & C_\psi S_\theta C_\phi + S_\psi S_\theta \\ C_\theta S_\psi & S_\psi S_\theta S_\phi + C_\psi C_\theta & S_\psi S_\theta C_\phi - C_\psi S_\theta \\ -S_\theta & S_\phi C_\theta & C_\phi C_\theta \end{bmatrix} \quad (7)$$

And,  $\Omega = \{\Omega_1, \Omega_2, \Omega_3\}^T$  denotes the angular velocity expressed in  $A$ , and  $I_f$  is the inertia matrix around the center of mass. Equation (8) gives the gyroscopic torque,  $G_a$ , and Equations (9)-(11) give each component of the torque:

$$G_a = \sum_{i=1}^4 I_r (\Omega \times e_z)(-1)^{i+1} \omega_i \quad (8)$$

$$\tau_a^1 = db(\omega_2^2 - \omega_4^2) \quad (9)$$

$$\tau_a^2 = db(\omega_1^2 - \omega_3^2) \quad (10)$$

$$\tau_a^3 = k(\omega_1^2 + \omega_3^2 - \omega_2^2 - \omega_4^2) \quad (11)$$

where,  $\tau_a = [\tau_a^1, \tau_a^2, \tau_a^3]^T$  denotes the airframe torques;  $k$  and  $b$  are proportional parameters that depend on the density of the air, the properties of the rotor blades, and other factors;  $d$  is the distance from the rotors to the center of mass of the quadrotor;  $\omega_i$  denotes the angular velocity of the rotor  $i$ ; and,  $I_r$  is the moment of inertia of a rotor around its axis.

## Fuzzy Logic Controller

As for flight guidance of UAVs, control systems are usually programmed to follow a planned path to reach to targets. However, as flight situations, health conditions, and other factors may vary during a mission, it is necessary that control systems adjust with the information from structural health monitoring in order to optimize the performance of the UAVs. Figure 3 shows the aforementioned control system using the integrated information of flight path and flight conditions simultaneously then determines the appropriate control strategies [8]. Flight conditions are mainly rotor performance and structural health integrity.

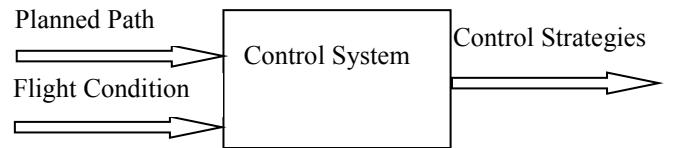


**Figure 3. A Control System Integrated with Flight Conditions**

In this current study, the flight condition and structural integrity were simulated and inputted to the control system. The fuzzy logic controller determined whether or not to continue a mission in case of component failures. Fuzzy logic is a fine choice for providing fault-tolerant control of the system. The set of rules can reconfigure the control parameters according to the health condition of the system. Figure 4 illustrates the Simulink model [9] implementing

the proposed approach. In this model, the flight condition is utilized to determine the health integrity of the system. The simulated condition of the rotors was evaluated with a health index, which was an input to the fuzzy logic controller. In this study, the given height was considered as the target of the mission. The fuzzy logic controller used the integrated information of targeted height as well as health index to guide the quadrotor to the target. It reconfigured the control surface as faults occurred; for example, if one or two rotors failed during the mission.

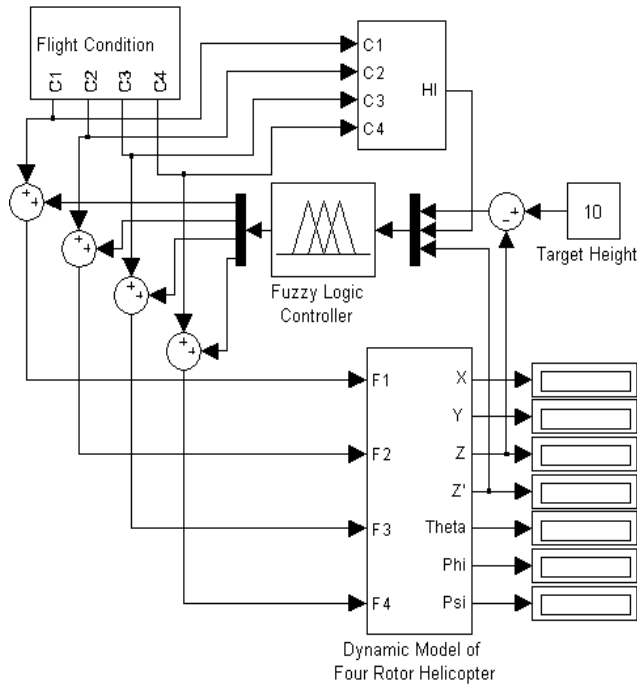


**Figure 4. Simulink Model of the Fuzzy Logic Control System**

## Results and Discussion

The input variables of the fuzzy logic controller were offset to the targeted height, vertical speed, and health index. Figure 5 shows the membership functions of the height offset, which is the difference of the current height to the targeted height. The membership functions represent when the quadrotor is close-up, mid-range, and far away from the targeted height. Figure 6 shows the membership functions of the speed settings, according to the offset height. If the quadrotor is close to the targeted height, the speed is low; if it is far away from the target, the speed should be high. Thus, based on the height offset and the speed of the quadrotor, the controller was designed to drive the offset to zero. At the same time, if the health condition changed as one or two rotors failed, the controller had to reconfigure the control strategies of the rotors.



**Figure 5. Membership Functions of Height Offset**

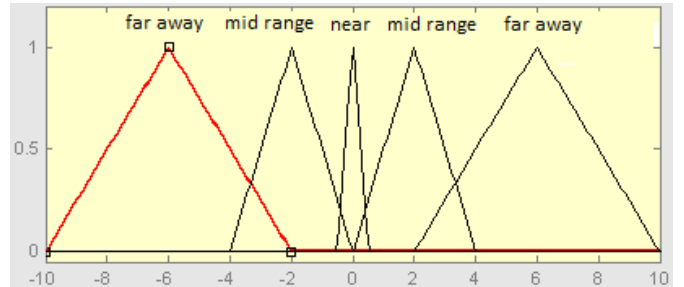


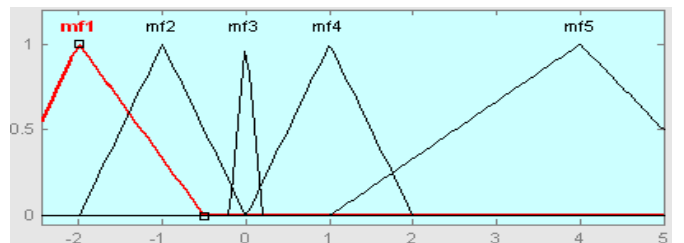
**Figure 6. Membership Functions of Vertical Speed**

The output of the fuzzy logic controller was the lift force of each rotor. The lift force is given by Equation (12):

$$f_i = -b\omega_i^2 e_3 \quad (12)$$

where,  $\omega_i$  is the rotating speed of rotor  $i$ , which can vary with the applied voltage.

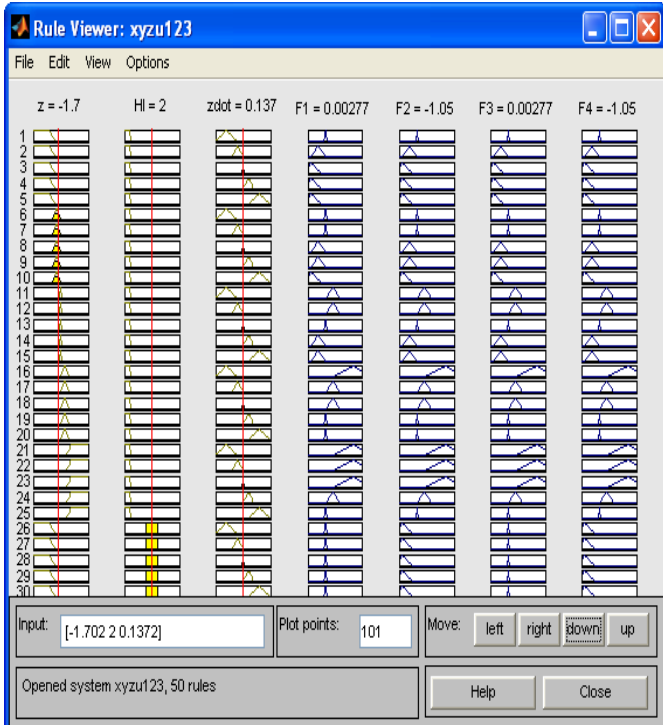
Membership functions of the output forces are presented in Figure 7, and 150 if-then rules were designed to determine the driving forces, according to the height offset, speed, and health index. Figure 8 shows the set of rules utilized by the fuzzy logic controller. Membership functions and rules need fine tuning to make the control parameters converge.



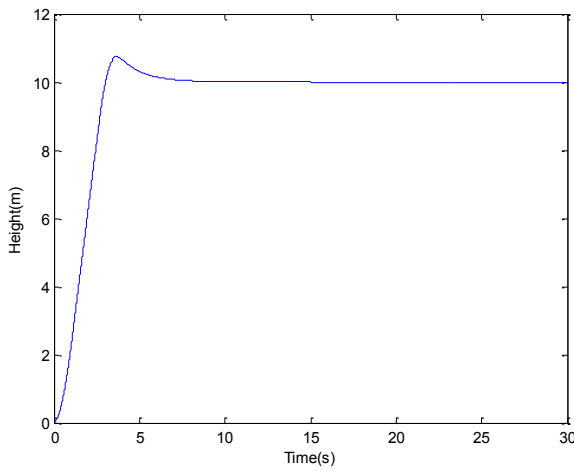
**Figure 7. Membership Functions of Output Forces**

Figure 9 shows the results of the quadrotor reaching the targeted height from the origin. It assumed that the health condition was perfect. As indicated from the graph, the helicopter climbed to the target under control of the fuzzy logic

controller; after a quick overshoot, it converged at the target height. The fuzzy logic controller also can provide fault accommodations when components fail. Figure 10 shows the simulation results when a fault occurred. The rotor labeled 1<sup>st</sup> failed at eight seconds. After the fault was identified, the health index was inputted to the controller. Based on the rules of the fuzzy logic controller, the output force for each rotor was reconfigured. From the graph, the quadrotor dropped first after the rotor failed. After the reconfiguration, the quadrotor climbed again and reached the target.



**Figure 8. Rule Viewer**



**Figure 9. Simulink Result with No Fault**

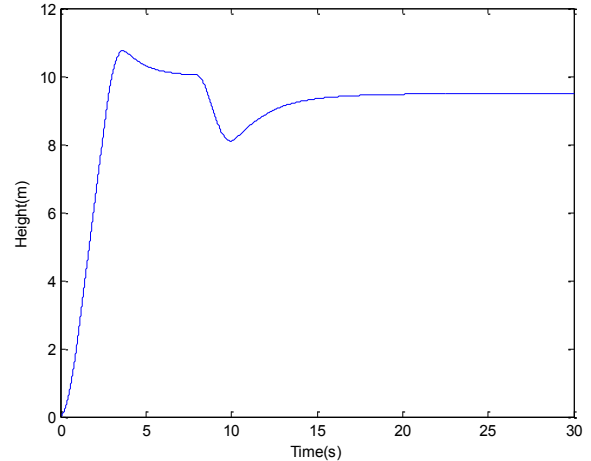


**Figure 10. Simulink Result with Fault Occurred**

## Conclusion

The goal of this study was to bring and keep the quadrotor to the desired vertical coordinate,  $z$ . In this study, a fuzzy logic controller was designed to provide fault accommodation under different health conditions of a quadrotor. Fuzzy logic is a fine choice for fault tolerant control. It is convenient to program and powerful in the reconfiguration of flight management, considering the health condition of the components. The initial setup of the fuzzy logic controller for the proposed application was simple. However, membership functions and rules needed fine tuning in order to optimize the control parameters. It is a tedious trial-and-error process. The number of rules increased dramatically when the identified fault modes were increased, which increased computation time. If a central microcontroller monitors all sensors, the efficiency of the control strategies would suffer with the increase of the fault modes. Multiple fuzzy logic controllers can be designed to run in parallel to increase the computational speed.

## References

- [1] Gao, H., Liu, C., Guo, D., & Liu, J. (2015). Fuzzy Adaptive PD Control for Quadrotor Helicopter. *Cyber Technology in Automation, Control, and Intelligent Systems (CYBER)*, 2015 IEEE International Conference, (pp. 281-286). Shenyang, China.
- [2] Choi, Y. C., & Ahn, H. S. (2015). Nonlinear Control of Quadrotor for Point Tracking: Actual Implementation and Experimental Tests. *IEEE/ASME Transactions on Mechatronics*, 20(3), 1179-1192.
- [3] Li, C. L., Yang, C. C., & Wu, C. J. (2006). Time-Optimal Control of a Hovering Quadrotor Helicopter.

- 
- Journal of Intelligent and Robotic Systems*, 45, 115-135.
- [4] Gao, Z., Ding, S. X., & Cecati, C. (2015). Real-Time Fault Diagnosis and Fault-Tolerant Control., *IEEE Transactions on Industrial Electronics*, 62(6), 3752-3756.
  - [5] Draganflyer V Ti PRO RC Gyro Stabilized Electric Helicopter. (n.d.). Retrieved November 7, 2015, from <http://www.rctoys.com/rc-toys-and-parts/DF-VTI/RC-HELICOPTERS.html>.
  - [6] Erginer, B., & Altug, E. (2007). Modeling and PD Control of a Quadrotor VTOL Vehicle. *Intelligent Vehicles Symposium, 2007 IEEE*, (pp. 894-899). Istanbul, Turkey.
  - [7] Tayebi, A., & McGilvray, S. (2006). Attitude Stabilization of a VTOL Quadrotor Aircraft. *IEEE Transactions on Systems Technology*, 14(3), 562-571.
  - [8] Bickraj, K., Pamphile, T., Yenilmez, A., Li, M., & Tansel, I. N. (2006). *Fuzzy Logic Based Integrated Controller for Unmanned Aerial Vehicles*. Paper presented at the Florida Conference on Recent Advances in Robotics (FCRAR 2006), Miami, Florida.
  - [9] Li, M., Demetgul, M., Li, X. H., Lago, H., & Tansel, I. N. (2009). *Fault Tolerant Fuzzy Logic Control for Four Rotor Helicopter*. Paper presented at the Florida Conference on Recent Advances in Robotics (FCRAR 2009), Jupiter, Florida.

## Biographies

**MING LI** is an assistant professor in the Department of Computer Science, Engineering and Physics at the University of Michigan-Flint. Dr. Li earned her Ph.D. in Mechanical and Materials Engineering from Florida International University in 2010. Her research interests include mechatronics, structural health monitoring, and robotics. Dr. Li may be reached at [minglilm@umflint.edu](mailto:minglilm@umflint.edu)

# A COMPARATIVE STUDY ON THE EFFECTIVENESS OF COATED AND UNCOATED TUNGSTEN CARBIDE TOOLS FOR DRY MACHINING OF Ti-6Al-4V

Muhammad P. Jahan, Western Kentucky University; Gregory K. Arbuckle, Western Kentucky University;  
Abdulhameed Dawood, Western Kentucky University

## Abstract

The dry and near-dry machining processes, commonly known as sustainable machining processes, are currently gaining popularity because of the increasing demand for green and environmentally friendly manufacturing processes. The objective of this study was to investigate the machinability of aerospace material Ti-6Al-4V (grade 5 titanium alloy) under dry machining conditions using both coated and uncoated tungsten carbide tools. An investigation was carried out to reduce tool wear and improve dry machining performance by applying a coating of titanium carbo-nitride (TiCN) and titanium aluminum nitride (TiAlN) on the tungsten carbide tools. Tool wear was found to be a serious issue in the machining of titanium alloys in dry conditions. The major problem of machining Ti-6Al-4V using uncoated carbide tools was alloying of workpiece materials to the tool surface, due to the lack of heat dissipation from the tool-workpiece interface and strong alloying tendency of Ti-6Al-4V. It was found that the adhesion to the cutting tool edges was significantly reduced for tools with TiCN and TiAlN coatings. Due to the minimal adhesion of the chips, tool wear was also reduced. In terms of surface finish, TiAlN-coated tools were found to provide lower average surface roughness compared to TiCN-coated and uncoated carbide tools. There was no significant difference in the machining time between coated and uncoated tools for the same machining conditions. Overall, surface roughness and tool wear were minimized with TiAlN-coated carbide tools during the machining of Ti-6Al-4V. The cutting speed of 50 m/min, feed rate of 0.5 mm/rev, and depth of cut of 0.3 mm with TiAlN-coated tools were found to be the optimum machining conditions for the dry machining of Ti-6Al-4V.

## Introduction

Titanium alloys are extensively used in aerospace and automotive industries due to their high specific strength (strength-to-weight ratio), superior mechanical and thermal properties, and excellent corrosion resistance. However, titanium alloys are commonly known as difficult-to-cut materials using conventional machining processes because of

their reactivity with tool materials, cutting speed limitation, chipping, and premature failure of the cutting tools [1-3]. The difficulty in the machining of titanium alloys is also associated with low thermal conductivity, high strength, and low young's modules of titanium [4]. Ti-6Al-4V, commonly known as grade 5 titanium alloy, is the most extensively used material among all titanium alloys, and has been found to have important applications in aerospace, automotive, and biomedical industries. Therefore, the machining of Ti-6Al-4V has been of great interest to researchers for many years.

Based on a recent report [5], the amount of used lubricants and coolant fluids was estimated to be around 38 Mt, which is expected to increase by 1.2% over the next few decades. Therefore, many researchers are focusing on the sustainable machining of aerospace materials in order to minimize carbon emissions into the environment and reduce the pollution generated from the machining processes [6]. Among the sustainable machining processes, dry machining, near-dry machining using minimum quantity lubrication (MQL), and cryogenic machining are the reported techniques for machining titanium alloys and other aerospace materials [5]. There have been many studies done on the machining of Ti-6Al-4V using MQL [6-9], high-pressure cooling [10], [11], and cryogenic machining conditions [12-14]. However, in this current study, that literature will not be discussed in detail, as the focus of this paper is on the effectiveness of coatings on the cutting tools, tool wear, and tool life during machining of Ti-6Al-4V.

Besides various cooling techniques, an investigation was carried out to enhance the machinability of titanium alloys by developing new cutting tools and providing various coatings on the existing cutting tool materials. Ezugwu and Wang [15] investigated the problems associated with the machining of titanium alloys and the possible reasons for tool wear and cutting tool failure during machining. They found that the straight tungsten carbide (WC-Co) cutting tools sustained their power in almost all machining conditions during machining of titanium alloys. They suggested that the chemical vapor deposition (CVD) coated carbides and ceramics could not be used, due to their reactivity with titanium and their relatively low fracture toughness and

poor thermal conductivity. They also proposed a new machining method of rotary cutting using ledge tools, which could be applied successfully for machining of titanium alloys. An attempt was also made to machine Ti-6Al-4V alloy with wurtzite boron nitride (wBN) cutting tools [16]. No significant difference was found between the wear mechanism of the wBN cutting tools and those of polycrystalline diamond (PCD) and polycrystalline cubic boron nitride (PCBN) tools. It was reported that the wBN-cBN composite tools could provide more economical machining of titanium alloys. Ezugwu et al. [17] investigated the effectiveness of cubic boron nitride (CBN) tools for machining of Ti-6Al-4V alloy with various coolant supplies. They found that the performance of CBN tools was poorer compared to that of uncoated carbide tools.

Che-Haron [18] investigated tool life and surface integrity during turning of Ti-alloy (Ti-6Al-2Sn-4Zr-6Mo) using two types of uncoated cemented carbide tools under dry cutting conditions. In his experiments, he used four different cutting speeds ranging from 45 m/min to 100 m/min and two different feed rates of 0.35 mm/rev and 0.25 mm/rev. The depth of cut was kept constant at 2.0 mm. The criteria used in his research to reject a tool were: 1) reaching the average flank wear to 0.4 mm or maximum flank wear to 0.7 mm; 2) getting notch at a depth of cut of 1.0 mm; 3) reaching a crater wear depth of 0.14 mm; 4) exceeding an average surface roughness,  $R_a$ , of more than 6  $\mu\text{m}$ ; and, 5) the occurrence of flaking or fracture. Considering these criteria, it was found that the coated tools provided higher tool life compared to uncoated tools. De Bruyn [19] considered high-speed machining of Ti-6Al-4V utilizing uncoated and PVD-coated carbide tools under dry conditions. They considered the tool life and the nature of the surface finish as the variables when analyzing cutting tool life. As per their study, PVD-coated carbide tools have comparatively higher tool life than uncoated tools.

Tuppen and Voice [20] developed models to predict tool life in the end milling of Ti-6Al-4V utilizing uncoated carbide tools under dry conditions. They utilized a central composite design (CCD) to build up the tool life model identified with essential cutting parameters. As indicated by their models, cutting rate was the principle element affecting tool life, after feed rate and pivotal depth of cut. He et al. [21] analyzed tool wear during the machining of particulate-reinforced titanium matrix composites (PTMCs), and observed that cracking and chipping of cutting tools occurred more often in uncoated tools, though pit wear was more common in coated tools. From the tool life analysis, it was found that the tool life of coated and uncoated carbide tools diminished rapidly at higher cutting velocities. They perceived that wet cutting was superior to dry cutting for coat-

ed carbide tools, and the utilization of oil-based coolant could extend the tool life of coated carbide tools.

Fanning [22] investigated the wear of cutting tools for turning Ti-6Al-4V with a specific end goal of creating suitable tool coatings. As per their discoveries, it was found that low thermal conductivity of titanium-based compounds caused a thermal exchange of the tool that prompted quick tool disintegration. They proposed that coating materials with thermal conductivity lower than that of the workpiece material could be utilized to enhance tool life for machining titanium-based alloys. Hosseini and Kishawy [23] presented another strategy for enhancing cutting tool life by utilizing the ideal estimations of speed and feed rate all through the cutting procedure. They also developed a mathematical model from the exploratory information of tool life. Enhancement methods were utilized for improving tool life, while keeping the metal removal rate constant.

Although a number of studies have been conducted on the feasibility of using coatings on the cutting tools for improving tool life and enhancing productivity, very few studies considered investigating the feasibility of titanium carbo nitride (TiCN) and titanium aluminum nitride (TiAlN) coated tools. Therefore, this current study investigated the effectiveness of the TiCN and TiAlN coatings on the carbide tools for dry machining of Ti-6Al-4V. A comparative study on the machinability of titanium alloys (Ti-6Al-4V) for coated (TiCN and TiAlN) and uncoated tools in dry machining was conducted. The effect of various operating parameters on machining time, tool wear, and surface roughness for both coated and uncoated tools was analyzed.

## Experimental Setup

A Haas Mini Mill machine tool was used to conduct the experiments in this current study. Figure 1 shows a photograph of the machine tool. This is a computer numerically controlled (CNC) machine tool integrated with a computer-integrated manufacturing (CIM) cell along with four other machine tools and assembly system. The machine tool had the option for automatic tool changing, which was used in this study to reduce the experiment time. The workpiece used in this study was Ti-6Al-4V, which is commonly known as Grade 5 titanium alloy or aerospace material. In order to cut the Ti-6Al-4V, four-fluted tungsten carbide tools with 1/8 inch cutter diameter were used. The feed rate and depth of cut were varied for three different settings. The cutting speed was kept at the fixed setting of 50 m/min, which was the highest capacity of the machine tool. The cutting speed was set at the highest available setting in order to maintain high-speed machining of the titanium alloys. For each parameter setting (a combination of cutting speed,

feed rate, and depth of cut), three slots of 1-inch length were machined. The machining time was recorded and the surface topography, roughness, and tool wear were analyzed. Table 1 presents the experimental conditions and parameters used in this study. The step-by-step experimental procedure is presented in Figure 2.

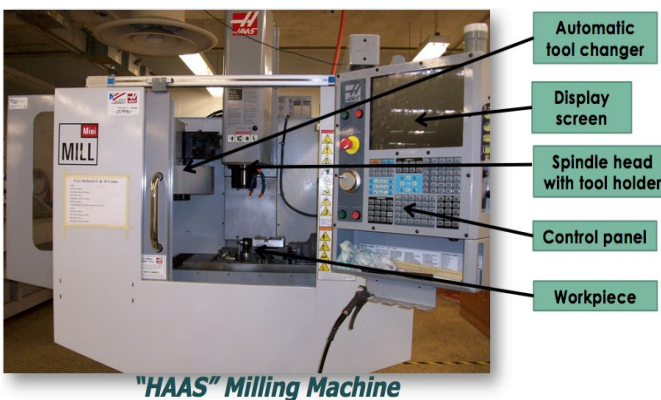


**Figure 1. Photograph of the Machine Tool (Hass Mini Mill) Used to Perform the Machining Experiments**

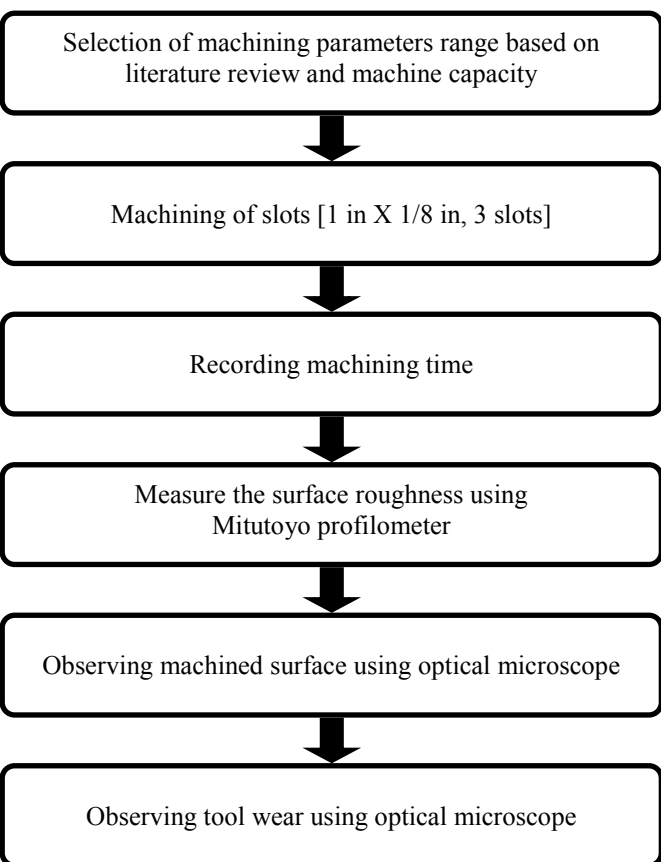


**Figure 2. Step-by-step Experimental Procedure Followed in This Study**

**Table 1. List of Experimental Conditions and Machining Parameters**

Experimental Condition	Machining Parameters
Workpiece	Ti-6Al-4V (3 in x 3 in x 0.5 in)
Cutting tool	Tungsten carbide (1/8 x 1/8 4F) – Coated and Uncoated
Types of coating	TiCN and TiAlN
Cutting fluid	No Cutting fluid (dry machining)
Cutting speed (m/min)	50 (Maximum limit of the machine tool)
Feed rate (mm/rev)	0.3, 0.5, 0.7
Depth of cut (mm)	0.3, 0.5, 0.7

## Results and Discussions

### Performance Comparison at Different Feed Rates

In order to compare the machining performance of coated and uncoated carbide tools, the effect of feed rate on the machining time, tool wear, and surface roughness was studied for uncoated, TiCN-coated and TiAlN-coated carbide tools. The feed rate was varied at 0.3, 0.5, and 0.7 mm/rev, while cutting speed and depth of cut remained unchanged at 50 m/min and 0.3 mm, respectively. Figure 3 shows the effect of feed rate on machining time, tool wear, and surface roughness during dry machining of Ti-6Al-4V using uncoated, TiCN-coated and TiAlN-coated carbide tools. It can be seen from Figure 3(a) that for both coated and uncoated carbide tools, the machining time decreased with an increase in feed rate. The machining times at different feed rates for TiCN- and TiAlN-coated carbide tools were found to be very similar. However, the uncoated carbide tools were found to provide slightly lower machining times at lower feed rates, although no significant difference in machining time was observed at higher depths of cut.

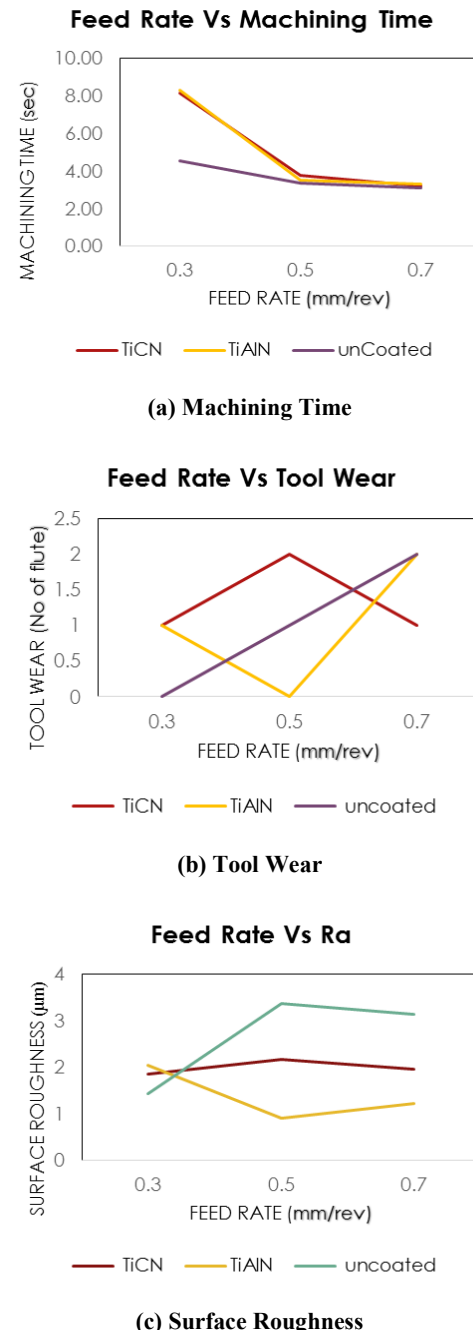
Figure 3(b) shows a comparison of the number of cutting edges/flutes affected at different feed rates for uncoated, TiCN-coated, and TiAlN-coated carbide tools. It can be seen that for uncoated carbide tools, the tool wear/number of worn out edges increased with an increase in feed rate. For the TiCN- and TiAlN-coated tools, the number of worn out edges was lower at higher feed rates compared to those of uncoated tools. Figure 3(c) indicates that the surface roughness obtained at higher feed rates, using TiCN- and TiAlN-coated tools, was significantly lower than that obtained with uncoated carbide tools. Although there was no significant difference in surface roughness at lower feed

rates, the difference became significant at higher feed rates. This was due to the fact that the increase in feed rate increased the amount of frictional forces at the tool-workpiece interface. The increased friction caused more heat generation, resulting in more wear in the cutting tool edges. However, the coating of TiCN and TiAlN sustained comparatively higher feed rates, thereby retaining the sharpness of the cutting edges at higher feed rate. The TiAlN was found to provide the smoothest surface finish among the three different types of cutting tools used in this study for dry machining of Ti-6Al-4V.

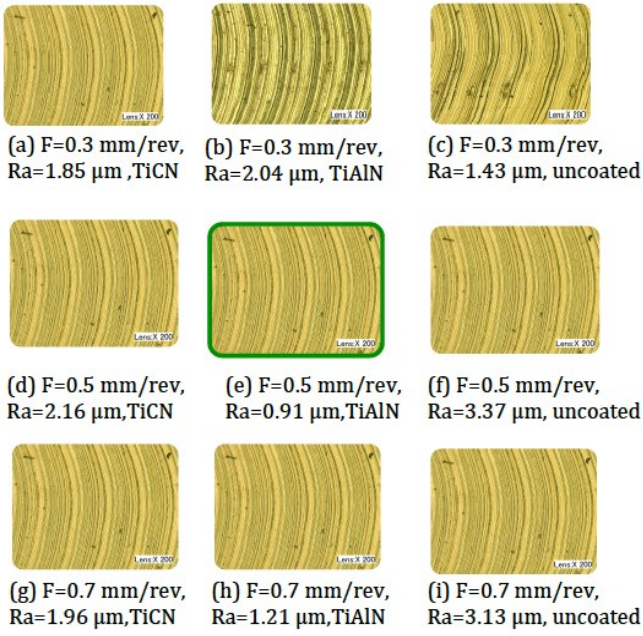
Figure 4 shows a comparison of the surface topography and roughness obtained by TiCN, TiAlN, and uncoated carbide tools at the different feed rates. It can be seen that for uncoated and TiCN-coated carbide tools, the average surface roughness increased with the increase of feed rate. However, interestingly, for TiAlN-coated tools, the surface roughness was higher at lower feed rates and decreased when higher feed rates were used. This indicated that the TiAlN coating was effective at comparatively higher feed rates. The lowest value of  $R_a$  was obtained at the feed rate of 0.5 mm/rev with the TiAlN-coated carbide tools. It was also found that surface roughness was higher when uncoated carbide tools were used at comparatively higher feed rates (0.5 and 0.7 mm/rev). On the other hand, the surface roughness was lower for uncoated carbide tools, when lower (0.3 mm/rev) feed rates were used for machining. The results indicated that the coatings on the tools were more effective when the machining was conducted at higher feed rates or at faster speeds. However, the coatings on the cutting tools were not very effective when the machining was carried out at lower feed rates.

Figure 5 shows a comparison of tool wear for the TiCN, TiAlN, and uncoated carbide tools for dry machining of Ti-6Al-4V at different feed rates. The number for tool wear indicates the number of worn out or affected flute/cutting edges of the tool. It can be seen from Figure 5 that tool wear was the most unpredictable, showing no confirmed trend against different feed rates or coatings. It was found that for machining at lower feed rates, e.g., 0.3 mm/rev, the uncoated carbide tool suffered less tool wear compared to the coated carbide tools. However, at higher feed rates, the coated carbide tools provided lower tool wear than those of uncoated tools. Among all three types of tools, the TiAlN-coated carbide tools suffered the least amount of tool wear in dry machining of Ti-6Al-4V. One important observation was the adhesion of chips on the cutting edge during machining at a feed rate of 0.5 mm/rev using uncoated carbide tools. The adhesion of chips at the cutting edge usually resulted in breakage of the cutting tool at the shank. This was due to improper heat dissipation from the cutting edges at higher feed rates. The coating on the cutting edges could reduce the

possibility of adhesion of chips at the cutting edge, as observed from Figure 5. The TiAlN-coated tools at moderately higher feed rates (0.5 mm/rev) provided the best results in terms of tool wear and surface finish.



**Figure 3. Effect of Feed Rate on Machining Time, Tool Wear, and Average Surface Roughness ( $R_a$ ) for Uncoated, TiCN-coated, and TiAlN-coated Carbide Tools [d.o.c. = 0.3 mm, cutting speed = 50 m/min]**



**Figure 4. Comparison of Surface Topography and Roughness of Ti-6Al-4V at Different Feed Rates for TiCN, TiAlN, and Uncoated Carbide Tools [d.o.c. = 0.3 mm, cutting speed = 50 m/min]**

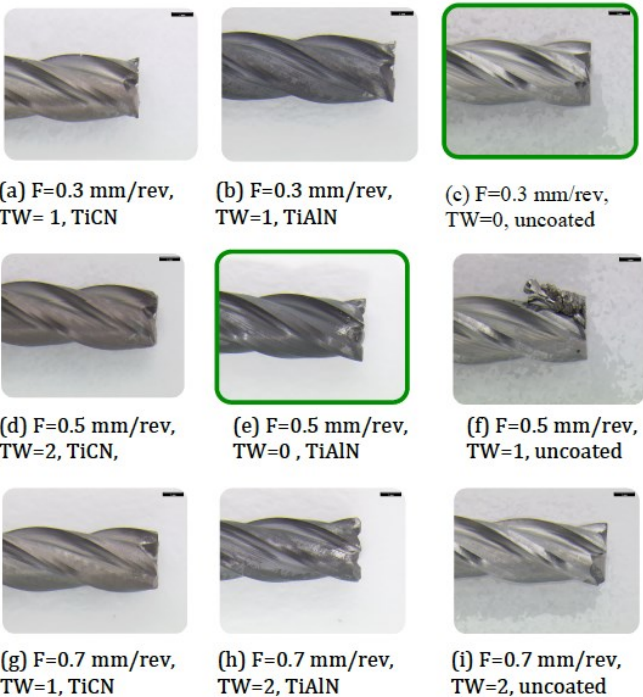


**Figure 5. Comparison of Tool Wear during Dry Machining of Ti-6Al-4V at Different Feed Rates for TiCN, TiAlN, and Uncoated Carbide Tools [d.o.c. = 0.3 mm, cutting speed = 50 m/min]**

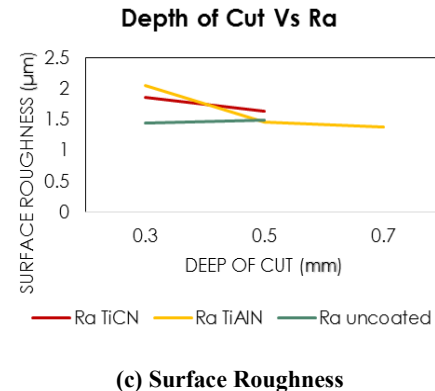
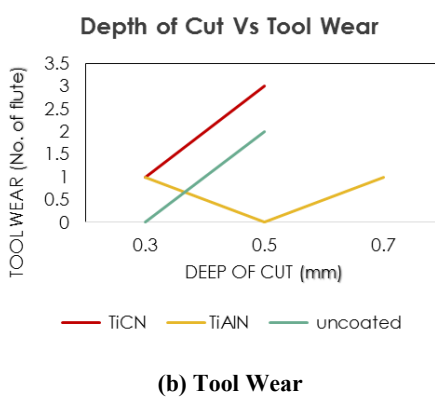
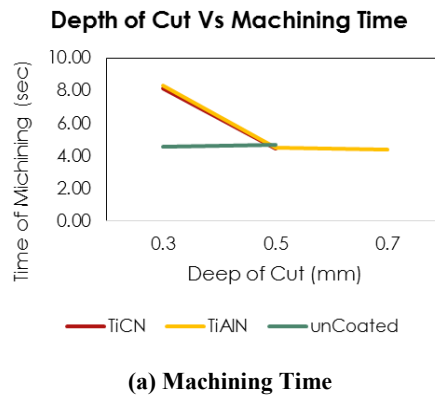
## Comparison of Performance at Different Depth of Cuts

Figure 6 shows the comparison of machining time, surface roughness, and tool wear during dry machining of Ti-6Al-4V using TiCN, TiAlN, and uncoated carbide tools at various depth of cuts. The depth of cut was varied at 0.3 mm, 0.5 mm, and 0.7 mm, while keeping the cutting speed at 50 m/min and feed rate at 0.3 mm/rev. It can be seen from Figure 6 that no data were available for machining at 0.7 mm depth of cut for uncoated and TiCN-coated carbide tools. This was because of tool breakage at 0.7 mm depth of cut. At least two attempts were made using each of the TiCN-coated and uncoated carbide tools for machining at 0.7 mm depth of cut, and the tools broke for both attempts. Only TiAlN-coated carbide tools could successfully machine the Ti-6Al-4V at 0.7 mm depth of cut, 50 m/min cutting speed, and 0.3 mm/rev feed rate.

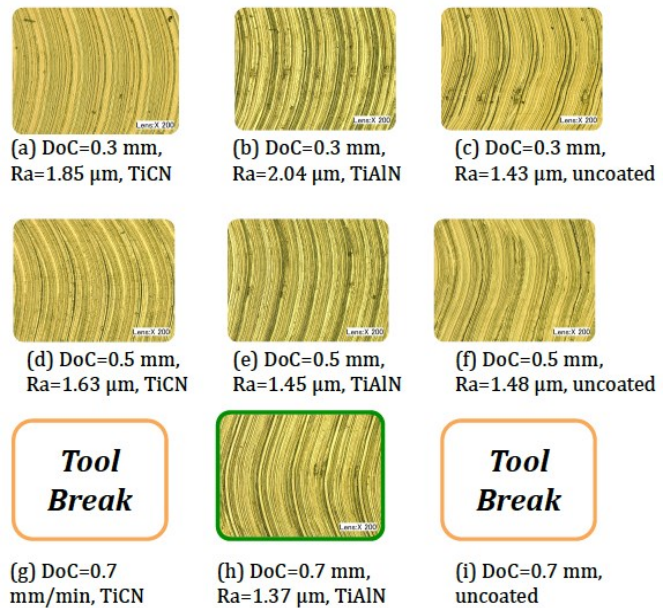
It can be seen from Figure 6(a) that for TiCN- and TiAlN-coated tools, the machining time slightly decreased with depth of cut, whereas for uncoated carbide tools, the machining time remained unchanged with the increase of depth of cut. The tool wear (number of affected cutting edges) was found to increase with the increase of depth of cut, as can be seen from Figure 6(b). This was due to the fact that an increase in the depth of cut causes the cutting tool to dig at higher depths and removes more material from the workpiece. The increased depth of cut also increased the frictional forces between the tool and the workpiece, causing the possible breakage of the tool. In case of TiAlN-coated carbide tool, there was no significant tool wear when machining was conducted at 0.5 mm depth of cut. For all three depths of cut, the TiAlN-coated tool was found to provide lower tool wear among the three types of cutting tools. Figure 6(c) shows a comparison of the surface roughness parameter,  $R_a$ , for machining of Ti-6Al-4V using TiCN-coated, TiAlN-coated, and uncoated carbide tools. The surface roughness was found to slightly decrease with the depth of cut for TiAlN- and TiCN-coated tools. However, no significant difference in surface roughness was observed with respect to the depth of cut for machining with uncoated carbide tools.

Figure 7 shows a comparison of surface topography and roughness obtained using TiCN, TiAlN, and uncoated carbide tools at different depths of cut. It can be seen that no data were available for machining at a 0.7 mm depth of cut for TiCN-coated and uncoated carbide tools because of the tool breakage. No significant trend in surface roughness was obtained against the depth of cut. The TiCN-coated tools were found to generate a rougher surface compared to TiAlN-and uncoated carbide tools. The TiAlN-coated car-

bide tool exhibited interesting results by providing the highest surface roughness at lower depths of cut and the lowest surface roughness at higher depths of cut. In the case of tool wear, the TiAlN-coated carbide tool exhibited the best performance among the three different types of tools, as can be seen from Figure 8.



**Figure 6. Effect of Depth of Cut on Machining Time, Tool Wear, and Average Surface Roughness ( $R_a$ ) for Uncoated, TiCN-coated, and TiAlN-coated Carbide Tools [cutting speed = 50 m/min, feed rate = 0.3 mm/rev]**



**Figure 7. Comparison of Surface Topography and Roughness of Ti-6Al-4V at Different Depths of Cut for TiCN, TiAlN, and Uncoated Carbide Tools [cutting speed = 50 m/min, feed rate = 0.3 mm/rev]**

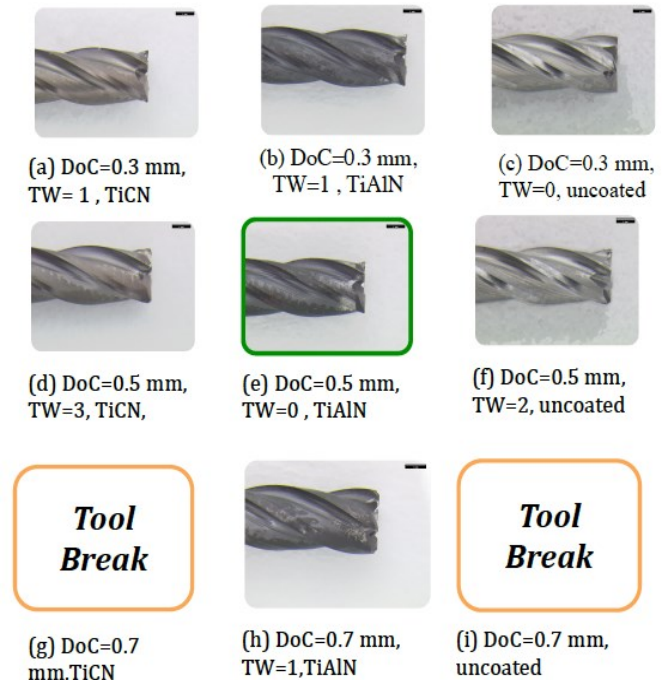


**Figure 8. Comparison of Tool Wear during Dry Machining of Ti-6Al-4V at Different Depths of Cut for TiCN, TiAlN, and Uncoated Carbide Tools [cutting speed = 50 m/min, feed rate = 0.3 mm/rev]**

## Conclusions

In this study, a comparative experimental investigation was carried out on the performance of uncoated and coated carbide tools for dry machining of Ti-6Al-4V. The effectiveness of TiCN- and TiAlN-coated carbide tools was evaluated in terms of machining time, surface roughness, and tool wear. The following conclusions were drawn from this study:

- The TiAlN-coated carbide tools provided improved machining performance compared to uncoated and TiCN-coated carbide tools. A cutting speed of 50 m/min, feed rate of 0.5 mm/rev, and depth of cut of 0.3 mm, while machining with TiAlN-coated tools, were found to be the optimum conditions for dry machining of Ti-6Al-4V.
- Dry machining using the TiAlN-coated carbide tools provided comparatively smoother surface finishes with lower average surface roughness. The surface roughness and the tool wear were comparatively higher for machining with uncoated tools.
- Tool wear was found to be unpredictable and the number of affected flutes increased with an increase in depth of cut and feed rate. The coating of TiAlN was found to be effective in reducing tool wear at higher feed rates and depths of cut.
- The machining of similar lengths of slots was found to be slightly faster with uncoated tools compared with the coated tools at lower feed rates and depths of cut. However, at higher settings, there was no significant difference in the machining time for coated and uncoated carbide tools.

## Ongoing and Future Research

In this paper, the authors present the partial results of the on-going funded research project on sustainable machining of aerospace materials. There is on-going research on the analysis of chip morphology for different machining conditions. Chips were collected during the machining at different cutting parameters with coated and uncoated carbide tools, and are currently under investigation. In addition, future research will focus on the cutting force analysis during the dry machining of Ti-6Al-4V using coated and uncoated carbide tools. It can be hypothesized from the results of this current study that there may be a reduction of cutting forces during the machining of Ti-6Al-4V with TiAlN-coated tools that resulted in the reduced tool wear and improved surface finish at higher cutting speeds, feed rates, and depths of cut. The application of green/environmentally friendly cutting fluids and minimum quantity lubrication (MQL) will be considered in the future research.

## Acknowledgement

The support from the WKU internal grant, RCAP 1 Award #13-8044, is acknowledged.

## References

- [1] Mhamdi, M., Boujelbene, M., Bayraktar, E., & Zghal, A. (2012). Surface integrity of titanium alloy Ti-6Al-4V in ball end milling. *Physics Procedia*, 25, 355-362.
- [2] Bajpai, V., Kushwaha, A. K., & Singh, R. K. (2013). Burr formation and surface quality in high speed micromilling of titanium alloy (Ti6Al4V). *Proceedings of ASME Conference. Paper # MSE2013-1216*, (pp. 1-8). Madison, WI.
- [3] Boswell, B., Islam, M., & Pramanik, A. (2013, July). Sustainable Machining of Aerospace Material. Paper presented at the World Congress on Engineering Conference, London, U.K.
- [4] Machado, A. R., & Wallbank, J. (1990). Machining of titanium and its alloys—a review. *Journal of Engineering Manufacture*, 204(1), 53-60
- [5] Debnath, S., Reddy, M. M., & Yi, Q. S. (2014). Environmental friendly cutting fluids and cooling techniques in machining: a review. *Journal of cleaner production*, 83, 33-47.
- [6] Zheng, X., Liu, Z., Chen, M., & Wang, X. (2013). Experimental study on micro-milling of Ti6Al4V with minimum quantity lubrication. *International Journal of Nanomanufacturing*, 9, 570-570.
- [7] Zhao, W., He, N., & Li, L. (2007). High speed milling of Ti6Al4V alloy with minimal quantity lubrication, *Key Engineering Materials*, 329, 663-668.
- [8] Sun, J., Wong, Y. S., Rahman, M., Wang, Z. G., Neo, K. S., Tan, C. H., et al. (2006). Effects of coolant supply methods and cutting conditions on tool life in end milling titanium alloy. *Machining Science and Technology*, 10(3), 355-370.
- [9] Li, K. M., & Chou, S. Y. (2010). Experimental evaluation of minimum quantity lubrication in near micro milling. *Journal of Materials Processing Technology*, 210, 2163–2170.
- [10] Ezugwu, E. O., Bonney, J., Da Silva, R. B., Machado, A. R., & Ugwoha, E. (2009). High productivity rough turning of Ti-6Al-4V alloy, with flood and high-pressure cooling. *Tribology Transactions*, 52(3), 395-400.
- [11] Nandy, A. K., Gowrishankar, M.C., & Paul, S. (2009). Some studies on high-pressure cooling in turning of Ti-6Al-4V. *International Journal of Machine Tools & Manufacture*, 49(2), 182-198.

- [12] Shokrani, A., Dhokia, V., & Newman, S. (2012). Study of the effects of cryogenic machining on the machinability of Ti-6Al-4V titanium alloy. *Proceedings of the EUSPEN Conference*, 2. 283-286. Bedford, UK.
- [13] Hong, S. Y., Markus, I., & Jeong, W. C., (2001). New cooling approach and tool life improvement in cryogenic machining of titanium alloy Ti-6Al-4V. *International Journal of Machine Tools and Manufacture*, 41(15), 2245-2260.
- [14] Davoudinejad, A., Chiappini, E., Tirelli, S., Annoni, M., & Strano, M. (2015). Finite Element Simulation and Validation of Chip Formation and Cutting Forces in Dry and Cryogenic Cutting of Ti-6Al-4V. *Procedia Manufacturing*, 1, 728-739.
- [15] Ezugwu, E. O., & Wang, Z. M. (1997). Titanium alloys and their machinability—a review. *Journal of materials processing technology*, 68(3), 262-274.
- [16] Bhawmik, S. K., Divakar, C., & Singh, A. K. (1995). Machining of Ti-6Al-4V alloy with a wBN-CBN composite tool. *Materials and Design*, 16(4), 221-226.
- [17] Ezugwu, E. O., Da Silva, R. B., Bonney, J., & Machado, A. R. (2005). Evaluation of the performance of CBN tools when turning Ti-6Al-4V alloy with high pressure coolant supplies. *International Journal of Machine Tools and Manufacture*, 45(9), 1009-1014.
- [18] Che-Haron, C. (2001). Tool life and surface integrity in turning titanium alloy. *Journal of Materials Processing Technology*, 118(1-3), 231-237.
- [19] De Bruyn, R. (2014). *Improving and implementing advanced milling techniques for the manufacture of selected titanium aerospace parts*. Doctoral dissertation, Stellenbosch University.
- [20] Tuppen, S., & Voice, W. E. (2012). U.S. Patent No. 8,141,225. Washington, DC.
- [21] He, J., Ding, W. F., Miao, Q., Zhao, B., Liu, Z. W., & Liang, Y. M. (2013). Experimental Investigation on Surface Topography for PTMCs during High Speed Grinding. *Applied Mechanics and Materials*, 423, 699-703.
- [22] Fanning, J. (2013). U.S. Patent No. 8,454,768. Washington, DC.
- [23] Hosseini, A., & Kishawy, H. A. (2014). Cutting Tool Materials and Tool Wear. *Machining of Titanium Alloys*. Springer Berlin Heidelberg.

## Biographies

**MUHAMMAD P. JAHAN** is an assistant professor in the Architectural and Manufacturing Sciences Department at Western Kentucky University. He earned his B.S. degree

from Bangladesh University of Engineering and Technology (Mechanical Engineering, 2004), and Ph.D. (Mechanical Engineering, 2010) from the National University of Singapore. Dr. Jahan is currently teaching at Western Kentucky University. His interests include advanced manufacturing, micro- and nano-manufacturing, lean manufacturing, and material characterization. Dr. Jahan may be reached at [muhammad.jahan@wku.edu](mailto:muhammad.jahan@wku.edu)

**GREGORY K. ARBUCKLE** is an associate professor and the Department Chair of the Architectural and Manufacturing Sciences Department at Western Kentucky University. He earned his B.S. degree (Mechanical Technology, 1996) from Indiana State University, M.S. degree (Industrial Technology, 1999) from Eastern Illinois University, and Ph.D. (Technology Management, 2004) from Indiana State University. Dr. Arbuckle is currently teaching at Western Kentucky University. His interests include quality assurance, robotics, automation, and 2+2 program development. Dr. Arbuckle may be reached at [greg.arbuckle@wku.edu](mailto:greg.arbuckle@wku.edu)

**ABDULHAMEED DAWOOD** is a graduate student at Western Kentucky University, where he is working on his Master of Science degree in Engineering Technology Management. He earned his B.S. degree (Optoelectronics Engineering, 2008) from the University of Technology, Baghdad, Iraq. His interests include sustainable machining and advanced manufacturing. Mr. Dawood may be reached at [abdulhameed.dawood566@topper.wku.edu](mailto:abdulhameed.dawood566@topper.wku.edu)

# INSTRUCTIONS FOR AUTHORS:

## MANUSCRIPT REQUIREMENTS

The INTERNATIONAL JOURNAL OF ENGINEERING RESEARCH AND INNOVATION is an online/print publication designed for Engineering, Engineering Technology, and Industrial Technology professionals. All submissions to this journal, submission of manuscripts, peer-reviews of submitted documents, requested editing changes, notification of acceptance or rejection, and final publication of accepted manuscripts will be handled electronically. The only exception is the submission of separate high-quality image files that are too large to send electronically.

All manuscript submissions must be prepared in Microsoft Word (.doc or .docx) and contain all figures, images and/or pictures embedded where you want them and appropriately captioned. Also, for all accepted manuscripts, each figure, image, or picture that was imported into your Word document must be saved individually as a **300dpi or higher JPEG (.jpg)** file and submitted separately; your manuscript and figure numbers must be used in the title of the file (e.g., **J13-F-18 Figure 4**); that means one additional file for each image imported into your manuscript. These 300dpi images do NOT need to be embedded in your manuscript. For tables or graphs created directly in Word, you do not need to submit them as separate files.

Included below is a summary of the formatting instructions. You should, however, review the sample Word document on our website ([www.ijeri.org/formatting\\_guidelines](http://www.ijeri.org/formatting_guidelines)) for details on how to correctly format your manuscript. The editorial staff reserves the right to edit and reformat any submitted document in order to meet publication standards of the journal.

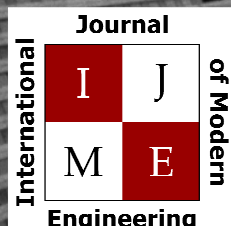
The references included in the References section of your manuscript must follow APA-formatting guidelines. In order to help you, the sample Word document also includes numerous examples of how to format a variety of scenarios. Keep in mind that an incorrectly formatted manuscript will be returned to you, a delay that may cause it (if accepted) to be moved to a subsequent issue of the journal.

1. **Word Document Page Setup:** Two columns with  $\frac{1}{4}$ " spacing between columns; Top of page =  $\frac{3}{4}$ "; Bottom of page = 1" (from the top of the footer to bottom of page); Left margin =  $\frac{3}{4}$ "; Right margin =  $\frac{3}{4}$ ".
2. **Paper Title:** Centered at the top of the first page with a 22-point Times New Roman (Bold), Small-Caps font.

3. **Page Breaks:** Do not use page breaks.
4. **Body Fonts:** Use 10-point Times New Roman (TNR) for body text throughout (1/8" paragraph indentation); 9-point TNR for author names/affiliations under the paper title; 16-point TNR for major section titles; 14-point TNR for minor section titles; 9-point TNR BOLD for caption titles for tables and figures; other font sizes as noted in the sample document.
5. **In-text Referencing:** List and number each reference when referring to them in the body of your document (e.g., [1]). The first entry must be [1] followed by [2], [3], etc., continuing in numerical order to the final entry in your References section. Again, see the sample Word document for specifics. Do not use the End-Page Reference utility in Microsoft Word. You must manually place references in the body of the text.
6. **Tables and Figures:** Center all tables and figures. Captions for tables must be above the table, while captions for figures are below; all captions are left-justified.
7. **Page Limit:** Manuscripts should not be more than 15 pages (single-spaced, 2-column format).
8. **Page Numbering:** Do not use page numbers.
9. **Publication Charges:** Manuscripts accepted for publication are subject to mandatory publication charges.
10. **Copyright Agreement:** A Copyright Transfer Form must be signed and submitted by all authors on a given paper before that paper will be published.
11. **Submissions:** All manuscripts and associated files must be submitted electronically.

**MANUSCRIPTS** should be submitted to Dr. Philip D. Weinsier, manuscript editor, at [philipw@bgsu.edu](mailto:philipw@bgsu.edu) along with a copy to [editor@ijeri.org](mailto:editor@ijeri.org).

**FILES** containing your high-quality images should ONLY be submitted to [philipw@bgsu.edu](mailto:philipw@bgsu.edu).



[www.ijme.us](http://www.ijme.us)

Print ISSN: 2157-8052  
Online ISSN: 1930-6628



[www.iajc.org](http://www.iajc.org)

## INTERNATIONAL JOURNAL OF MODERN ENGINEERING

### **ABOUT IJME:**

- IJME was established in 2000 and is the first and official flagship journal of the International Association of Journal and Conferences (IAJC).
- IJME is a high-quality, independent journal steered by a distinguished board of directors and supported by an international review board representing many well-known universities, colleges and corporations in the U.S. and abroad.
- IJME has an impact factor of **3.00**, placing it among the top 100 engineering journals worldwide, and is the #1 visited engineering journal website (according to the National Science Digital Library).

### **OTHER IAJC JOURNALS:**

- The International Journal of Engineering Research and Innovation (IJERI)  
For more information visit [www.ijeri.org](http://www.ijeri.org)
- The Technology Interface International Journal (TIIJ).  
For more information visit [www.tiji.org](http://www.tiji.org)

### **IJME SUBMISSIONS:**

- Manuscripts should be sent electronically to the manuscript editor, Dr. Philip Weinsier, at [philipw@bgsu.edu](mailto:philipw@bgsu.edu).

For submission guidelines visit  
[www.ijme.us/submissions](http://www.ijme.us/submissions)

### **TO JOIN THE REVIEW BOARD:**

- Contact the chair of the International Review Board, Dr. Philip Weinsier, at [philipw@bgsu.edu](mailto:philipw@bgsu.edu).

For more information visit  
[www.ijme.us/ijme\\_editorial.htm](http://www.ijme.us/ijme_editorial.htm)

### **INDEXING ORGANIZATIONS:**

- IJME is indexed by numerous agencies. For a complete listing, please visit us at [www.ijme.us](http://www.ijme.us).

Contact us:

**Mark Rajai, Ph.D.**

Editor-in-Chief  
California State University-Northridge  
College of Engineering and Computer Science  
Room: JD 4510  
Northridge, CA 91330  
Office: (818) 677-5003  
Email: [mrajai@csun.edu](mailto:mrajai@csun.edu)



[www.tiji.org](http://www.tiji.org)



[www.ijeri.org](http://www.ijeri.org)

The International Journal of Engineering Research & Innovation (IJERI) is the second official journal of the International Association of Journals and Conferences (IAJC). IJERI is a highly-selective, peer-reviewed print journal which publishes top-level work from all areas of engineering research, innovation and entrepreneurship.



## **IJERI Contact Information**

General questions or inquiries about sponsorship of the journal should be directed to:

Mark Rajai, Ph.D.

Founder and Editor-In-Chief

Office: (818) 677-5003

Email: [editor@ijeri.org](mailto:editor@ijeri.org)

Department of Manufacturing Systems Engineering & Management

California State University-Northridge

18111 Nordhoff St.

Room: JD3317

Northridge, CA 91330